INTERIM REPORT

Accession No. EGG-TFBP-0567

Contract Program or Project Title: Thermal Fuels Behavior Program

Subject of this Document: Severe Core Damage Assessment Program Experiment Requirements

Type of Document: Experiment Requirements

Author(s): J. M. Broughton

Date of Document: March 1980

Responsible NRC Individual and NRC Office or Division: M. L. Picklesimer

Prepared for
U.S. Nuclear Regulatory Commission
Washington, D.C. 20555

INTERIM REPORT

EGG-TFBP-5067
MARCH 1980

SEVERE CORE DAMAGE ASSESSMENT PROGRAM

EXPERIMENT REQUIREMENTS

J. M. Broughton

U.S. Department of Energy
Idaho Operations Office • Idaho National Engineering Laboratory

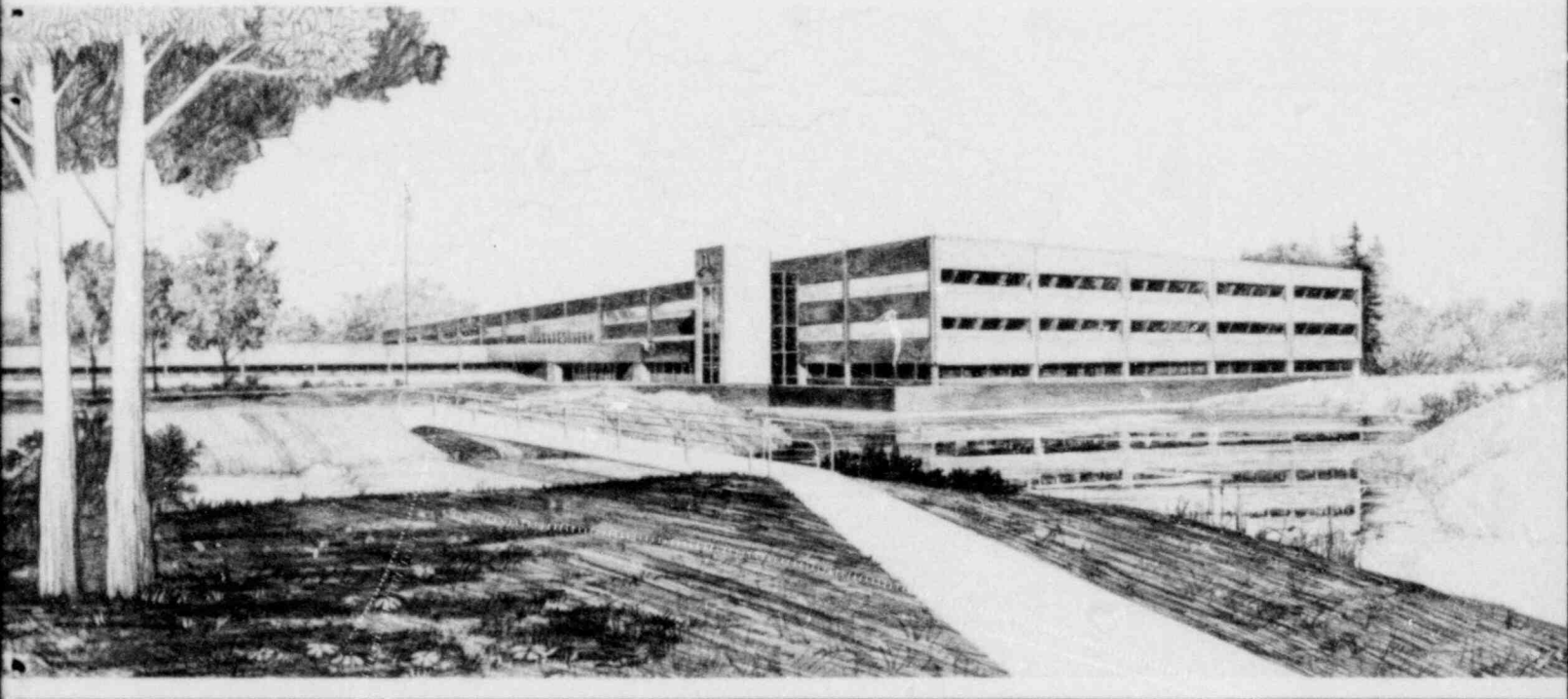

Prepared for the
U.S. Nuclear Regulatory Commission
Under DOE Contract No. DE-AC07-76ID01570
FIN No. A6041

EG&G Idaho

EG&G Idaho, Inc.

FORM EG&G-398
(Rev. 11-79)

INTERIM REPORT

Accession No. _____

Report No. EGG-TFBP-5067

Contract Program or Project Title: Thermal Fuels Behavior Program

Subject of this Document: Severe Core Damage Assessment Program Experiment Requirements

Type of Document: Experiment Requirements

Author(s): J. M. Broughton

Date of Document: March 1980

Responsible NRC Individual and NRC Office or Division: M. L. Picklesimer

This document was prepared primarily for preliminary or internal use. It has not received full review and approval. Since there may be substantive changes, this document should not be considered final.

EG&G Idaho, Inc.
Idaho Falls, Idaho **83415**

Prepared for the
U.S. Nuclear Regulatory Commission
Washington, D.C.
Under DOE Contract No. **DE-AC07-76ID01570**
NRC FIN No. A6041

INTERIM REPORT

SEVERE CORE DAMAGE ASSESSMENT PROGRAM EXPERIMENT REQUIREMENTS

J. M. Broughton

MARCH 1980

Approved:

R R Hobbins

R. R. Hobbins, Manager
Program Development and Evaluation Branch

R. K. McCardell

R. K. McCardell, Manager
PBF Experiment Specification and Analysis Branch

P. E. MacDonald

P. E. MacDonald, Manager
Light Water Reactor Fuel Research Division

FOREWORD

This experiment requirements document (ERD) discusses the range of PWR system response during a small break LOCA transient; the TMI-2 accident, and the estimated response and condition of the core; and the primary modes of fuel rod behavior during a small break LOCA. Data requirements are proposed for Severe Core Damage Tests in the Power Burst Facility for the NRC Light Water Reactor Safety Research Program.

ACKNOWLEDGEMENTS

The author wishes to thank Dr. S. L. Seiffert, Ms. B. A. Cook, Dr. D. L. Hagrman, Dr. G. A. Reymann, Mr. R. E. Mason, and Dr. F. S. Gunnerson for their assistance with the detailed review of fuel rod behavior. The final review by Dr. R. R. Hobbins and Mr. R. A. Cushman was invaluable. The patient efforts of Kim Culbertson and the other text processors are also acknowledged.

ABSTRACT

The PWR core response during hypothetical small break LOCA transients and the TMI-2 accident is reviewed with regard to the system response, core damage, and the coolability of the damaged core. The primary modes of fuel rod behavior are identified. The current understanding of these phenomena are discussed; the available and applicable data reviewed; the controlling parameters and ranges of interest are identified; and experimental data requirements proposed. A heat transfer model for long term cooling of a damaged PWR core, such as the TMI-2 core, is formulated. An experimental program to be conducted in the Power Burst Facility (PBF) is proposed. The program is structured to characterize fuel damage during conditions basically similar to a small break LOCA with cladding temperatures of approximately 2300 K, and to provide limited hydrodynamic and heat transfer data regarding the coolability of a highly fragmented and partially liquified core. The data will be used to: (a) evaluate the behavior of PWR fuel rods in a bundle configuration under system conditions similar to that of a small break LOCA; (b) evaluate more extensive out-of-pile data sets which are pertinent to specific phenomena; and, (c) develop and verify the relevant requirements for fuel behavior models. The system operation, test train design, fuel rod design, and the primary measurement requirements for performing the tests are presented.

SUMMARY

On March 28, 1979, at approximately 4:00 am. the Three Mile Island Unit 2 (TMI-2) B&W pressurized water reactor (PWR) suffered a small break loss-of-coolant accident (LOCA). The accident was initiated by a loss of normal feedwater to the steam generators resulting in a turbine trip. During the resultant events, normal for this transient, the electromatic relief valve opened to relieve excess pressure, but failed to reseat when pressure was reduced. This circumstance allowed continued coolant discharge from the reactor coolant system and, as a result of numerous subsequent events, the reactor core was uncovered, resulting in severe core damage and substantial coolant flow blockage.

As a consequense of the TMI-2 accident, the NRC has directed that a severe core damage assessment program be established to characterize fuel behavior and core damage as fuel rod temperatures rise to above fuel melting under a variety of system conditions. This document defines a series of experiments to: (a) characterize fuel behavior and core damage, primarily from cladding oxidation, embrittlement, fuel rod fragmentation and fuel rod melting with peak cladding temperatures of at least 2300 K; (b) monitor fission product release to evaluate the effects of UO_2 dissolution by molten α-Zr(O) and pellet fragmentation on fission product release; and (c) evaluate the hydrodynamic and heat transfer characteristics of a "rubble bed" formed from fragmented and prior molten fuel rods. A separate experiment requirements document which addresses the data requirements at fuel temperatures ranging from 2300 to 3200 K will be published at a later date.

The data from this program are a necessary addition to the various data sets acquired from the out-of-pile experimental programs. These in-pile data will provide invaluable calibration points against which the applicability of the out-of-pile data to nuclear rods under the actual accident conditions will be evaluated and verified. For particular conditions where out-of-pile data are

nonexistent or unattainable, these tests should provide a basic understanding or affirmation of postulated fuel behavior and core damage during small break LOCA conditions. These tests are not intended to be all inclusive or direct simulations of fuel behavior during all possible small break LOCA/flow starvation accident scenarios. However, the data from this program will bound the anticipated range of fuel behavior and a model verified against both the out-of-pile and in-pile data sets should be capable of accurately assessing the fuel behavior and probable core damage resulting from transients of this type.

During a small break LOCA transient, the system conditions which result in fuel damage can be characterized by a slow depressurization and reduced core flow. If the core flow rate decreases sufficiently, the core may uncover by boiling. If cladding temperatures increase sufficiently because of the reduced cladding surface heat transfer and the system pressure drops below the fuel rod internal pressure, the zircaloy cladding will balloon and rupture. At temperatures greater than 2245 K, the oxygen stabilized alpha-zircaloy will melt and could dissolve a significant fraction of the UO_2. Resolidification of the liquified fuel rod material may cause extensive blockages of coolant subchannels. Quenching of the embrittled cladding will result in fragmentation of the fuel rods thus creating a large rubble bed composed primarily of slag (previously molten material), and fragmented ZrO_2 and UO_2. Fission products will be released to the system when the cladding is ruptured, and additional fission product release can occur from dissolution of UO_2, and also from pellet fragmentation and desintering.

Cladding ballooning is primarily controlled by temperature, local temperature gradients, stress, and strain rate. At high strain rates, typical of a large break LOCA transients, the cladding ballooning and rupture zone is generally restricted to a few diameters in length. However, significant cladding deformation can occur over the entire high temperature zone at slow heating rates. Steam oxidation of the cladding interior surface could be enhanced if the fuel rods were to experience a "sausage" type deformation.

Zircaloy cladding becomes severely embrittled at high temperatures in an oxidizing environment. Zircaloy oxidation is primarily a function of temperature, time at temperature, and the initial oxide layer thickness. Review of the existing oxidation data indicate that the data are very limited at temperatures greater than about 1800 K. Precipitation of zirconium hydrides at low temperatures could further embrittle the cladding. However, due to the extremely high temperatures involved, $\geq$ 2250 K, hydrogen pickup at the cladding inside surface (at least in the high temperature zone) would be minimal; consequently, detrimental effects from hydriding are expected to be minimal in comparison to oxygen embrittlement. Accepted embrittlement criteria are basically restricted to room temperature conditions and cladding fragmentation from thermal shock upon quenching. Brittle fracture of the cladding also occurs at elevated temperatures, but this is not currently modeled.

When the oxygen stabilized alpha-zircaloy (α-Zr(O)) melts and redistributes, extensive dissolution of the UO_2 pellets is possible. The primary criterion for dissolution is intimate contact between the molten α-Zr(O) and the UO_2. Results from out-of-pile cladding meltdown experiments graphically illustrate this phenomenon.

Gaseous fission products, which have accumulated in the fuel rod free void volume, will be released to the reactor system when the cladding ruptures. Fuel fragmentation and possibly desintering upon quench could result in a significant increase in volatile and gaseous fission product release. Peak fuel temperatures, temperature rise rate, and time at temperature are the primary controlling parameters for gaseous fission product release. Fuel dissolution may result in nearly 100% release of the fission products contained in the dissolved UO_2.

A model describing the rubble bed fluid dynamics and heat transfer from fuel fragments is proposed. The pressure drop across the rubble pile is shown to be a function of the bed geometry, superficial fluid velocity and bed properties. However, the minimum

fluidizing velocity is a function only of the characteristic particle dimension and properties. The heat transfer is shown to follow a Nusselt number-Reynolds number power law relationship. Data from out-of-pile separate effects tests are required to determine the leading coefficients and exponents applicable to a rubble bed formed from fuel rod fragments and previously molten fuel rod material.

The severe core damage test program in the PBF is designed to evaluate the behavior of PWR fuel rods in a bundle configuration, under system conditions of a relatively slow depressurization and a reduced coolant flow. The basic objectives of the test program are to characterize core damage with respect to: oxidation, embrittlement, fuel rod melting, fuel rod fragmentation and rubble bed heat transfer.

To achieve the goals of this program, a series of eight tests is proposed for the Power Burst Facilities (PBF). The program is divided into five high priority tests and three relatively low priority tests. The fuel rod temperature rise rate, time at peak temperature and rod internal pressure will be varied in these tests. Some tests will be terminated with a slow cooldown to preserve the bundle integrity. Other tests will be quenched to fragment the rods and form a rubble bed. The hydrodynamic and heat transfer characteristics of the rubble bed will be evaluated by varying the coolant flow.

CONTENTS

FOREWORD iii

ACKNOWLEDGEMENTS iv

ABSTRACT v

SUMMARY vi

I. INTRODUCTION 1

II. SYSTEM THERMAL HYDRAULIC AND CORE RESPONSE DURING SMALL BREAK LOCA TRANSIENTS 3

1. Calculated System Response 3
2. Review of TMI-2 Core Damage 9
3. Conclusions 16

III. FUEL ROD BEHAVIOR 20

1. Cladding Ballooning and Rupture 20
2. Zircaloy Oxidation, Hydrogen Uptake, Embrittlement and Fragmentation 24

2.1 Zircaloy Oxidation 24
2.2 Hydrogen Uptake and Precipitation of Hydrides 33
2.3 Zircaloy Cladding Embrittlement and Fragmentation . . 35

3. Fuel/Cladding Interaction 46

3.1 Zircaloy-UO_2 Chemical Interaction 48
3.2 Experimental Results 50

3.2.1 Review of KfK Single Rod Tests 50
3.2.2 Review of PBF PCM-1 Test 54
3.2.3 Review of KfK Bundle Tests 59
3.2.4 Summary of Experimental Results 61

4. Fission Gas Release 62

4.1 MATPRO-11 Gas Release Model 63
4.2 Other Mechanisms Influencing Fission Gas Release . . 64

5. Conclusions 65

IV. PROPOSED MODEL FOR LONG TERM COOLING OF A DAMAGED CORE. . . . 67

1. Proposed Model. 67
2. System Fluid Dynamics 69
3. Rubble Bed Heat Transfer. 72
4. Conclusions 74

V. SEVERE CORE DAMAGE ASSESSMENT TEST PROGRAM. 75

1. Test Requirements and Objectives. 75
2. Feasibility of PBF Testing. 78
3. Test Program. 80

VI. EXPERIMENT REQUIREMENTS 84

1. Test Train Operational Requirements 84
2. Fuel Rods 85
3. Instrumentation 85
4. Postirradiation Examination 91

VII. CONCLUSIONS 93

VIII. REFERENCES. 94

APPENDIX A: POTENTIAL FOR VAPOR EXPLOSION. 100

FIGURES

1. Westinghouse Zion nodalization for small cold-leg-break, Reference 11. 5

2. System depressurization during a small cold-leg-break, Reference 11. 6

3. Core inlet flow rate during a small cold-leg-break, Reference 11. 7

4. Calculated peak cladding temperature history for the 25.81 cm small cold-leg break, Reference 11 8

5. Three Mile Island, Unit-2 system pressure history 11

6. System configuration during core dryout and heatup at approximately 2.8 hours, P ≅ 1200 psig, Reference 2 12

7. Estimated core coolant mixture level history, Reference 2 . . 13

8. Calculated peak cladding temperature for the hot bundle of the TMI-2 core with a minimum core mixture level of 4.0 ft., Reference 12 15

9. Map of core coolant temperatures at the core exit between 240 and 330 minutes after turbine trip, Reference 2 17

10. Cladding ballooning of Rod-1, -2, and -3 from PBF Test LOC-3. 21

11. Example of extended or "sausage" cladding deformation showing the effect of axial steam flow, Reference 23. 22

12. Cladding ballooning of the high pressure (~4.8 MPa) irradiated fuel rod (Rod-4) from PBF Test LOC-3. 23

13. Schematic of pellet/cladding contact showing inner and outer surface oxidation 26

14. Cladding cross section illustrating oxidized zircaloy microstructures 27

15. Comparison of calculated (solid lines) and measured ZrO_2 thicknesses for six temperatures, Reference 27. 30

16. Growth of zircaloy oxide layers as a function of temperature from Hofmann and Politis30. 32

17. Linear power generation due to oxidation for a rod of initial diameter 1.25×10^{-2} m as a function of initial oxide thickness, Reference 27 34

18. Transition zone in partially oxidized cladding showing a change from alpha plus beta two-phase material to prior beta phase with grain boundary alpha along beta grains. . . . 36

19. Cladding fracture with grain boundary alpha along prior beta grains and hydride needles (~1020 ppm H_2) within beta grains. 37

20. Fracture map for fuel rods tested under power cooling mismatch conditions, Reference 31 40

21. Hodson-Rittenhouse[34] isothermal data for the fast cooled cladding compared with the 0.65 and 0.70 wt% and the 90 and 95% filled criteria 41

22. Specimen ductility as a function of deformation temperature and fraction of wall thickness (F_W) consisting of transformed β-phase 42

23. Exposure temperature versus exposure time, in steam, with the curves drawn to show temperatures above which the ring specimens were ductile under diametral impact strains of 0.150 in, Reference 34. 44

24. Figure similar to Figure 23, but with curves drawn to show temperature below which the ring specimens had no ductility under impact loading, Reference 34. 44

25. Comparison of the ANL data for slow cooled cladding with the slow cooled embrittlement criterion, Reference 27 47

26. Isothermal phase diagrams for the ternary U-Zr-O system, for temperatures of 1273 (A), 1773 (B), and 2273 K (C), Reference 45. 49

27. Melting temperatures in the U-Zr-O ternary system, Reference 58. 51

28. Equilibrium psudo-binary phase diagram between UO_2 and α-Zr(O), Reference 58 52

29. Rods heated in He (a) and steam (b) at different heatup rates, Reference 47 53

30. Melting behavior of rods with spacers heated in He (a) and steam (b), Reference 47 55

31. Several orientations of the cladding at 0.67 m showing typical zircaloy-UO_2, zircaloy-steam interactions 57

32. Uranium distribution in the inner oxide layer at several orientations of the 0.30 m elevation, Reference 52. 58

33. Photographs of bundles heated in steam at 0.25, 2. and 4. K/s to peak temperatures of 2323, 2273 and 2323 K, respectively, Reference 50. 60

34. Schematic of damaged core long term cooling model 68

35. Comparison of heat transfer model with data, C_5, C_6, I and J for liquid water, the others for air, Reference 54. 73

36. Schematic of test bundle instrumentation. 90

A-1 Possible chain of events in large scale vapor explosion, Reference A-16. 102

A-2 Illustration of spontaneous nucleation model, Reference A-3 . 105

A-3 Description illustration of pressure detonation model, Reference A-3 106

TABLES

1. Summary of Fuel Rod Damage Mechanisms and Controlling Variables and Direct Coupling Between Mechanisms. 77

2. Test Parameters 79

3. Test Program. 81

4. Test Fuel Rod Nominal Dimensions. 86

5. Fuel Rod Measurement Requirements 87

6. Test Train and System Measurement Requirements. 88

7. Postirradiation Examination Requirements. 92

I. INTRODUCTION

Light water reactor safety research sponsored by the U.S. Nuclear Regulatory Commission (NRC)[1] has been directed towards the development and assessment of computer models which describe the behavior of a reactor system and core during selected, hypothetical design basis accidents. On March 28, 1979, the Three Mile Island Unit 2 (TMI-2) B&W pressurized water reactor (PWR) experienced a severe thermal transient[2] which resulted in extensive and severe core damage and extensive fission product release to the containment. The initiating event was a loss of normal feed water to the steam generators resulting in a turbine trip. These events are anticipated to occur with moderate frequency and are normally terminated without incident. However, during this particular transient, the electromatic relief valve which opened, as planned, to relieve excess system pressure failed to close when the system pressure decreased. This condition permitted continued coolant discharge which eventually resulted in a partial coolant uncovery of the core with fuel rod heatup in the uncovered region. The resultant core damage was probably much greater than that anticipated to result from selected, hypothetical design basis accidents.

As a direct result of the TMI-2 accident, the NRC has initiated a severe core damage assessment program designed to evaluate fuel rod and core response during accidents beyond the design basis. The proposed program would eventually extend the data obtained from ongoing PBF programs[3-6] to conditions of gross fuel melting and possibly interaction with support structures and the pressure vessel. The test program proposed herein, termed the PBF Severe Core Damage Tests, will provide data to evaluate fuel rod and bundle behavior under system conditions which will drive the fuel rods through a slow heatup to peak cladding temperatures of at least 2300 K with cladding ballooning and rupture in a manner similar to that which could occur during a small break LOCA. At a later date, an experimental program designed to provide the desired fuel behavior data at temperatures from 2300 to about 3100 K will be addressed in a subsequent ERD.

Accurate and detailed knowledge of fuel behavior during small break LOCA conditions, such as obtained from this test program, will substantially improve NRC's capability to realistically evaluate potential plant damage and thus potential danger to the public resulting from these types of transients. The out-of-pile tests are designed to systematically evaluate the modes of fuel behavior which occur. However, it is not possible to duplicate in out-of-pile experiments all facets of the nuclear environment or the integrated fuel rod and core behavior that would occur. Therefore, these tests will provide an invaluable bench mark against which the out-of-pile data can be evaluated. The test program is structured to provide data at critical points over the complete range of interest. Additionally, these tests will provide integral data regarding the dominant processes and primary coupling mechansims between the system hydrodynamics and the fuel rod bundle response, and also between the various fuel behavior modes. Finally, the applicability and capability of the NRC Fuel Rod Analysis Program (FRAP)[7] to predict the behavior of PWR fuel rods during these conditions will be assessed from the data.

In Section 2, the range of system and fuel rod response during a small break LOCA transient are discussed. The primary modes of fuel behavior are identified. In Section 3, the current understanding of these fuel behavior modes is reviewed, the applicability of existing data and/or models discussed, the primary controlling parameters identified, and the range of interest of these parameters is specified. A relatively simple model of the fluid dynamics (pressure drop and minimum fluidization velocity) and heat transfer from a fragmented core is proposed in Section 4. The test program is presented in Section 5. Experiment requirements regarding the fuel rod, test train, facility operation and measurements are discussed in Section 6.

II. SYSTEM THERMAL HYDRAULIC AND CORE RESPONSE DURING SMALL BREAK LOCA TRANSIENTS

As a consequence of the TMI-2 accident, the NRC has requested that a series of scoping calculations be performed using RELAP-4 [8] by The Code Assessment and Applications Program.[9-11] The purpose of these calculations is to evaluate the system response of specific Babcock and Wilcox[9], Combustion Engineering[10], and Westinghouse[11] plants to various break sizes, break locations, and determine the effect of operational variations of various reactor components. The results of the calculations evaluating various break sizes of the Westinghouse Zion Unit 1 plant are summarized in Section 2.1. The results from the other calculations are not evaluated explicitly as the primary purpose of discussing these results is to illustrate the basic small break LOCA thermal-hydraulic boundary conditions which would result in a severe thermal transient of the core. There is not a great deal of experience in performing these calculations and the various models which were used have not been verified for these conditions. Also, the effect of the various system components on the system thermal hydraulic response is not necessarily known.

In Section 2.2 the results of the NRC evaluation[12] of fuel damage in the TMI-2 core are reviewed. From this review, the primary modes of fuel behavior which would be expected to occur during a small break LOCA transient are identified for detailed evaluation in Section 3.

1. Calculated System Response

Scoping calculations were performed for small cold leg breaks (25.81 cm^2, 6.45 cm^2, and 3.23 cm^2) for a Westinghouse pressurized water reactor (PWR). These calculations were performed

using RELAP4/MOD7[8,a] and the system nodalization, shown in Figure 1, which was based on guidelines developed by the RELAP4/MOD6 code assessment effort at INEL.

The calculated system depressurization for the 25.81 cm^2 and 6.45 cm^2 breaks is shown in Figures 2.a and 2.b respectively. The system depressurization was characterized by a relatively rapid subcooled depressurization until saturated conditions were reached within the system. The rate of depressurization then decreased substantially until accumulator flow was initiated or the calculation was terminated. The calculated system pressure for the 25.81 cm^2 calculation held constant at about 8.5 MPa between approximately 40 and 270 seconds because the primary and steam generator secondary pressures equalized. The calculated system depressurization for the 6.45 cm^2 break never reached the saturation pressure. At about 700 seconds, water began flowing back into the pressurizer causing condensation. The pressurizer was rapidly refilled when the high pressure injection exceeded the break flow. The system became water solid at 1692 seconds and the calculation was terminated.

The calculated core inlet flow rate during the transient for the 25.81 cm^2 and 6.45 cm^2 breaks is shown in Figures 3.a and 3.b respectively. For both cases, the core inlet flow rapidly decreases during the subcooled depressurization. However, core inlet flow was predicted to go to zero only for the 25.81 cm^2 break. Core uncovery was predicted to start at about 800 seconds because of liquid boiloff.

The calculated cladding surface temperature of the upper core slab during the transient for the 25.81 cm^2 break is shown in Figure 4. Cladding temperatures began to increase at about 930 seconds and the fuel rod was quenched when accumulator flow was initiated at 1007 seconds. A peak temperature of approximately 665 K

---

a. Identified internally as Version 87 and stored at INEL under Configuration Control Number C001007 (RELAP4/MOD7) and H009982B (Steam Tables).

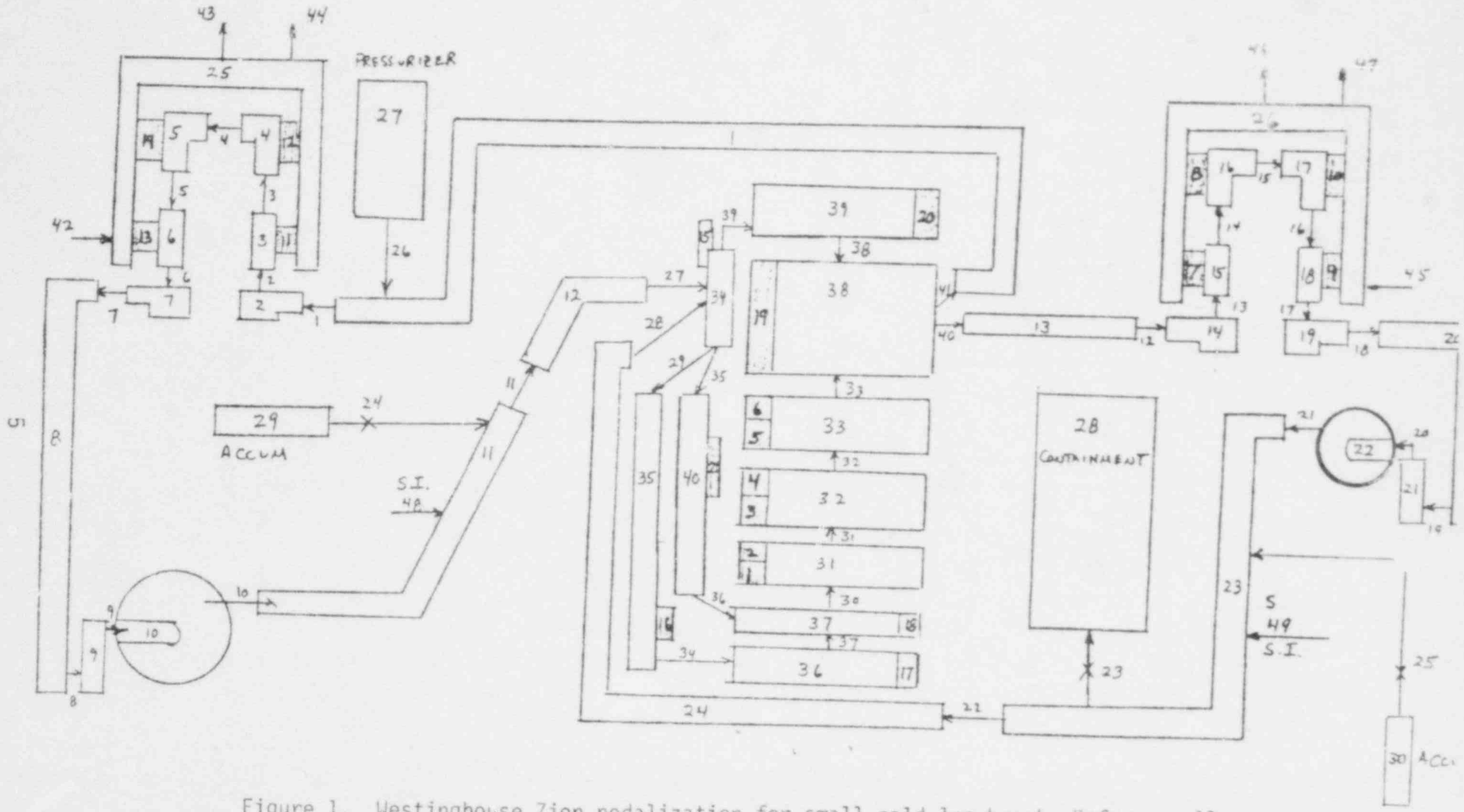

Figure 1. Westinghouse Zion nodalization for small cold-leg break, Reference 11.

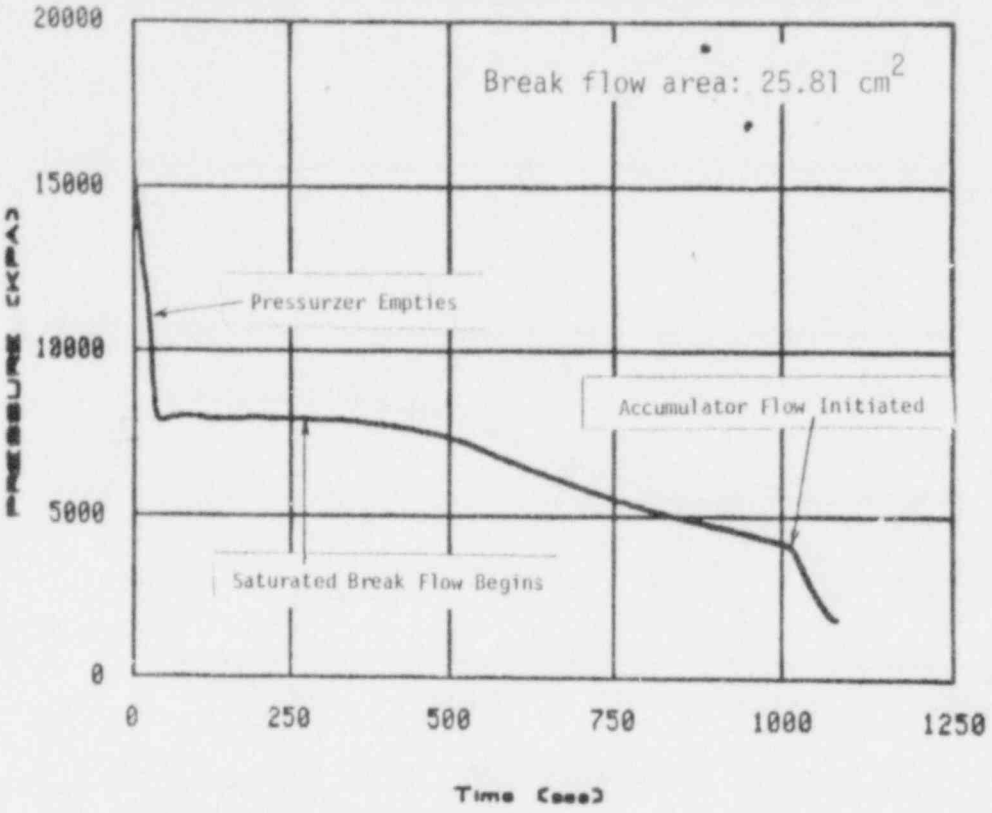

2.a

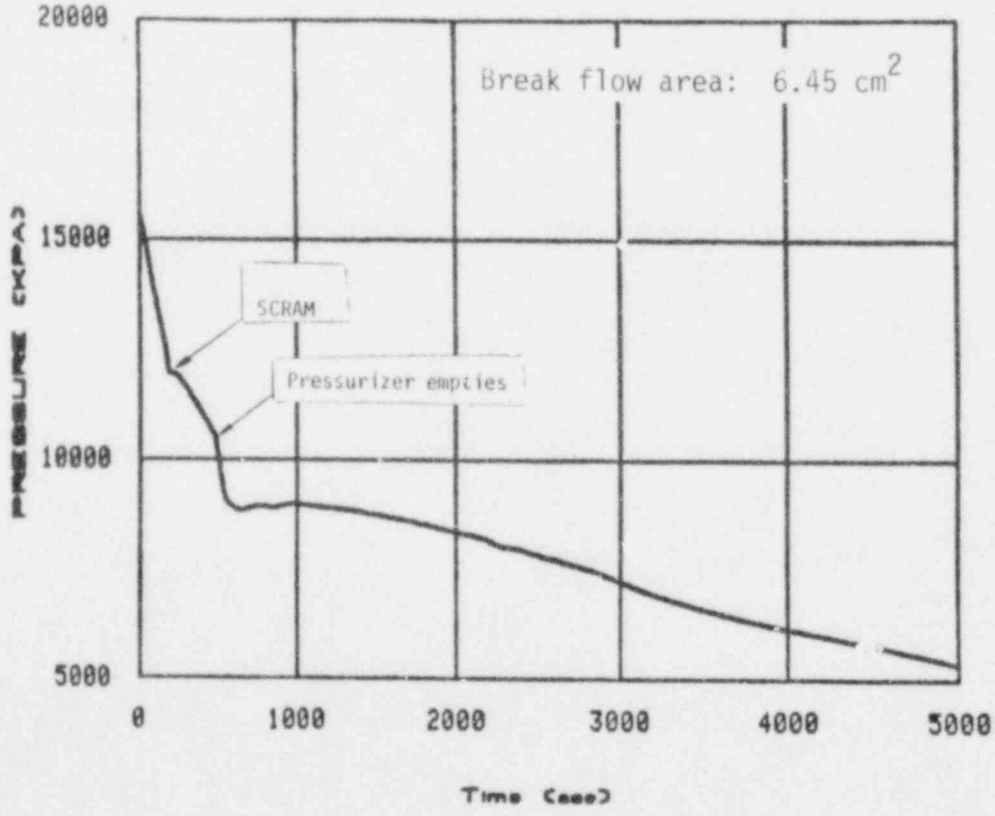

2.b

Figure 2. System depressurization during a small cold-leg break, Reference 11.

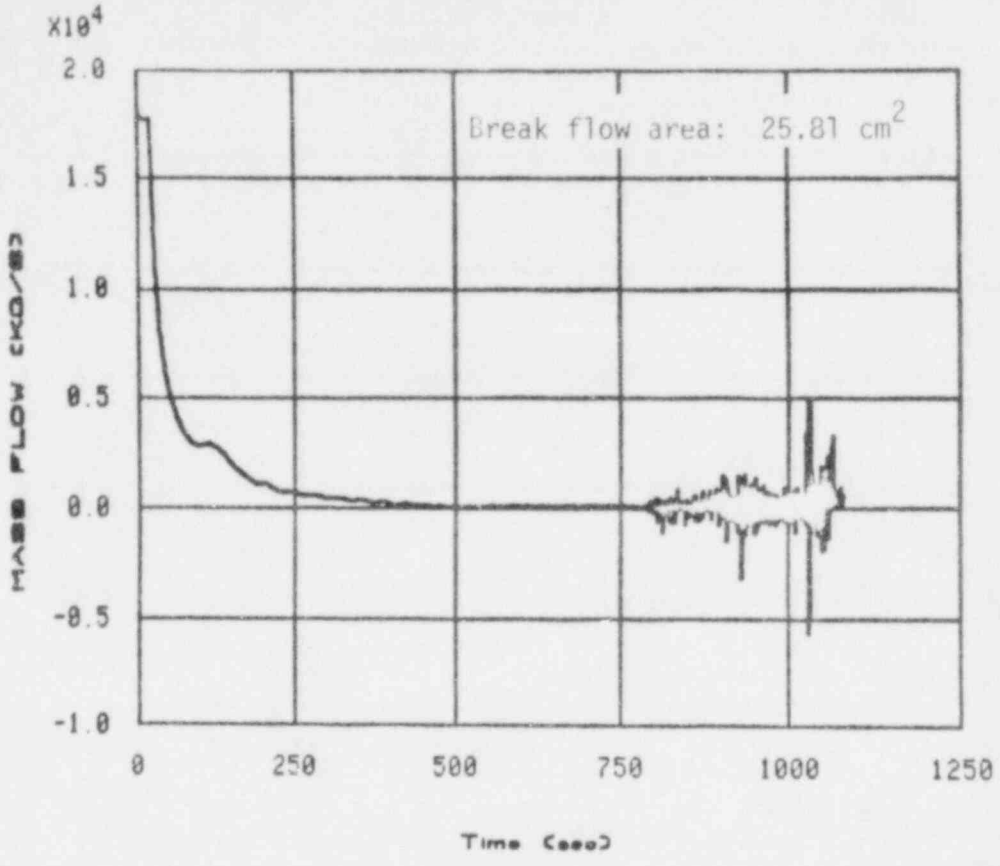

3.a

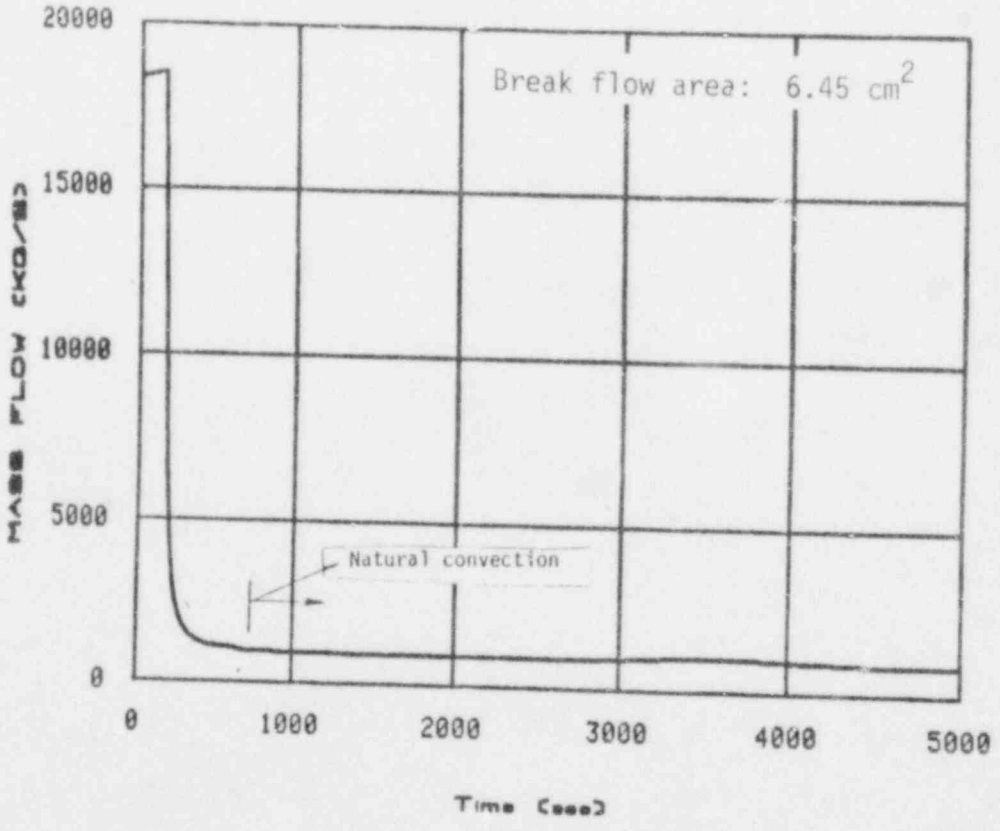

3.b

Figure 3. Core inlet flow rate during a small cold-leg break, Reference 11.

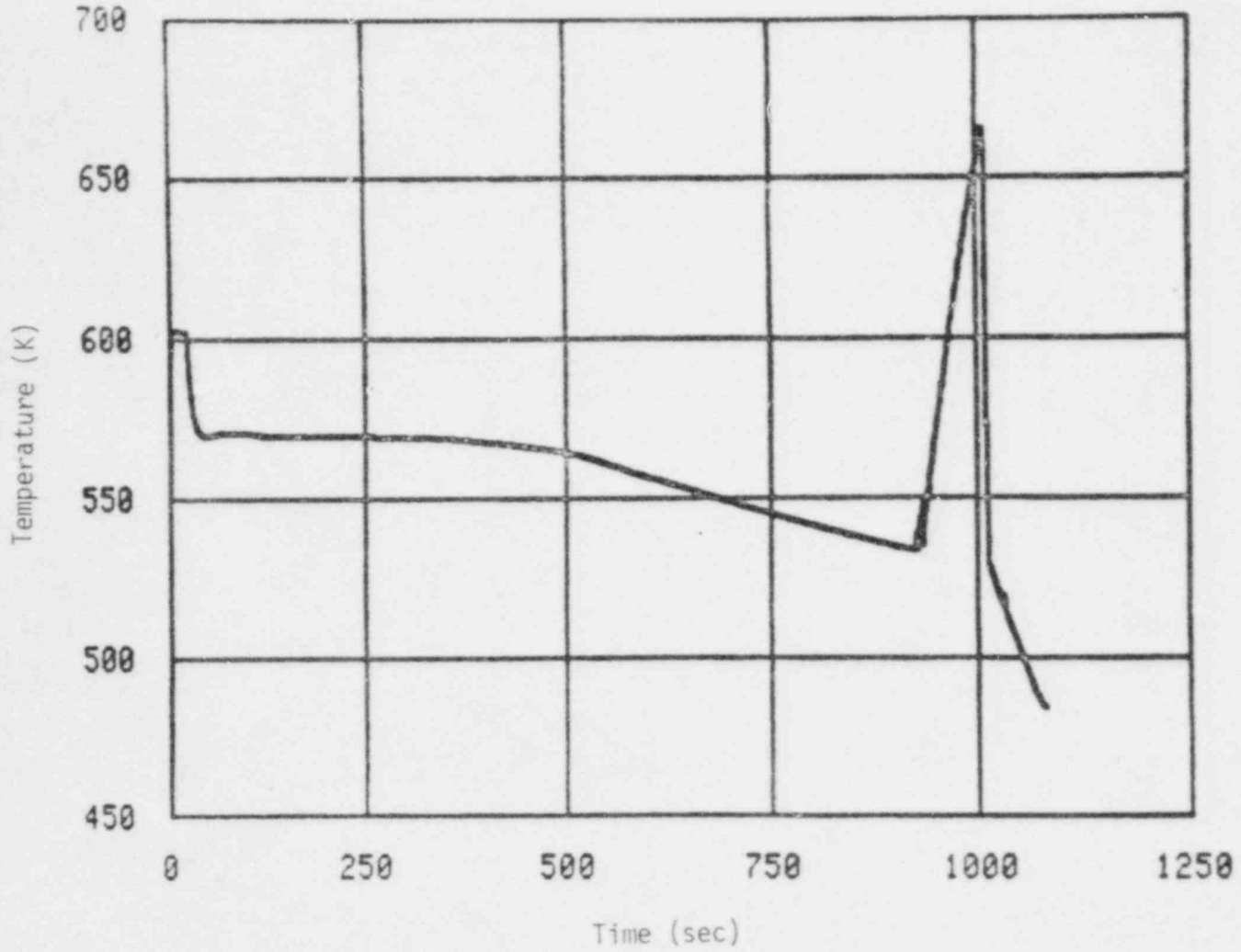

Figure 4. Calculated peak cladding temperature history for the 25.81 cm^2 small cold-leg break, Reference 11.

was calculated, and the cladding heatup rate was about 1.5 K/s. The intent of these calculations was not necessarily to predict cladding temperatures, but rather to evaluate the system response over a variety of conditions. There were known deficiencies in the core heat transfer models which resulted in too large a heat transfer coefficient in the voided region of the core. Additional calculations have recently been performed which correct (at least partially) most of these deficiencies, and a peak cladding temperature of about 1425 K was obtained without consideration for cladding metal/water reaction. Also, this calculation predicts that large core flows will occur when the accumulator flow is initiated. Recent unpublished experimental data indicate that core reflood may not occur immediately after the accumulator flow enters the system, in which case the thermal transient would continue to even higher temperatures.

A wide range of system and core thermal-hydraulics could be obtained depending upon the specific nature and conditions of the transient. An important result is that if the core remains covered, no significant core damage will occur. The thermal-hydraulic boundary conditions which could result in core damage are basically characterized by (a) a slowly fluctuating system pressure, and (b) a very low core coolant flow which is insufficient to remove the energy generated by decay heat without the occurrence of boiling and eventually core uncovery. After core uncovery, heat transfer by convection and radiation would probably be insufficient to prevent increased fuel rod temperatures. If the transient were to continue unchecked, the core would eventually melt.

2. Review of TMI-2 Core Damage

The TMI-2 accident was initiated by a loss of normal feedwater to the steam generators resulting in a turbine trip. The reactor coolant system responded to this initiating event in a normal manner and during the course of events, documented in Reference 2, the power operated relief valve (PORV) opened to relieve system pressure, as intended, and should have closed when the pressure was reduced

sufficiently. Instead, it remained open, thereby allowing continued coolant discharge from the reactor primary cooling system, and causing a further decrease in reactor coolant system pressure. The resulting system pressure history for TMI-2 during the following 15 hours is shown in Figure 5. Uncovering of the core began about 1.7 hours into the accident when the A-loop pump was shut down.

The system configuration during the period of core uncovery and heatup is shown in Figure 6. Both coolant pumps were off and the core liquid level had decreased below the top of the fuel rods. Large voids consisting of hydrogen, gaseous fission products and steam had formed in both coolant loops. These large voids, which occurred because of insufficient cooling water, prevented core cooling by natural circulation through the core after the pumps were shut down. The estimated core liquid level from 100 to 210 minutes is shown in Figure 7. The core liquid level was estimated, in Reference 2, to reach a minimum height of about 0.91 m (3 feet) above the bottom of the active core at about 138 minutes (approximately 35 minutes after core uncovery started). The core liquid level was then estimated to slowly increase until at about 185 minutes. Only the top 5 feet of the core was uncovered. The core liquid levels then decreased again and beyond about 200 minutes the estimated core liquid level was undetermined when the EPRI study[2] was published in July 1979. Considerable uncertainty still exists, at the time of publication of this document, concerning the liquid level during the accident and Figure 7 should only be considered as representative of what may have occurred.

After the core was uncovered, damage occurred because the heat transfer from the fuel rods to the steam and surrounding support structures was insufficient to remove decay heat without a significant increase in cladding temperatures. The TMI-2 core temperatures were calculated using a computer code developed within the NRC Fuel Behavior Branch[12]. The calculation accounts for core water level as a function of time, variable water/steam properties, oxidation heat, temperature varying fuel rod material properties, steam flow rate, and rod-to-steam heat transfer including both convection and radiation heat transfer.

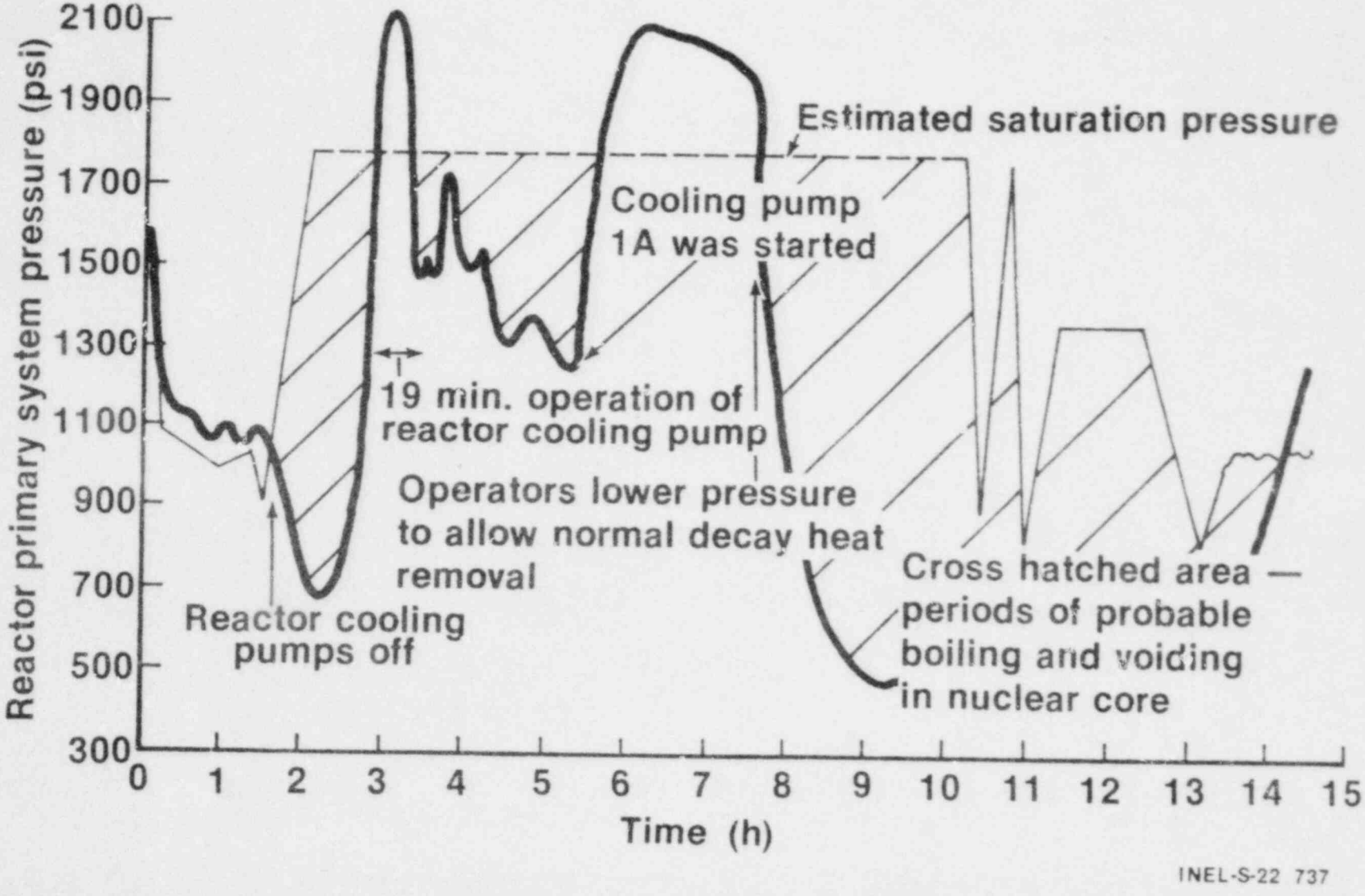

Figure 5. Three Mile Island, Unit-2 system pressure history.

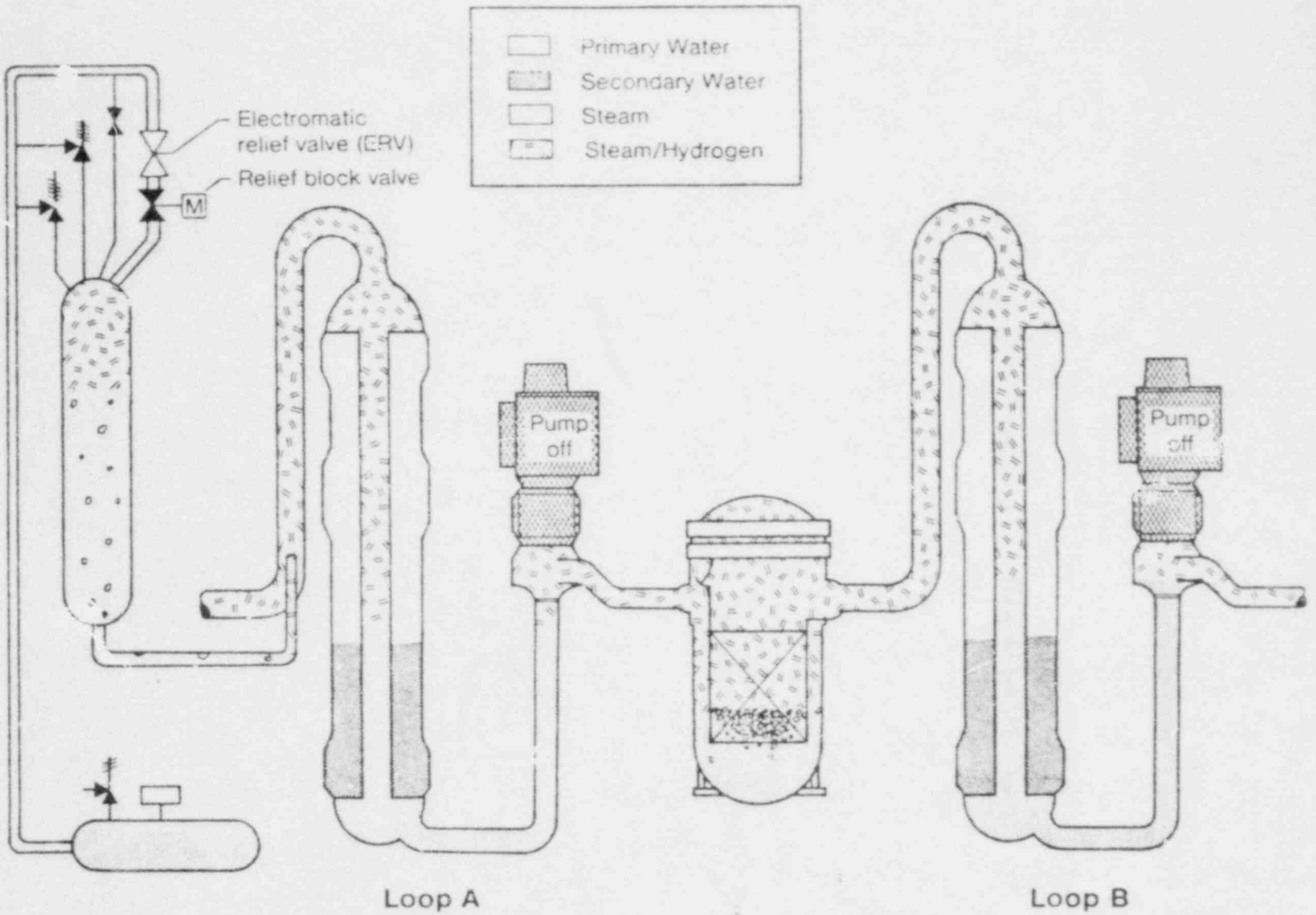

Figure 6. System configuration during core dryout and heat up at approximately 2.8 hours, P ≅ 1200 psig, Reference 2.

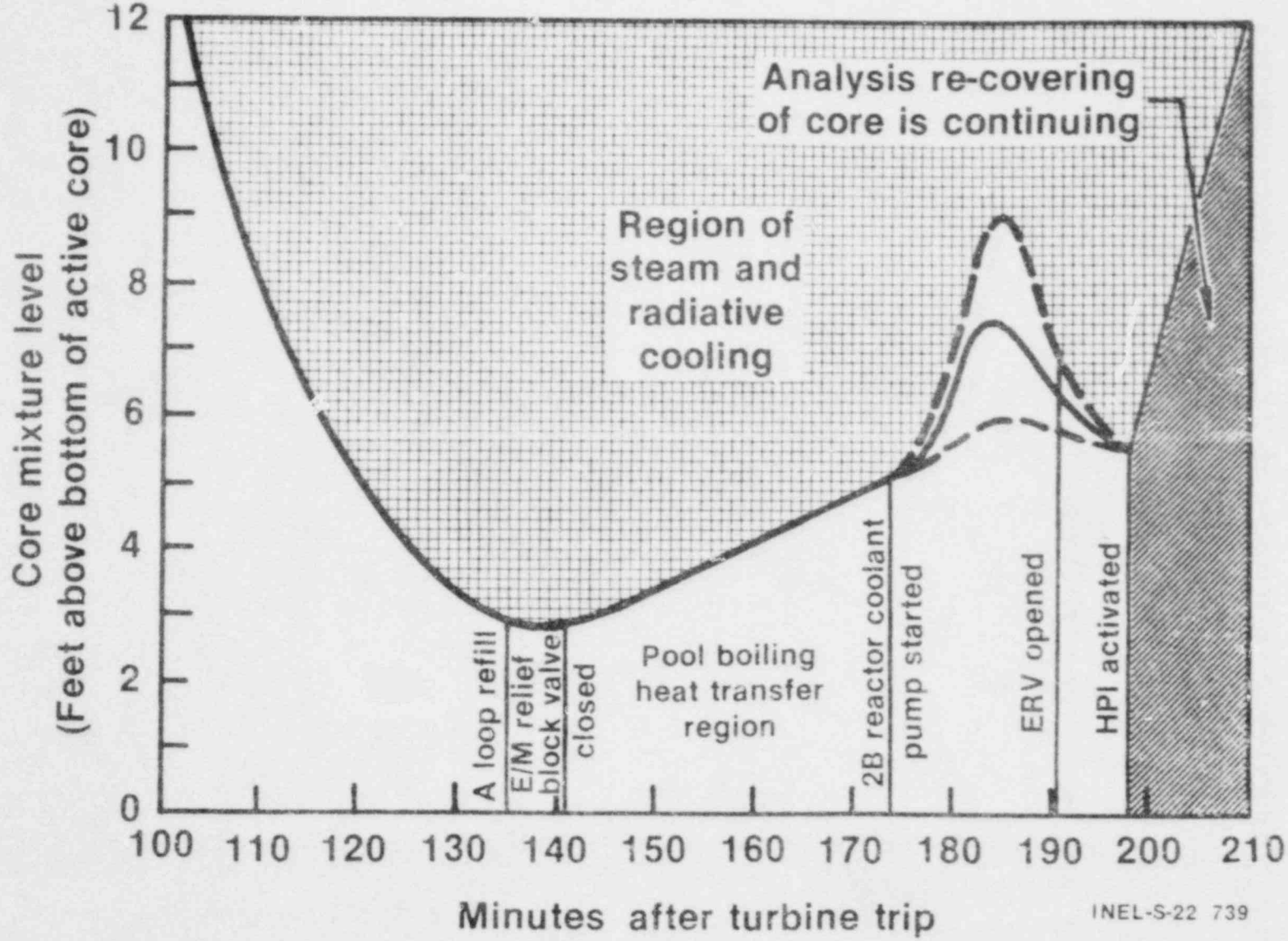

Figure 7. Estimated core coolant mixture level history, Reference 2.

The calculated fuel rod temperature history is shown in Figure 8 for a liquid level history which decreased to 1.22 m at a rate of 4.27 m/hr and was held constant at 1.22 m for 46 minutes. The calculated temperatures at one foot intervals from 0 to 2.1 m are plotted in Figure 8. Fuel rod temperatures in excess of 2550 K were calculated and at least the top 0.91 m of the fuel rod cladding was calculated to melt. (The melting temperature of α-Zr(O) is about 2245 K.) Severe cladding oxidation was calculated for at least the top 1.22 m of the core, with an oxide thickness of only about 0.24 mm at the time of cladding melting.

Additional calculations were made assuming minimum liquid levels of 1.52 m and 0.91 m. For the case with a minimum liquid level of 1.52 m, peak fuel rod temperatures were approximately 1975 K at the top of the fuel rod. For the case when all but 0.91 m of the fuel rod was uncovered, calculated peak fuel rod temperatures were greater than 3300 K, which is greater than the UO_2 melting temperature of approximately 3100 K. Cladding melting was calculated down to about 2.00 m from the bottom of the fuel rod.

The following scenario is postulated for fuel rod response during the TMI-2 transient. Cladding ballooning and rupture probably occurred when cladding temperatures were between 1033 and 1089 K. The axial elevation of the rupture was probably at about 0.3 m from the top for rods near the core center and about 0.9 m for peripheral rods. Cladding rupture would permit steam to enter the cladding and oxidize the inner surface near the rupture when temperatures rose above 1245 K. In the cooler regions of the cladding sufficient hydrose absorption may have occurred that hydrides may have formed and precipitated during quench. With the long times at elevated temperatures, severe cladding embrittlement probably occurred primarily from oxidation and oxygen absorption. As the fuel rod temperatures continued to rise, a complex reaction between the β-phase zircaloy (β-Zr), oxygen stabilized alpha-phase zircaloy (α-Zr(O)) and the UO_2 pellets may have occurred where intimate contact existed between the fuel and cladding. The β-Zr will reduce the UO_2 matrix

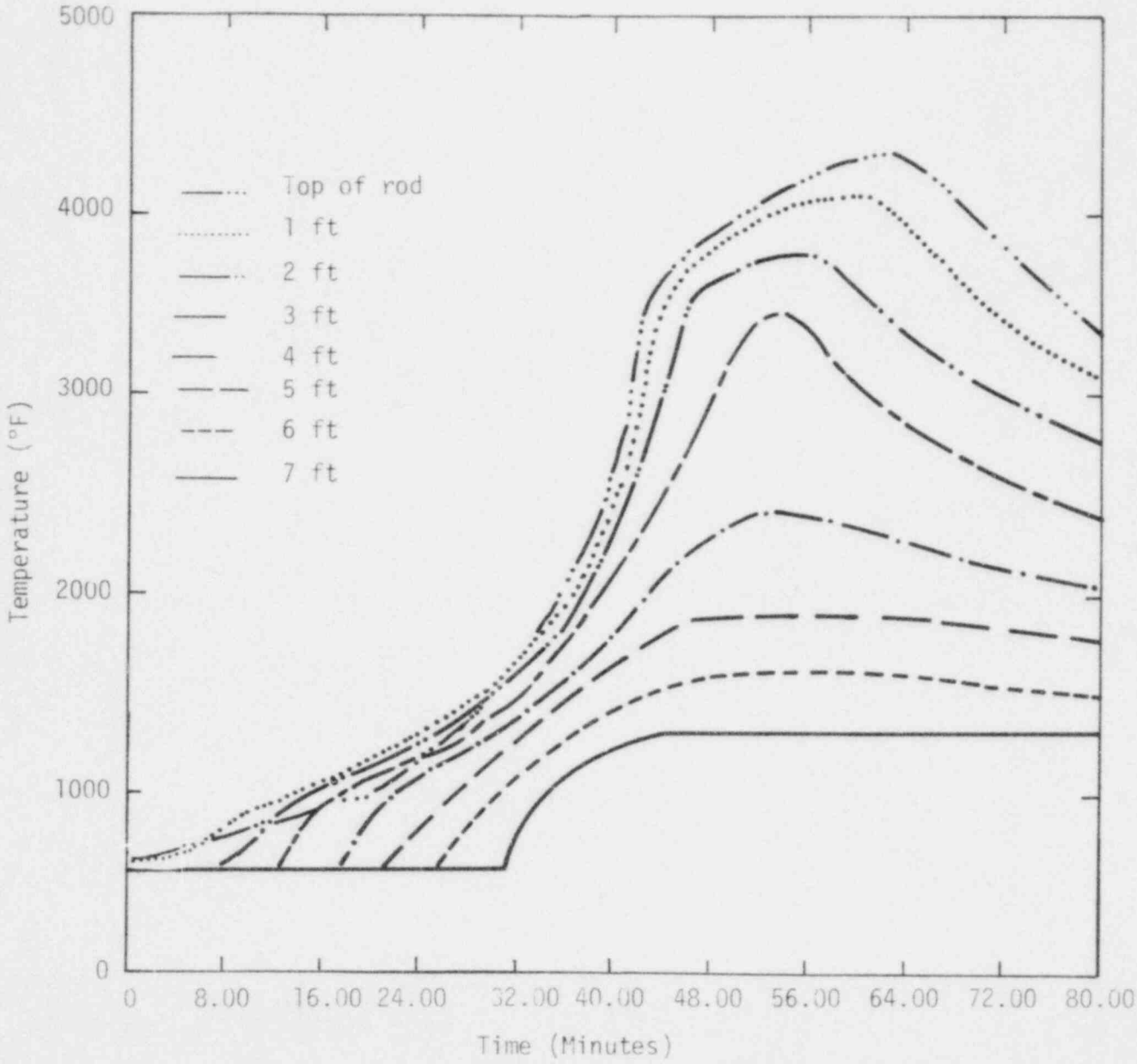

Figure 8. Calculated peak cladding temperatures for the hot bundle of the TMI-2 core with a minimum core mixture level of 4.0 ft, Reference 12.

forming α-Zr(O) and a uranium rich intermetalic compound which could be liquid depending upon the uranium and oxygen concentrations. At temperatures above 2250 K the zircaloy cladding was molten and the rate of the UO_2 reduction process may have increased significantly. Molten α-Zr(O) would have dissolved UO_2, and the dissolution of the UO_2 pellets could have been significant. The molten material would have flowed down into the bottom of the core, possibly blocking coolant flow channels as it resolidified in the cooler regions of the core.

The first indication of fission product release was found on the air sample monitor chart at 145 minutes. The estimated time for the initial cladding rupture was approximately 142 minutes, which is in excellent agreement with the observed fission product release. The fuel/cladding reaction, which may have occurred at the high cladding temperatures, would probably have resulted in almost 100% fission product release from the UO_2 involved in the reaction. Additional fission product release could have occurred during core quench because of extensive fragmentation and desintering of the fuel pellets.

When the core was quenched, extensive fuel rod fragmentation probably occurred because the cladding was severely embrittled over at least one-third to one-half of the core. If fragmentation occurred, then the fragments would have collected on intact grid spacers and rod stumps thus forming a large rubble pile. A map of core coolant outlet temperatures recorded between 240 and 330 minutes is shown in Figure 9. Very high temperatures were measured throughout the central region indicating that coolant flow channels were blocked (or nearly blocked) which caused the coolant flow to redistribute into peripheral bundles and the remaining, relatively unblocked, bundles within the central region of the core.

3. Conclusions

Based upon the preceding evaluation of recent RELAP4 calculations and the estimated core response during the TMI-2 accident, the

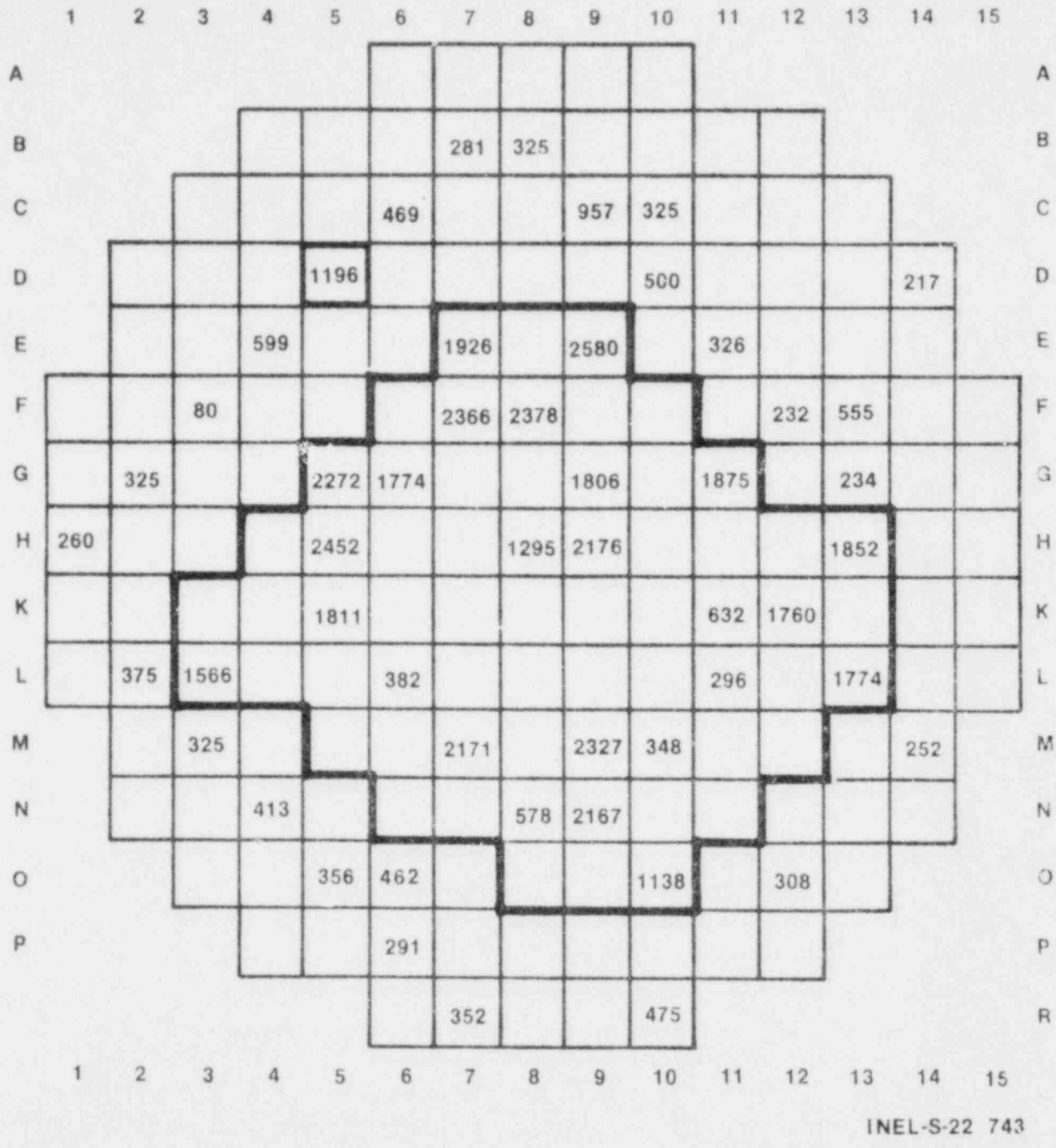

Figure 9. Map of core coolant temperatures at the core exit between 240 and 330 minutes after turbine trip, Reference 2.

following conclusions can be made concerning the anticipated system and core response during small break LOCA's.

1. The system depressurization would be slow, on the order of 0.005 MPa/sec, and could vary. The system pressure could increase, decrease, or remain stable for extended periods.

2. Core damage would not be expected unless the core was uncovered.

3. The cladding would balloon and rupture if temperatures reached 1033 to 1089 K provided the system pressure decreased sufficiently.

4. Two-sided, oxidation could occur near the cladding rupture at temperatures above 1245 K.

5. Hydrogen absorption could occur at the cladding inside surface, primarily in the cooler regions, and hydrides may form during quench.

6. The cladding would be severely embrittled by oxidation and oxygen absorption if the transient continued for long times with cladding temperatures of at least 1245 K.

7. A complex interaction between the zircaloy cladding and UO_2 pellets could occur, resulting in significant dissolution of the UO_2 matrix by molten α-Zr(O).

8. Extensive fragmentation of the fuel rods would probably occur at quench.

9. Massive releases of fission products could occur.

10. The configuration of the core would be drastically altered. A non-homogeneous anisotropic rubble bed, probably consisting of fuel rod fragments and previously molten materials would form at least within the lower center of the core.

To prevent the resultant core mass from causing a melt-through of the reactor pressure vessel, a means must be provided to remove the decay heat. This cooling must be a long term process. the heat transfer in such a conglomerate would be highly complex and variable. Additional information is required concerning both the basic configuration of the rubble pile and the heat transfer characteristics of the various components primarily at low flow conditions.

III. FUEL ROD BEHAVIOR

From the review of system and fuel rod response which could occur during a small break LOCA, such as the TMI-2 core experienced, the primary modes of fuel behavior were identified. These phenomena are discussed in the following section, the relative significance assessed, and the controlling variables identified.

1. Cladding Ballooning and Rupture

Cladding ballooning under a wide variety of conditions has been under intensive investigation in both out-of-pile[13-23] and in-pile[24-26] experiments. This work has been concentrated on the definition of strain as a function of stress, temperature, irradiation, and oxidation histories and on determining the rupture strain. For most transients, the cladding strain rate is high and uniform circumferential strains greater than 10% were generally restricted to the immediate vicinity of the rupture. Photographs of three of the rods from the PBF LOC-3 Test[25] are shown in Figure 10. The general characteristics of the cladding deformation for these rods were consistent with that observed during the out-of-pile tests.

E. D. Hindle of the United Kingdom Atomic Energy Authority has performed a series of tests in steam to evaluate cladding ballooning at relatively low strain rate between 900 and 1079 K.[22,23] Typical rod deformations during these tests are shown in Figure 11. Cladding circumferential strain was generally uniform along the entire heated length with burst strains as great as 60 - 65%. In later tests, burst strains were as great as 97%. These results may be an artifact of the test method; however, if such large circumferential strains over an extended axial length were to occur on a nuclear fuel rod the flow and circulation of steam within the fuel/cladding gap could be enhanced significantly after rod failure.

A photograph of the high pressure irradiated fuel rod in the LOC-3[25] test is shown in Figure 12. Circumferential strains of

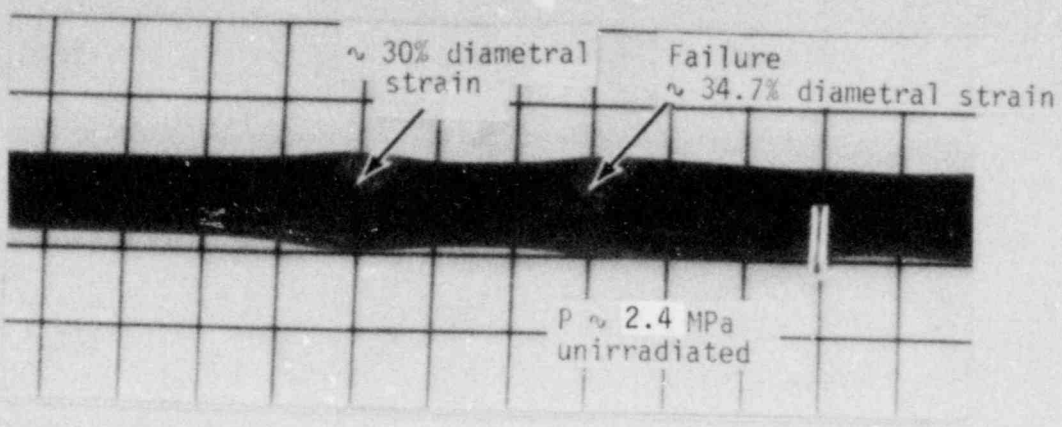

Rod 1

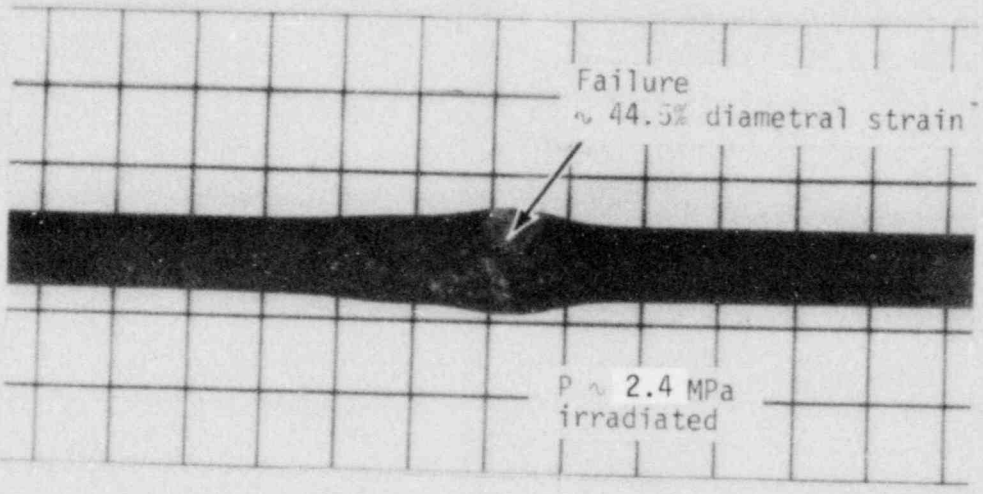

Rod 2

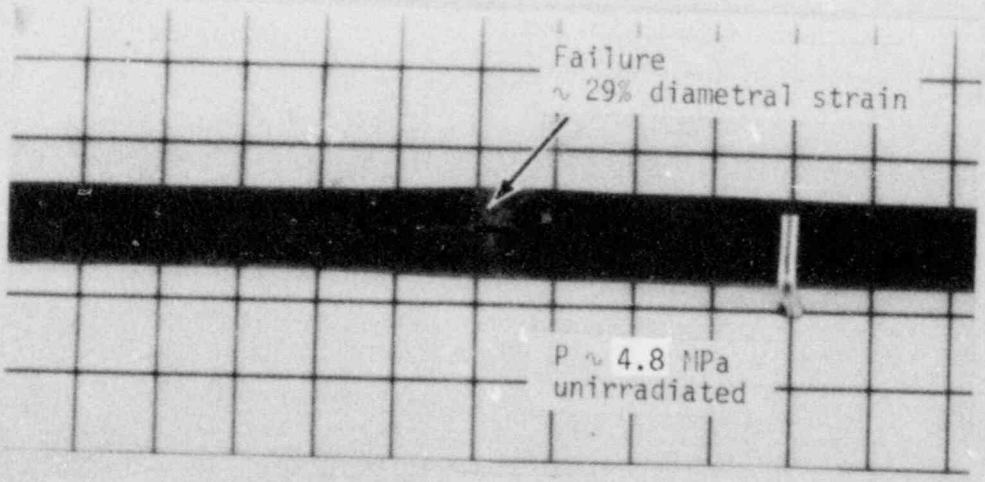

Rod 3

Figure 10. Cladding ballooning of Rod-1, -2 and -3 from PBF Test LOC-3.

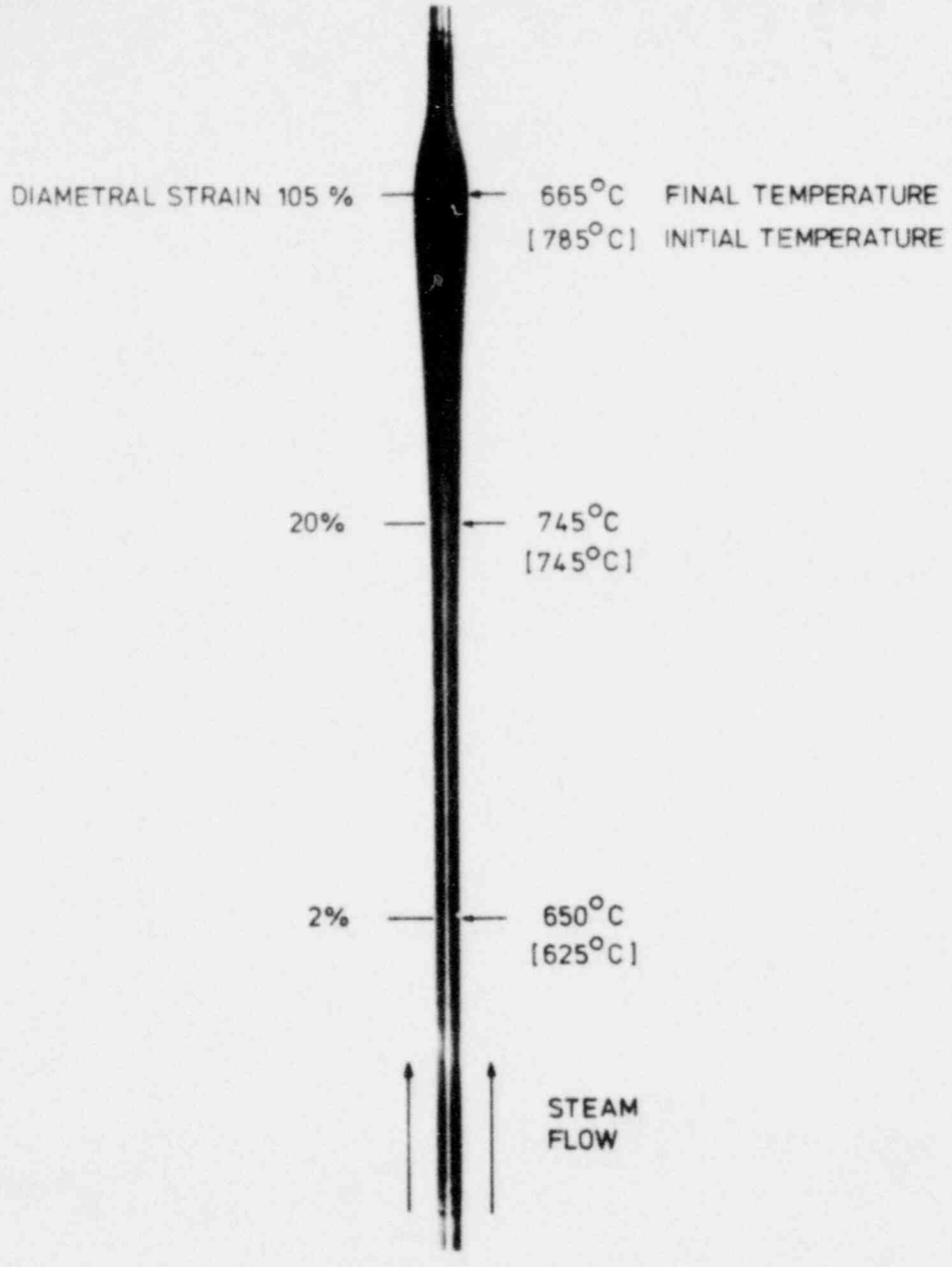

Figure 11. Example of extended or "sausage" cladding deformation showing the effect of axial steam flow, Reference 23.

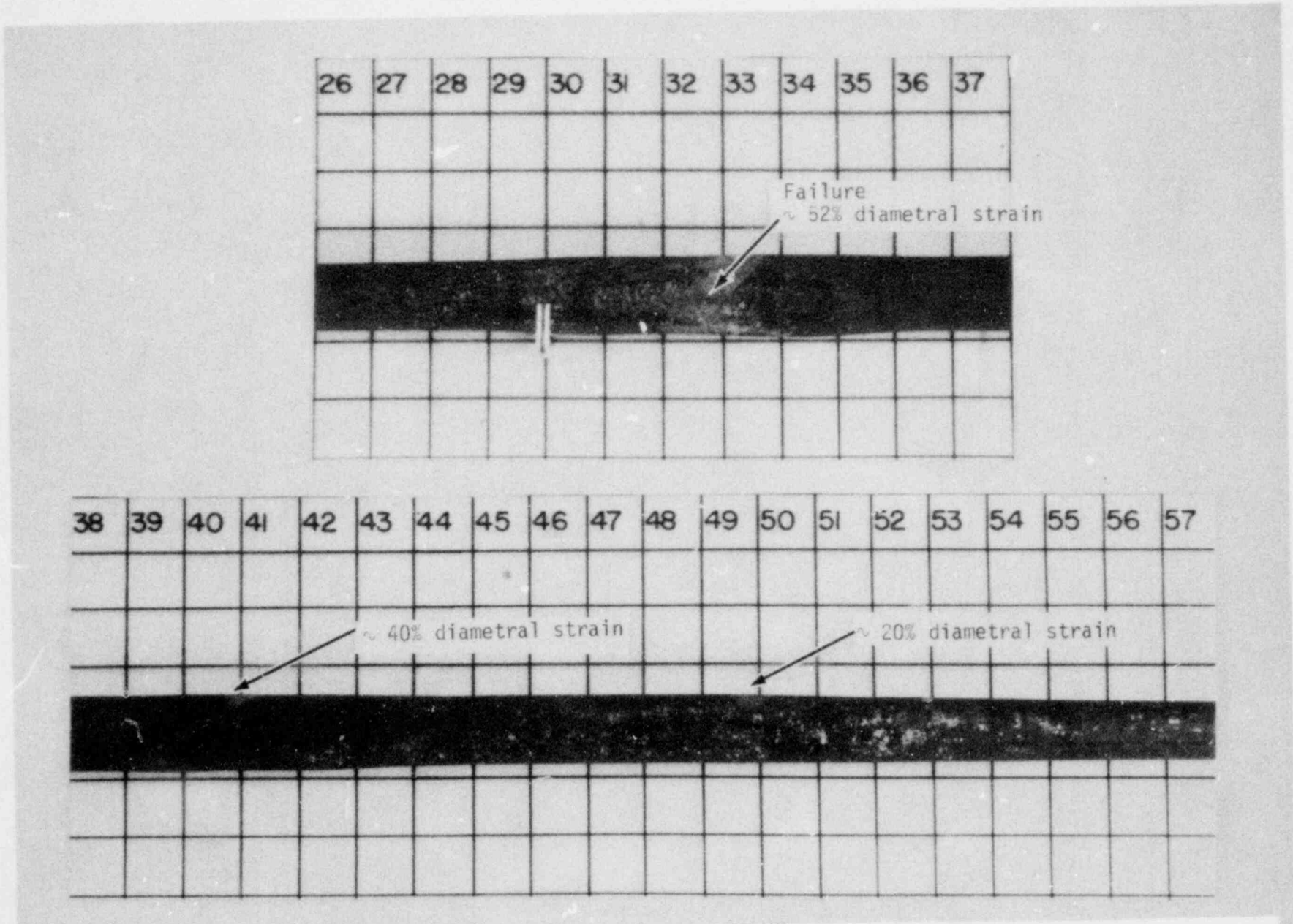

Figure 12. Cladding ballooning of the high pressure (~ 4.8 MPa) irradiated fuel rod (Rod 4) from PBF Test LOC-3.

at least 20% extended over the entire high temperature region from about 0.2 to 0.5 m. The rod ruptured at about 0.32 m with approximately 52% strain. Although the strain rate should have been high, the appearance of the deformation is quite similar to the low strain rate data published by Hindle.

Cladding deformation would probably affect the oxidation at the inside surface and the chemical interaction between zircaloy and UO_2. If the deformation were minimal with little deformation outside the rupture zone, the flow of steam into the fuel rod would be limited and oxidation would be restricted to the region adjacent to the rupture. Also, the potential for intimate fuel/cladding contact would be increased with respect to "sausage" type cladding ballooning. Extended or "sausage" type cladding deformation could enhance the circulation of steam within the gap and thus possibly increase the oxidation, but it would reduce the potential for intimate fuel/cladding contact. The flow and circulation of steam within the fuel rod is not currently modeled.

2. Zircaloy Oxidation, Hydrogen Uptake, Embrittlement and Fragmentation

The kinetics of zircaloy oxidation have been measured by numerous experimentors and are modeled in MATPRO-11.[27] Various embrittlement criteria have been postulated to correlate zircaloy embrittlement with the degree of oxidation. Hydrogen uptake may occur at the cladding inside surface, primarily within cooler regions, concurrent with oxidation. Hydrides may precipitate during quench if the solubility limit has been exceeded. These processes, models and related data are reviewed below. The controlling parameters are identified, and limitations in the models and data are assessed.

2.1 Zircaloy Oxidation

High temperature ($T \geq 1250$ K) exposure of zircaloy cladding to a steam-water environment may produce severe oxidation of the cladding.

The degree of oxidation is strongly dependent upon time at temperature, and significant energy is released during the exothermic reaction.

To help visualize the cladding oxidation, an idealized cross section through the cladding wall of an intact fuel rod with fuel/cladding contact is shown in Figure 13. The outside surface has been oxidized from high temperature exposure to the two-phase (steam-water) coolant. This oxidation is shown as a layer of zirconium dioxide (ZrO_2), and is followed by a layer of oxygen-stabilized alpha zircaloy [α-Zr(O)] of approximately equal thickness. The central region of the cladding is beta-phase zircaloy (β-Zr). All three materials; ZrO_2, α-Zr(O), and β-Zr can coexist at high temperatures provided there is sufficient oxygen supply.

When the inside surface of the cladding is in contact with the fuel, at high temperature, a layer of α-Zr(O) is produced inside of which is a uranium rich intermetallic layer, and inside of this layer is another α-Zr(O) layer containing some uranium. The source of oxygen for this reaction comes from oxygen in the UO_2.

The oxidation and embrittlement of zircaloy cladding from high temperature film boiling operation has been extensively evaluated.[28] A typical example of the microstructures observed in zircaloy oxidized under film boiling conditions for about 100 seconds is shown in Figure 14. Microstructural features such as outer, single-layer surface oxide (ZrO_2), outer and inner layers of oxygen-stabilized alpha-zircaloy, and the prior beta field are illustrated. The inner surface oxygen-stabilized alpha layer formed when there was fuel-cladding contact resulting from collapsed cladding. The cladding does not exhibit an oxygen-stabilized alpha layer where there was an open gap, indicating that the UO_2 is the source of oxidation at the inside surface for intact fuel rods. The results from this study show that reaction between the cladding and coolant led to rapid external oxidation and multilayered buildup of ZrO_2. Oxygen diffusion from the surface oxide layer induced the

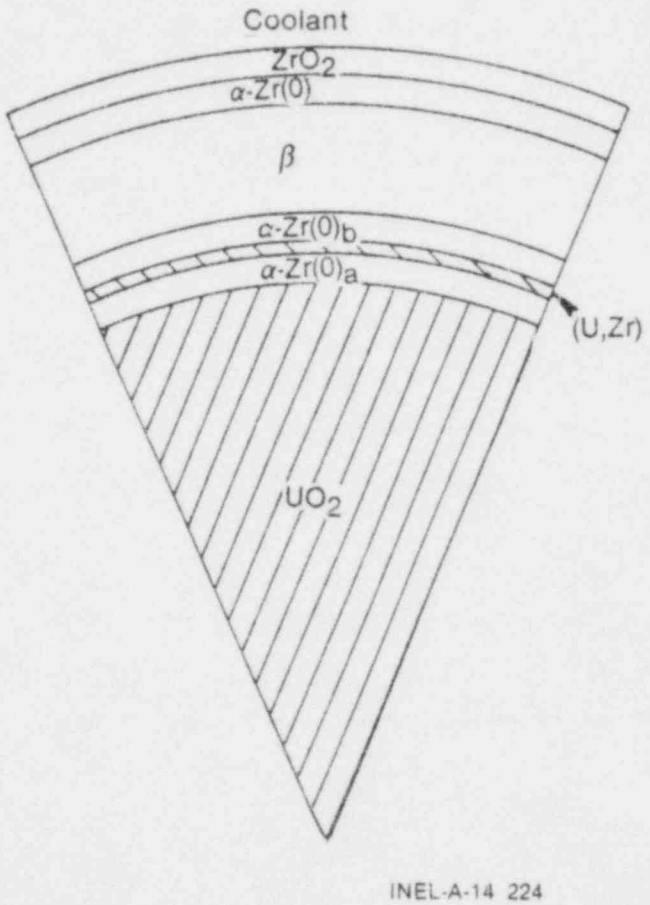

Figure 13. Schematic of pellet/cladding contact showing inner and outer surface oxidation.

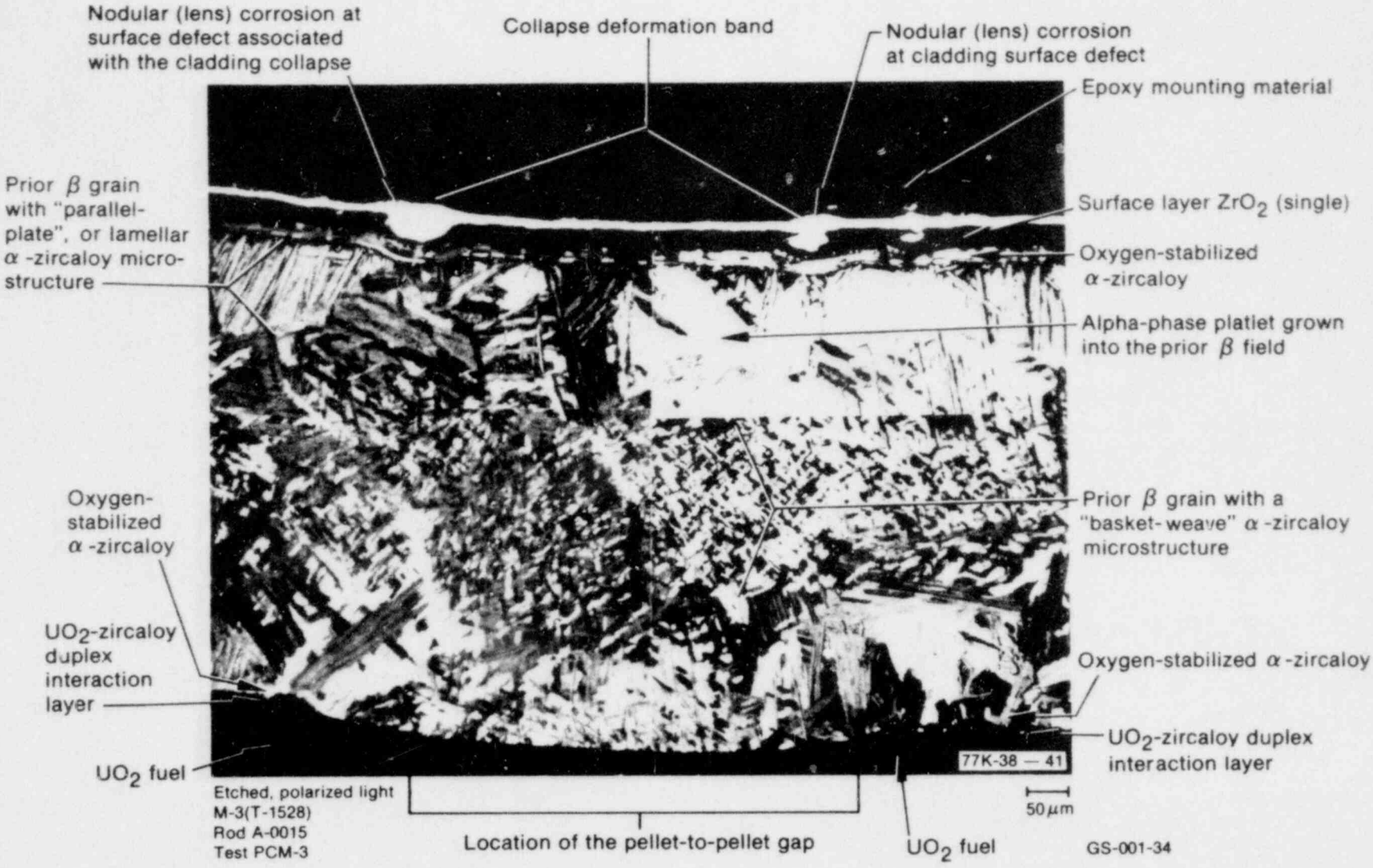

Figure 14. Cladding cross section illustrating oxidized zircaloy microstructures.

formation of oxygen-stabilized alpha-zircaloy and alpha-zircaloy incursions from the parent beta phase. Rods which operated in film boiling experienced severe oxidation on the cladding inside surface in the areas where there was contact between the fuel and cladding. At these locations, two oxygen-stabilized alpha layers formed, sandwiching a thin uranium rich intermetallic layer.

The analysis of the TMI-2 accident and evaluation of fuel rod behavior during the transient indicate that cladding temperatures probably exceeded 2250 K. At such temperatures the zircaloy cladding would rapidly oxidize and become severely embrittled. If sufficiently embrittled, the fuel rods would fragment when quenched, i.e., rewet. A detailed discussion on the chemical interaction between UO_2 and zircaloy when in intimate contact is presented in Section 3.3. In the absence of pellet-cladding contact, oxidation of the inside surface of unruptured cladding proceeds by vapor transport of the oxygen across the fuel-cladding gap, and thin layers of ZrO_2 and α-Zr(O) form.

If the cladding balloons and ruptures, steam will enter the gap and oxidation would proceed on the cladding inside surface in the immediate vicinity of the rupture. Layers of ZrO_2 and oxygen-stabilized alpha zircaloy of approximately the same thickness would form. Oxidation on the inside surface releases hydrogen which may be absorbed by the cladding. The accumulation of hydrogen in the gap from the oxidation process retards the pentrating of steam into the gap and thus limits the oxidation process at the cladding inside surface, except in the immediate vicinity of the rupture. Hydrogen uptake is discussed further in Section 3.2.2.

The zircaloy oxidation reaction proceeds according to the relationship:

$$Zr + 2H_2O \rightarrow ZrO_2 + 2H_2 + \text{Heat} \qquad (1)$$

The kinetics of zircaloy steam oxidation were measured by J. V. Cathcart, et al.,[29] and found to obey a parabolic rate equation between 1255 and 1773 K.

$$\frac{dk}{dt} = \frac{1}{k} A \exp(-B/RT) \quad (2)$$

where

k = the kinetic parameter (eg., weight gain, layer thickness)
t = time (seconds)
A,B = constants
T = temperature (Kelvin)
R = universal gas constant (8.314 J/mole-K).

Equation (2) has been incorporated into MATPRO-11[27] for use with FRAP-T[7] when calculating the oxide thickness, the oxygen-stabilized alpha layer thickness, and the weight gain during high temperature fuel rod transients.

A comparison of calculated oxide thickness versus the square root of time at temperature (isothermal conditions) with measured oxide thickness from various experiments[29] is shown in Figure 15. The uncertainty bands for the data are indicated and, in general, the calculated oxide thicknesses are in excellent agreement with data. Above 1773 K only limited data are available and as yet the model has not been compared against the higher temperature data. Peak cladding temperatures during these experiments are planned to be approximately 2300 K, which is significantly higher than the temperatures for which the model has been verified. It is also possible that the phase change of the zirconium dioxide at about 1850 K causes a discontinuity in the oxidation kinetics with substantial increase in the oxidation rate. However, depending upon the specific transient, the time at temperature between 1773 and 2300 K may be very short and the resultant oxidation could be insignificant.

The oxygen profile in the beta phase zircaloy must be accurately known or calculated to evaluate the cladding embrittlement. The oxygen concentration in the beta phase zircaloy may be determined by

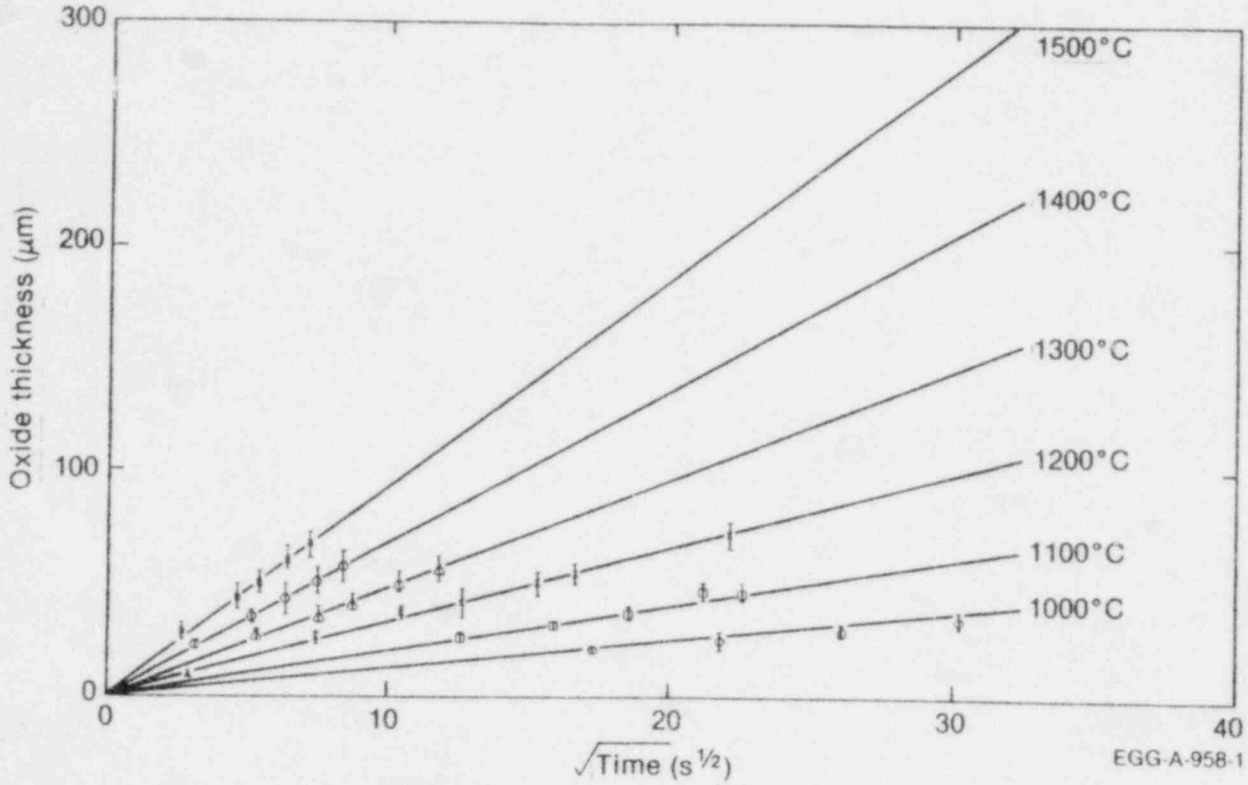

Figure 15. Comparison of calculated (solid lines) and measured ZrO_2 thicknesses for six temperatures, Reference 27.

MATPRO-11, using a finite difference form of Fick's law of diffusion[30]. The diffusion coefficient for oxygen in the β-Zr is expressed as a function of temperature in the form of an Arrhenius equation. The diffusion coefficient has been accurately measured;[31] and the physical system sufficiently satisfies the basic assumptions if (a) the material is homogeneous and isotropic β-Zr and (b) the cladding is isothermal. With the exception of isothermal cladding conditions these conditions are satisified for many transients. Non-isothermal transients have been modeled by Pawel.[32] This model integrates the oxidation over time by breaking the transient into relatively small isothermal steps.

The formation of oxygen-stabilized alpha layers on the cladding inside surface only occurs when there is intimate pellet-cladding contact. The layer thickness is calculated by rearranging and integrating Equation (2). The integrated result is incorporated into the COBILD high temperature oxidation code within MATPRO-11. Hofmann's data[33] provide an extensive basis for this formulation. The formation of the thin uranium-alloy zircaloy layer is not modeled currently because its effect on the thermal and mechanical properties of the cladding is considered negligible.

The calculated oxygen-stabilized alpha layer thicknesses on the cladding surfaces are shown in Figure 16 as a function of cladding temperature and compared with Hofmann's data.[33] The standard deviation for the thickness of the outer of the two inside surface layer, is $\pm$18% for temperatures less than 1600 K, and for the innermost layer is $\pm$16% for temperatures less than 1760 K. The agreement is relatively good, however, the constants A and B, from Equation (2), were derived from the data. The model should be compared, if possible, with the other unrelated data to obtain an independent evaluation. Again, data are only available up to about 1773 K.

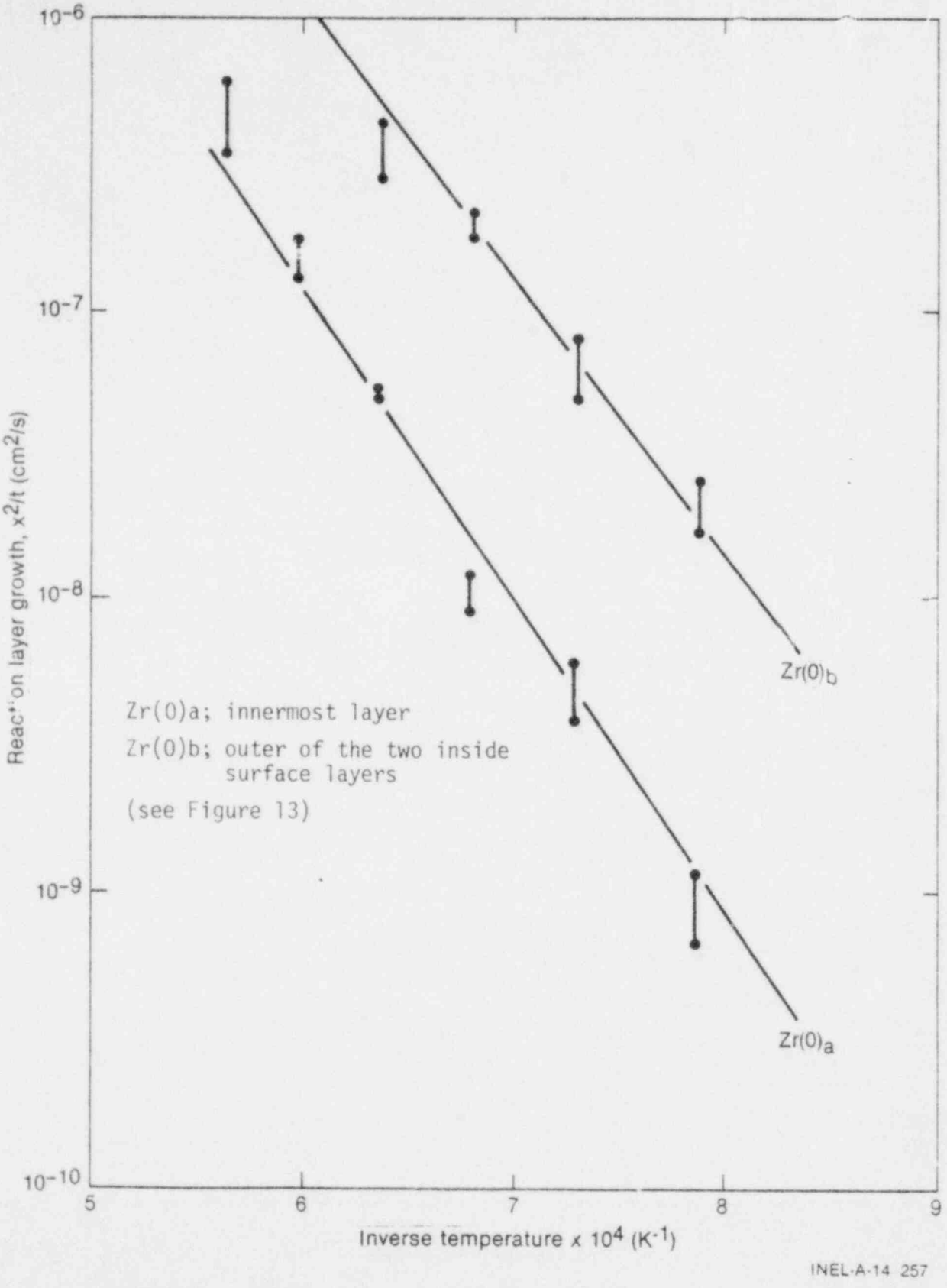

Figure 16. Growth of zircaloy oxide layers as a function of temperature from Hofmann and Politis[30].

Zircaloy oxidation is an exothermic process, and the heat of reaction may be significant during a small break LOCA transient, and also during the planned tests. The oxidation heating rate is modeled in MATPRO-11 as a combination of two factors; (a) the heat of reaction from converting zircaloy to zircaloy dioxide and, (b) the heat of solution of the dissolved oxygen in the base metal beneath the oxide layer. The heat generation per unit length is calculated from an algebraic equation relating the linear heat generation to the heat of reaction, changes in the effective oxide layer thickness, and time.

A plot of the calculated linear power generation as a function of the initial oxide layer thickness and reaction temperature (up to 1773 K) is shown in Figure 17. For thin oxide layers the linear power generation is calculated to increase very rapidly with increasing temperature. However, above about 10 μm of oxide thickness the rate of change of power with reaction temperature decreases significantly. Depending upon the temperature history during a small break LOCA transient, the relative influence on the overall fuel rod thermal response can vary substantially as a result of the heat of oxidation and oxygen solution. If cladding temperatures were to rise rapidly up to the temperature range of 1300 to 1600 K, before significant oxidation could occur, then the heat generation from oxidation may be sufficient to produce rapid cladding heating to temperatures above the zircaloy melting temperature. Conversely, if the surface heat transfer is sufficient to keep cladding temperatures relatively low until a significant oxide layer has formed, the oxidation heat generation could be relatively insignificant throughout the transient.

2.2 Hydrogen Uptake and Precipitation of Hydrides

Oxidation of the inner surface of ruptured cladding releases two moles of hydrogen for every mole of oxygen reacted. This free hydrogen diffuses throughout the fuel/cladding gap, and depending primarily upon cladding temperature and the hydrogen partial pressure, hydrogen will be absorbed by the zircaloy cladding.[34] In the high

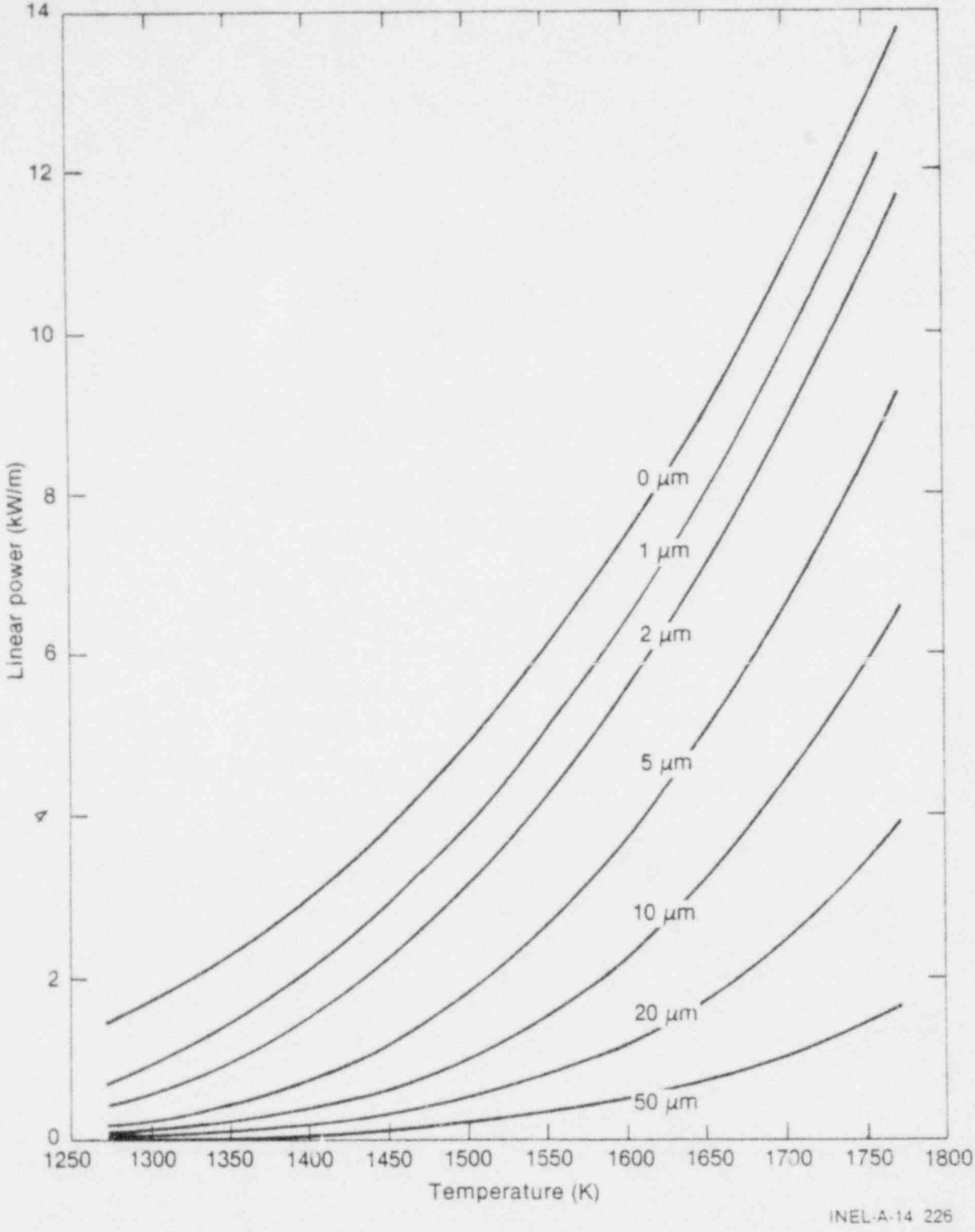

Figure 17. Linear power generation due to oxidation for a rod of initial diameter 1.25×10^{-2} m as a function of initial oxide thickness, Reference 27.

temperature (> 800 K) regions of the cladding, the dissolved hydrogen concentration will probably not exceed a few hundred ppm. However, in the lower temperature regions, probably near the bottom of the fuel rod, the dissolution of hydrogen could be significant with concentration levels possibly reaching several thousand ppm. When the dissolved hydrogen concentration exceeds the terminal solid solubility, precipitation of zirconium hydrides would occur at grain boundaries. The terminal solubility limit would probably not be exceeded except during quench when temperatures drop below 700 K. Precipitation of hydrides degrades the cladding structure, and if severe, can cause a complete breakdown locally of the cladding structure.

Figure 18 shows a typical example of hydriding in the alpha plus beta two-phase region and prior beta matrix from the PBF tests.[28] The hydrogen pickup that can occur under these circumstances is illustrated. The reoriented hydrides which precipitate during beta quenching may induce crack initiation and propagation during cooldown of oxidized cladding as shown in Figure 19.

Hydride precipitation would, in general, be inconsequential during small break LOCA transients because of the extensive damage that has probably already occurred to the fuel rod. However, cladding embrittlement due to hydriding could further contribute to fuel rod damage, primarily in regions outside the oxidation zone and it could be of consequence during post irradiation handling of test rods.

2.3 Zircaloy Cladding Embrittlement and Fragmentation

Zircaloy cladding is embrittled by oxidation, oxygen absorption, and, at low temperatures, by hydriding. Zircaloy oxidation and oxygen absorption follow a parabolic rate law as oxygen diffusion introduces an oxygen gradient beneath the oxide layer. The extent of the oxidizing reaction, and hence, embrittlement is primarily a function of temperature and time. Thus, the cladding ductility at a given temperature decreases with oxidation.

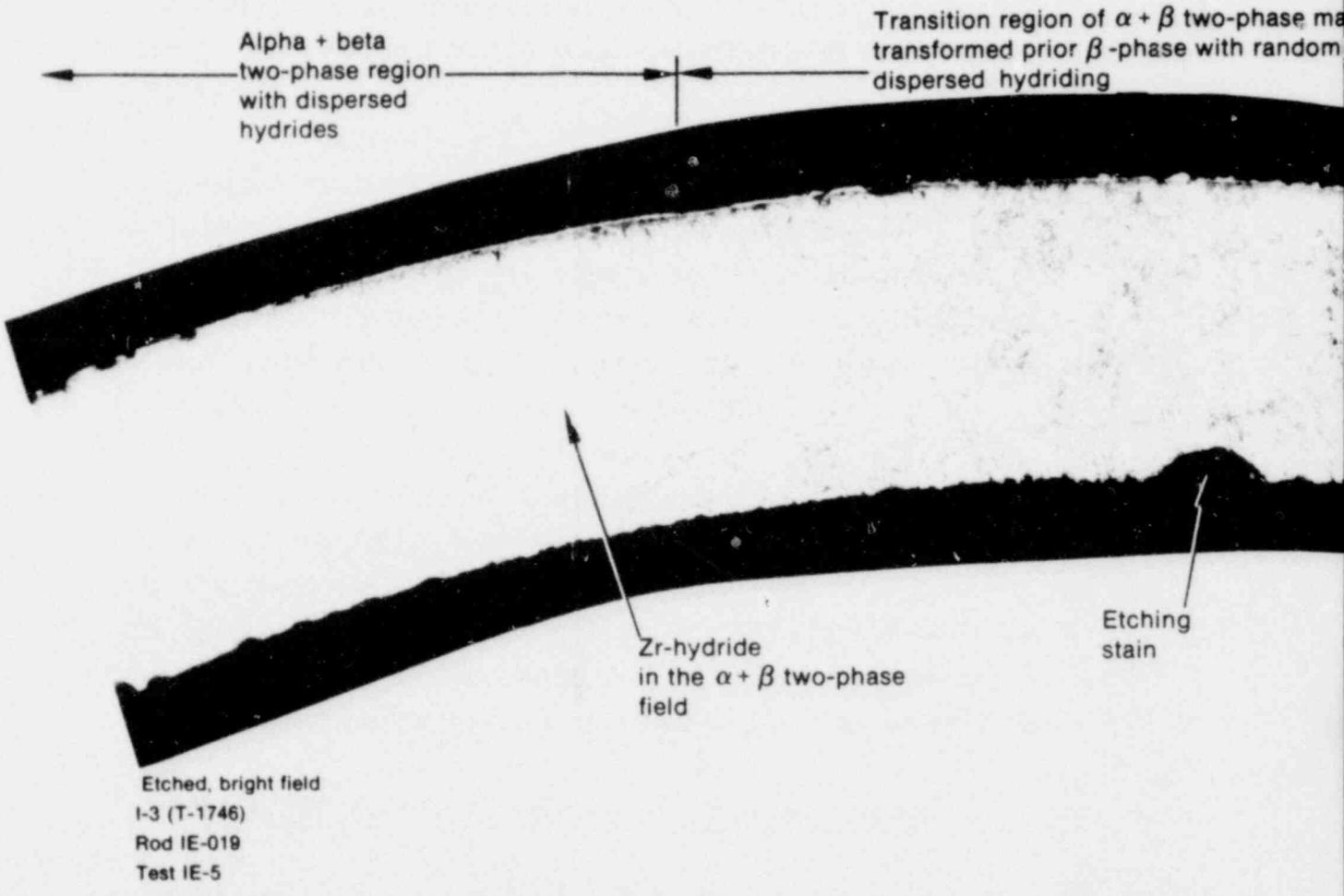

Figure 18. Transition zone in partially oxidized cladding showing a chang
phase with grain boundary alpha along beta grains.

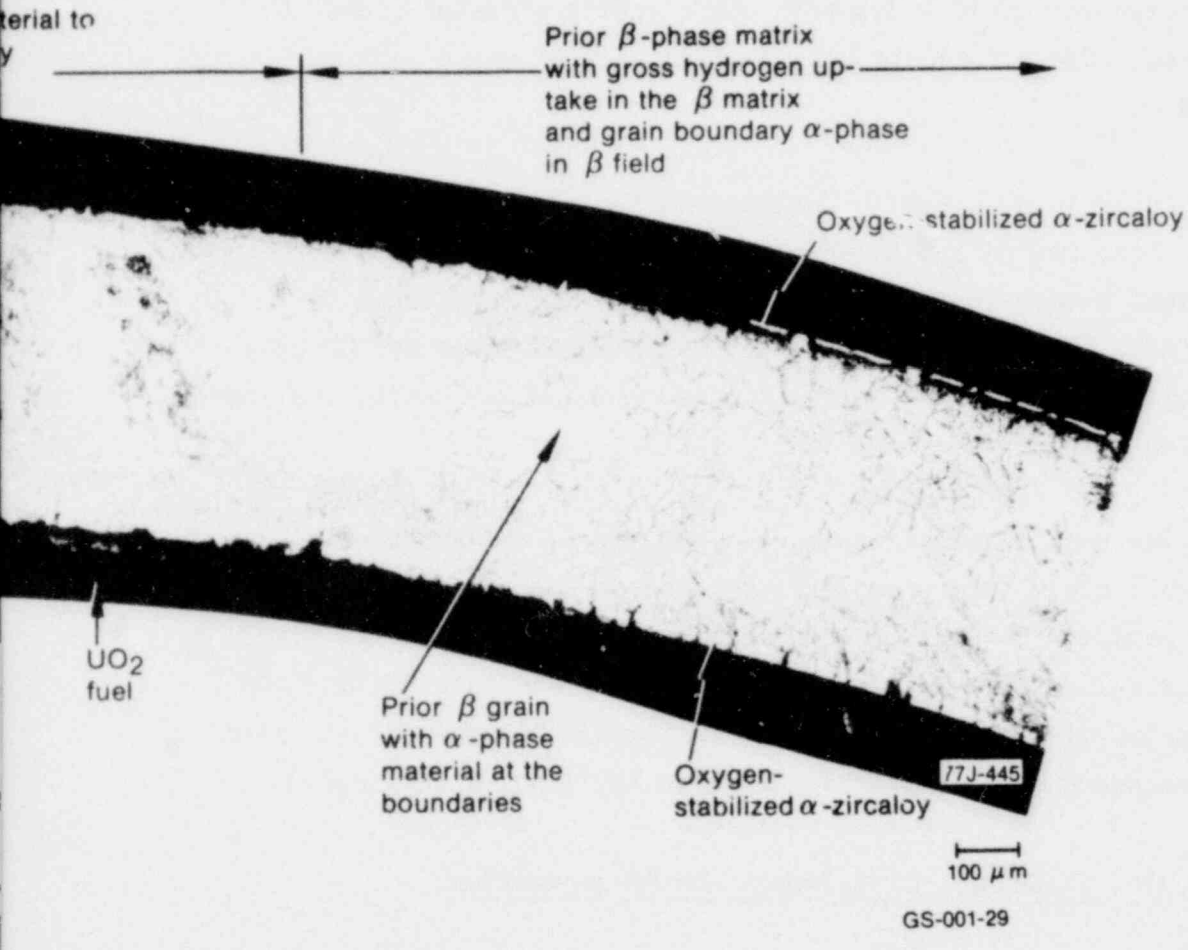

e from alpha plus beta two-phase material to prior beta

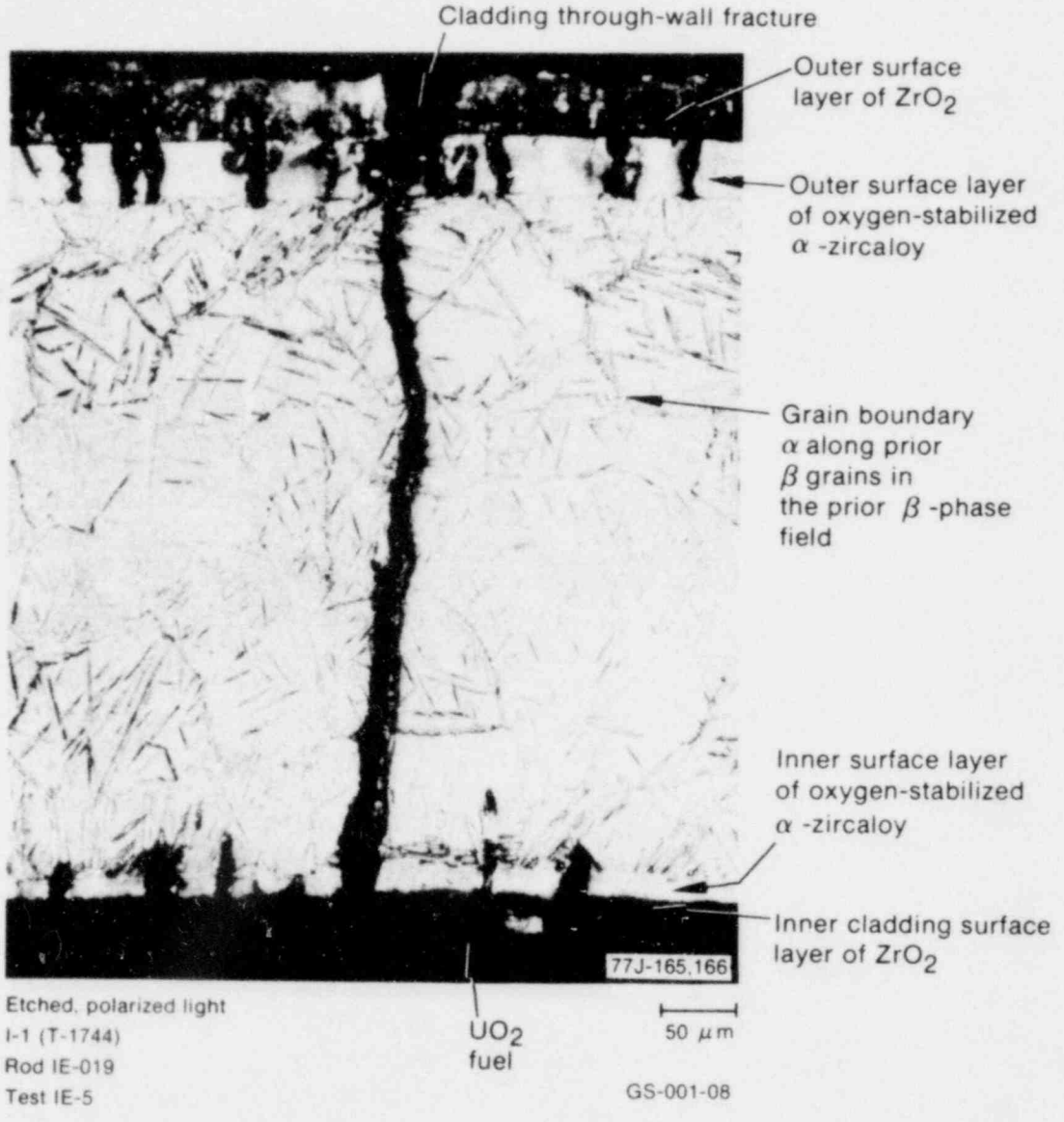

Figure 19. Cladding fracture with grain boundary alpha along prior beta grains and hydride needles (~ 1020 ppm H_2) within beta grains.

As the cladding oxidizes and oxides form on the surface, large fractions of the beta material may be converted into α-Zr(O), and oxygen also diffuses into the untransformed beta meterial. The untransformed beta material remains somewhat ductile, depending upon the dissolved oxygen concentration and temperature. When the transient is terminated and cladding temperatures decrease, the cladding becomes brittle at a given temperature depending upon the dissolved oxygen concentration and cooling rate. At room temperature, which is the applicable temperature for most embrittlement criteria, the mechanical properties of oxidized cladding depend upon (a) the extent of prior beta, (b) the beta phase oxygen concentration, and (c) the presence of alpha incursions.

The embrittlement criteria which have been proposed are based upon the following: fraction of wall thickness which remains in the beta phase;[35] impact energy required to cause a brittle fracture;[36] and maximum oxygen content in the beta phase.[37-39] The criteria based upon the oxygen content in the beta phase zircaloy were selected for MATPRO-11.[27] Pawel[38] suggested the values of 0.7 wt% for the average oxygen concentration in the beta phase, together with a 95% saturation condition as the critical criteria for embrittlement at room temperature, where embrittlement is defined as fracture with no plastic deformation. Reymann[27] modified these criteria slightly to be 0.65 wt% and 90%, respectively. It was further stipulated that the cooling rate must be at least 100 K/sec, and that the cladding would be considered fully embrittled if the temperature ever reached 1700 K without regard for time at temperature. The criterion of no more than 0.65 wt% oxygen concentration is required because the ductility of beta phase zircaloy decreases with increasing dissolved oxygen concentration which implies a critical concentration limit, at temperature, in weight percent to induce complete embrittlement. Physically, the percent saturation limit of 95% is reasonable, because brittle oxygen-stabilized alpha precipitates form, generally as incursions from the alpha layer extending into the beta phase, as the oxygen content of beta zircaloy approaches saturation. The presence of oxygen-stabilized alpha

incursions is always associated with a loss of cladding ductility. These incursions may also form during cooling because as the temperature decreases so does the oxygen solubility, often making the beta phase super-saturated with oxygen.

Comparisons of the embrittlement criteria postulated by Pawel[38] and in MATPRO-11 with data from PBF[28] and ORNL[33] are shown in Figures 20 and 21, respectively. The film boiling times for all the data associated with rod fracture, except three, fall above the limiting conditions for embrittlement, in Figure 20, as defined by Pawel. The three fractures which do not satisfy either embrittlement criteria were from PBF rods which were operated in film boiling with breached cladding. Subsequent metallographic examination revealed that the cladding had sustained significant hydriding which substantially reduced the cladding ductility. A significant number of the rods fall above the embrittlement criteria without suffering cladding fracture. Two of these rods (Rods IE-008 and IE-020) were subjected to ring compression ductility tests and indicated 2% and 0% ductility, respectively. These results indicate that rods which exceeded the embrittlement criteria but did not fail have little, if any ductility.

In MATPRO-11 instantaneous embirttlement is assumed to occur above 1700 K since all but one of the rods which attained temperatures above 1700 K were brittle, and the criteria as defined are valid only for room temperature embrittlement. Hobson and Rittenhouse[37] showed that oxidized zircaloy is brittle also at elevated temperatures. Specimen ductility is shown in Figure 22 as a function of deformation temperature and the fraction of wall thickness of oxidized tubes consisting of transformed β-phase zircaloy. The figure is subdivided into three regions: the region to the right, characterized by open circles represents ductile specimens with relatively low oxidation. The central region, bounded by the two dashed lines, represents specimens which were moderately oxidized that fractured but only after some plastic strain. The left hand region, represents highly oxidized specimens which fractured without detectable plastic deformation. The

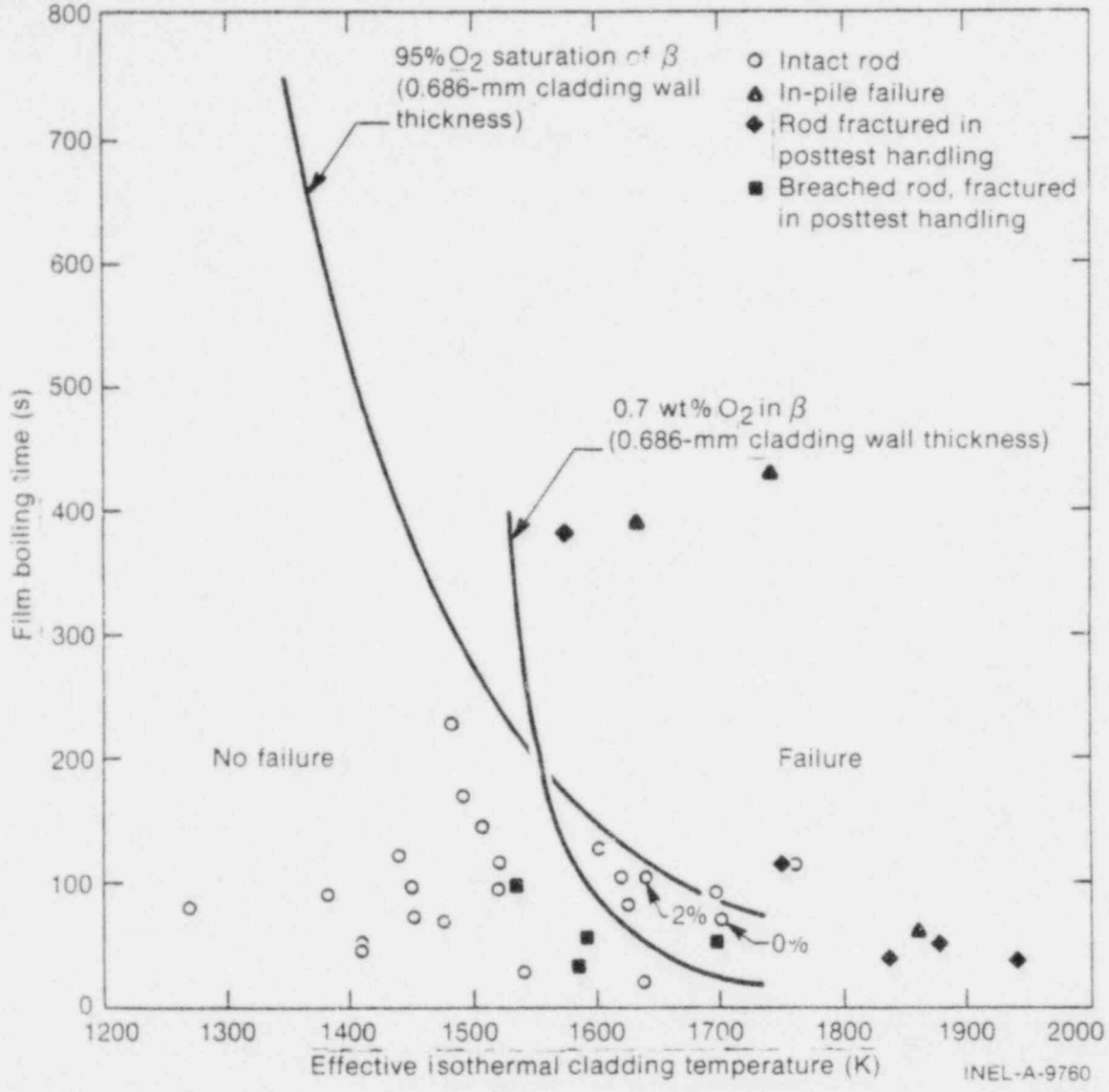

Figure 20. Fracture map for fuel rods tested under power cooling mismatch conditions, Reference 31.

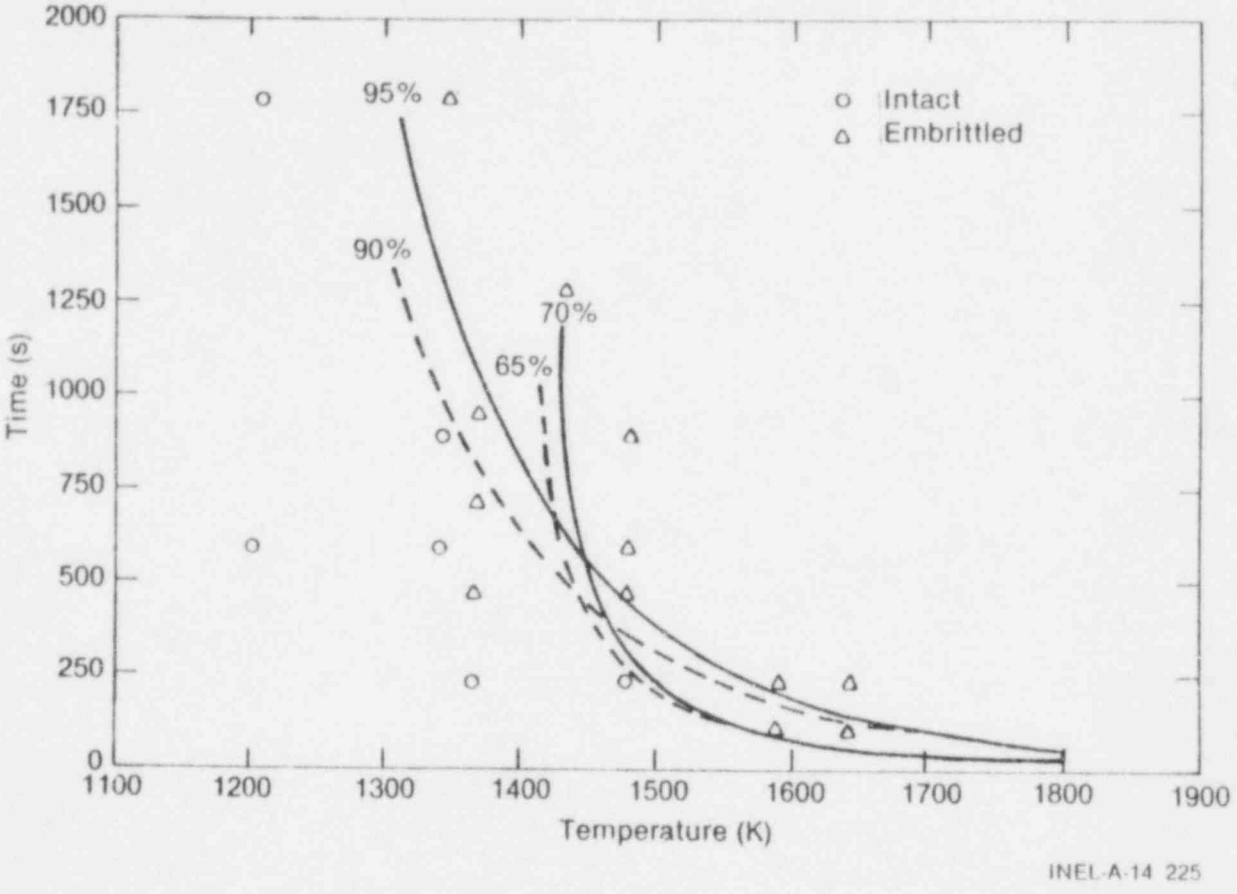

Figure 21. Hodson-Rittenhouse[34] isothermal data for the fast cooled cladding compared with the 0.65 and 0.70 wt% and the 90 and 95% filled criteria.

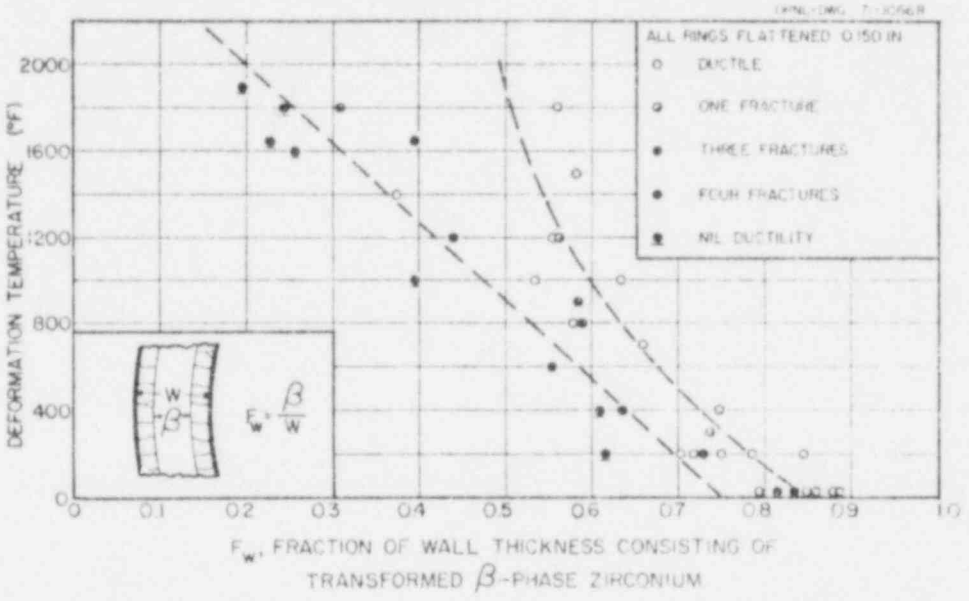

Figure 22. Specimen ductility as a function of deformation temperature and fraction of wall thickness (F_W) consisting of transformed β-phase.

dashed line separating the zero-ductility region from the partial ductility region is independent of the deformation imposed and therefore defines the zero-ductility temperature of the cladding as a function of microstructure and deformation temperature.

The implied functional relationship between cladding ductility, deformation temperature and microstructure is critical with respect to understanding the fracture characteristics of a fuel rod during quench and rewet. The transition from ductile to brittle cladding implies that as fuel rods are quenched, the fuel rods may fracture before the rewet temperature is reached. Also, fuel rod fragment size may vary with embrittlement and the quench front temperature gradient. Rewetting generally occurs at approximately 700 to 800 K (800 to 980 F), and the fraction of wall thickness consisting of transformed β-phase zircaloy which corresponds to nil ductility at this temperature is about 0.5 compared with about 0.72 at room temperature, (see Figure 22). Therefore, if sufficient oxidation occurs, cladding embrittlement can occur at elevated temperatures in these tests.

Hobson and Rittenhouse[37] proposed the plots, shown in Figures 23 and 24, of total ductility and nil ductility temperatures as a function of isothermal steam exposure followed by a rapid cooldown. The data in these figures extend only to 1300 K and are not amenable to extrapolation to temperatures of 2300 K.

Chung and Kassner[40] recently proposed an embrittlement criterion specifically designed to define the cladding conditions which would withstand thermal shock from quench and rewet. This criterion is:

> The calculated thickness of the cladding with $\leq$0.9 wt% oxygen, based on the average wall thickness at any axial location, shall be greater than 0.1 mm.

Therefore, cladding fragmentation would be expected if the wt% oxygen was greater than 0.9, or if the wall thickness, with an oxygen concentration $\leq$ 0.9 wt% was less than or equal to 0.1 mm.

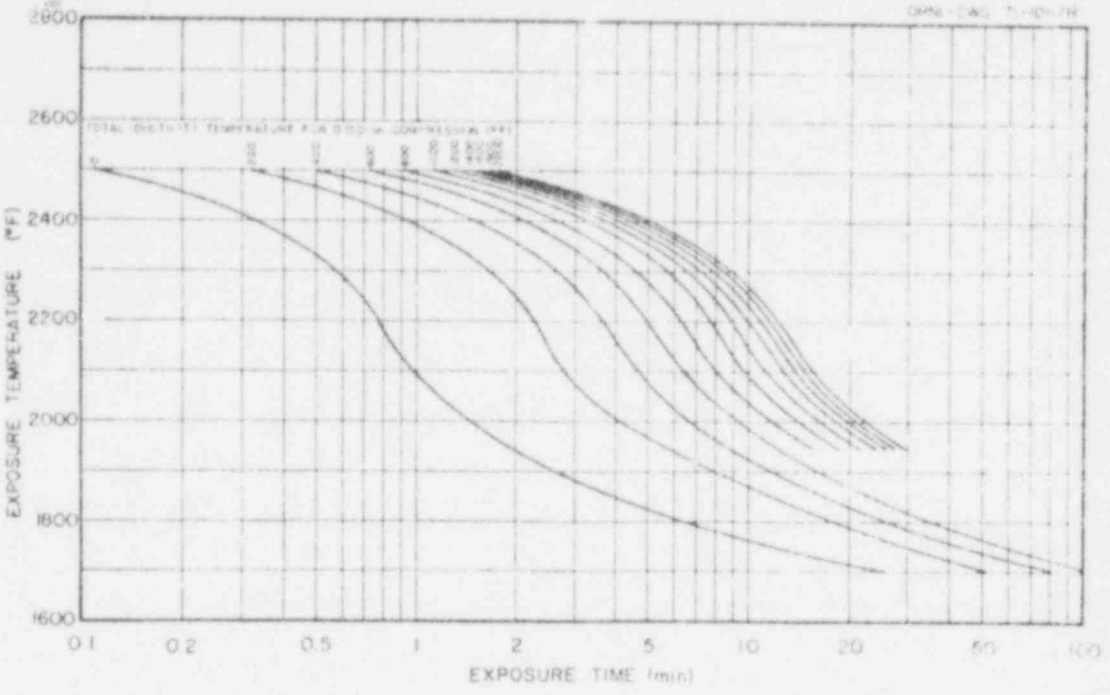

Figure 23. Exposure temperature versus exposure time, in steam, with the curves drawn to show temperatures above which the ring specimens were ductile under diametral impact strains of 0.150 in, Reference 34.

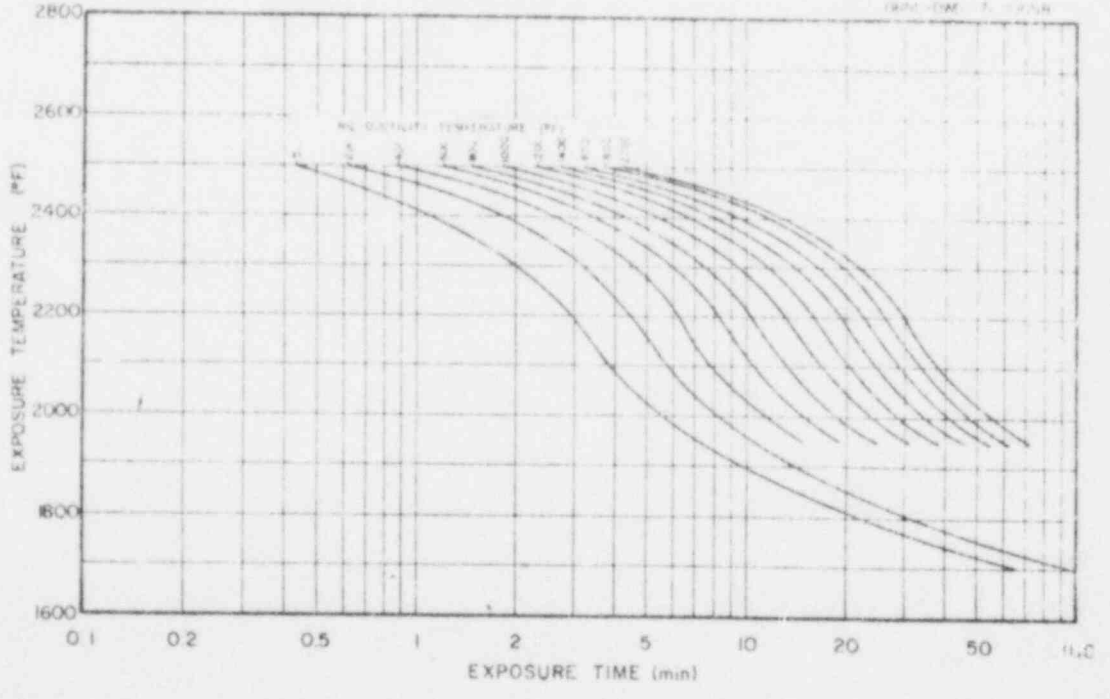

Figure 24. Figure similar to Figure 23, but with curves drawn to show temperature below which the ring specimens had no ductility under impact loading, Reference 34.

Extensive breakup and fragmentation of three rods have occurred during PBF PCM tests.[41,42] Two rods failed during film boiling, and the rods suffered massive breakup (i.e. fragmentation of the fuel and cladding) when the tests were quenched. The other rod failed at rewet after 5.2 minutes of film boiling. The cladding on the rod which failed at 5.2 minutes fractured and fragmented extensively; however, little fuel was lost. The fuel fragments remaining in the flow shroud from test PCM-1[41], were almost equally divided between particles of about 0.04 and 0.2 mm mean diameter, and the fuel rods from test PCM-5[42] primarily fragmented into particles of 0.2 mm or greater mean diameter. For both tests, the cladding in the fragmented zone had totally reacted, and was either all zirconium dioxide or a combination of zirconium dioxide and oxygen stablized alpha zircaloy. Peak temperatures during PCM-1 were greater than 2100 K, whereas during PCM-5 peak cladding temperatures did not exceed 1900 K. Although the evidence is not conclusive, this may be indicative that fuel rod fragmentation varies with temperature and probably oxidation of both fuel and cladding.

During test PCM-1 a large fraction of the fuel desintered to approximately grain size particles when the fuel was quenched. Posttest metallurgical examination of fuel rods indicated that only those rods which operated at temperatures greater than 1900 K in the unrestructured zone experienced grain boundary separation. At such elevated temperatures the UO_2 grain boundary strength in tension is essentially zero, such that intergrannular failure can be expected from thermal stresses generated during fuel rod quench and rewet. A threshold temperature of approximately 1900 K for extensive grain boundary fracture was assessed[43] based upon the equicohesive temperature for UO_2. Postirradiation examination of the fuel rod from test PCM-1 showed extensive oxidation of UO_2 to U_4O_9. Steam oxidation of the UO_2 is observed to initiate preferentially along grain boundaries which would tend to weaken the boundaries and enhance fuel fragmentation upon quenching.

This test program will be structured to preserve the bundle from selected tests with highly oxidized and embrittled test rods and to fragment the bundle during the remaining tests to evaluate the heat transfer characteristics of the resulting rubble bed.

Different embrittlement criteria for slow cooled cladding, which is how tests must be terminated to preserve the fuel rod structure, are stipulated in MATPRO-11. For cladding cooldown rates less than 100 K/s, the cladding is considered embrittled if the prior beta phase thickness with 1% oxygen by weight or more is less than 0.3 mm. A comparison of the Argonne data[39,44,45] with slow cooled cladding (5 K/s) using this criterion is shown in Figure 25. In general, these data support the criterion. However, there are trends which may indicate that the minimum thickness may be less than 0.3 mm at the lower temperatures, and greater than 0.3 mm at temperatures greater than approximately 1600 K. At temperatures below about 1400 K more than half of the specimens, 13 vs 11, with less than 0.3 mm of zircaloy thickness containing more than 1% oxygen are intact, whereas at temperatures greater than about 1600 K there were three specimens that failed above the 0.3 mm criterion. The effect of slow cooling and this criterion must be considered when handling the intact bundles, and when evaluating the data from the metallographic examination.

3. Fuel/Cladding Interaction

At temperatures above about 1525 K, a molten uranium/zirconium mixture may form. Beta-phase zircaloy melts at approximately 2123 K, and α-Zr(O) melts at approximately 2245 K. The molten α-Zr(O) will dissolve the UO_2 if there is intimate contact. If this molten material were generated in sufficient quantity, severe blockage of coolant flow channels could occur due to relocation and freezing of the liquid.

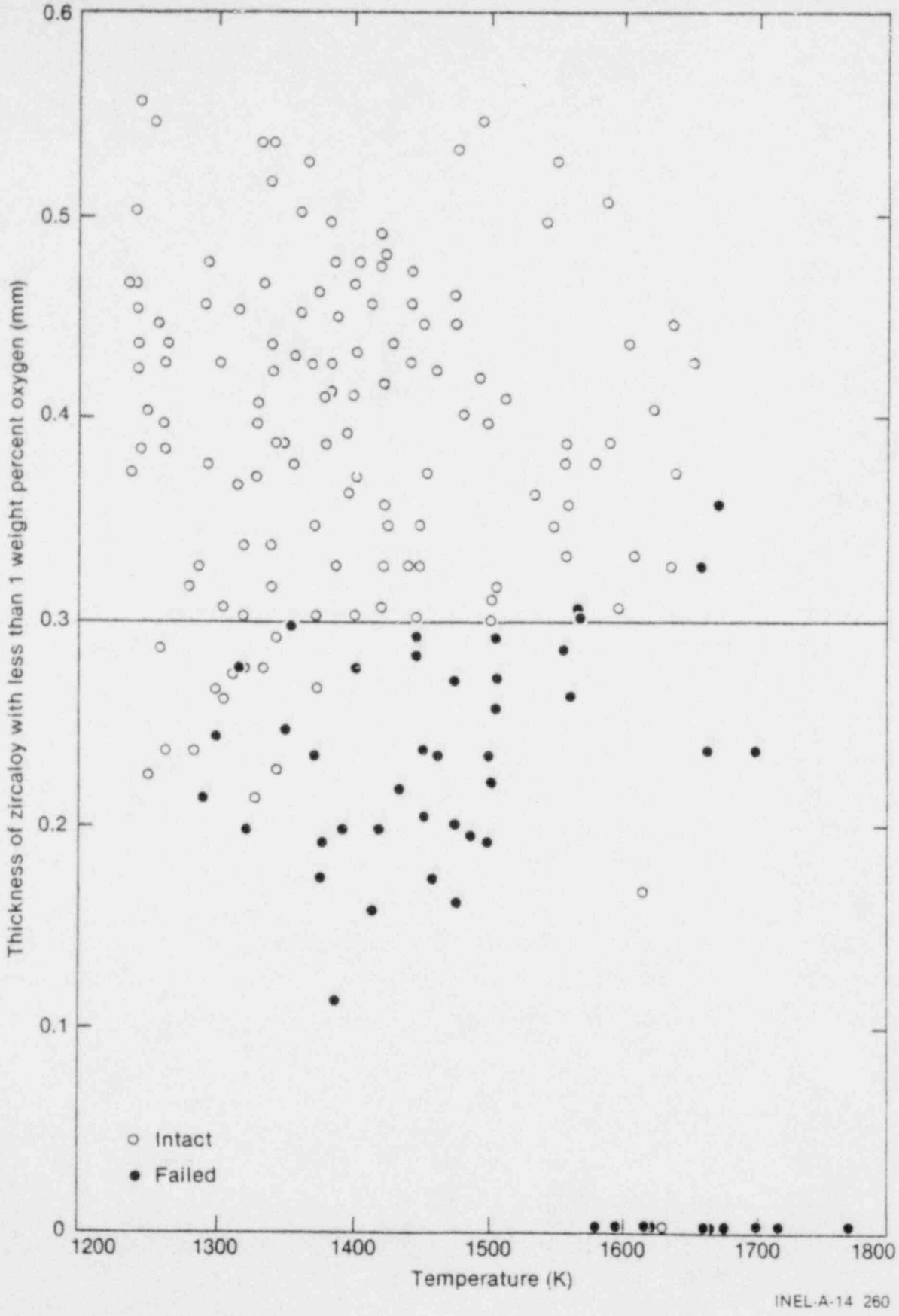

Figure 25. Comparison of the ANL data for slow cooled cladding with the slow cooled embrittlement criterion, Reference 27.

The equilibrium thermodynamics of the ternary uranium-zirconium-oxygen system and the quasi-binary α-Zr(O)--UO_2 system are reviewed in Section 3.1. Results from the KfK out-of-pile core meltdown experiments and the in-pile PBF test PCM-1 are then reviewed in Section 3.2.

3.1 Zircaloy-UO_2 Chemical Interaction

The equilibrium thermodynamics of the ternary uranium-zirconium-oxygen (U-Zr-O) system have been evaluated by Politis,[46] Hofmann,[47] and Hofmann and Politis[33]. This work evaluated the ternary phase field boundaries over a wide range of composition and temperature.

Isothermal ternary phase diagrams for the uranium-zirconium-oxygen system at 1273, 1773 and 2273 K are shown in Figure 26. Results from Hofmann's and Politis' investigations[33,46,47] indicate that UO_2 and Zr react to produce α-Zr(O) containing 30 percent oxygen. A solid solution (δ-U, β-Zr) may also coexist with the UO_2/α-Zr(O) system; and at 1273 K, as shown in Figure 26.a, no liquid is present. At temperatures less than 1273 K, a thin zirconium dioxide layer on the cladding inside surface completely inhibited the UO_2/Zr reaction[33]. However, at temperatures greater than 1273 K, a thin ZrO_2 layer was rapidly dissolved by the β-phase zirconium forming α-Zr(O) and the uranium/zirconium reaction proceeded. The growth of the reaction layers followed a parabolic rate law, and the diffusion of oxygen into the β-phase zirconium was determined to be the rate limiting process.

At 1773 K, the phase diagram for the ternary system changes substantially as shown in Figure 26.b. The (δ-U, β-Zr) alloy begins to melt at approximately 1300 K, and at 1773 K some uranium rich liquid is present throughout much of the phase diagram except at the highest oxygen and zirconium concentrations.

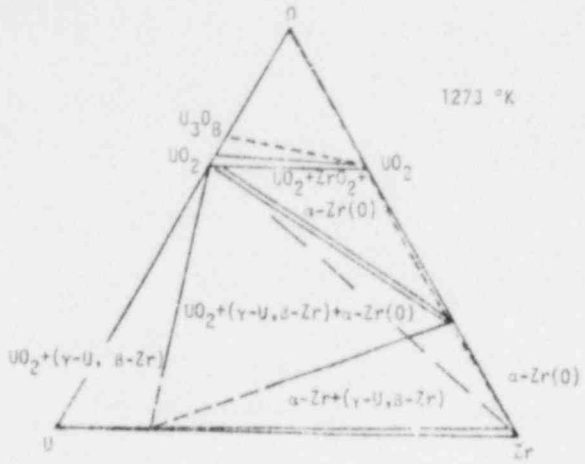

Adjustment of equilibrium after 144 hours.

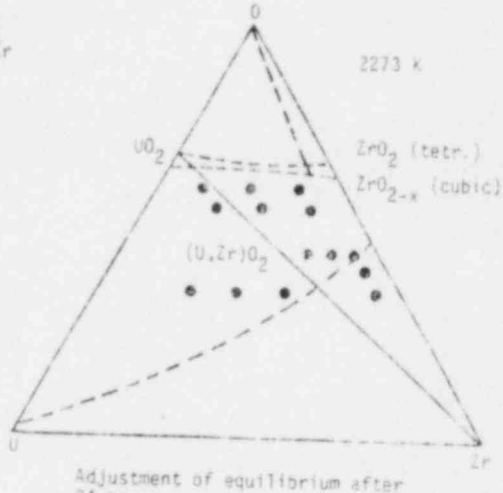

Adjustment of equilibrium after 24 hours.

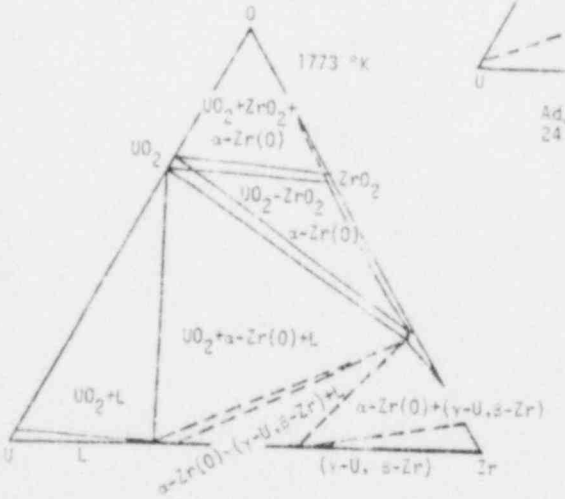

Adjustment of equilibrium after 16 hours.

Figure 26. Isothermal phase diagrams for the ternary U-Zr-O system for temperatures of 1273 (A), 1773 (B), and 2273 K (C), Reference 45.

At 2273 K, much of the complexity of the system has disappeared, as shown in Figure 26.c. A liquid exists at low oxygen concentrations. With increasing oxygen concentrations, uranium zirconium dioxide formed until gradually the solid oxide became a continuous phase encasing the liquid. At the highest oxygen concentrations, UO_2 and ZrO_2 are the equilibrium phases.

The melt diagram for the uranium-zirconium-oxygen system is shown in Figure 27. Melt temperatures generally increase with increasing concentrations of both zirconium and oxygen. Zirconium has a higher melt temperature than uranium, and the presence of oxygen tends to further increase the melting temperature.

Molten α-Zr(O) will dissolve UO_2 if in contact. This dissolution reaction is shown in the pseudo-binary phase diagram between UO_2 and α-Zr(O), Figure 28. The eutectic conditions are approximately 2100 K and 5 mol% UO_2. The solubility of UO_2 increases with temperature to 23 mol% at 2650 K. Also at this temperature a second liquid is formed with a solubility of 85 mol% UO_2. It is evident from this diagram that a large volume of UO_2 could be dissolved by molten α-Zr(O) given sufficient time and provided there was intimate contact. The kinetics of this dissolution process are not well understood and significant work is required in this area before the process can be expressed analytically.

3.2 Experimental Results

A detailed out-of-pile experimental investigation on the initial phase of a core meltdown was conducted by KfK.[48-52] The primary objective of the investigation was to determine how the different fuel element components; UO_2 pellets, zircaloy cladding, inconel-spacers, guide tubes and control rods influence the fuel rod and core meltdown.

3.2.1 Review of KfK Single Rod Tests.[48] Simulated fuel rods electrically heated at different rates in helium are shown in Figure 29.a. For all rods, the beginning of melting was measured at

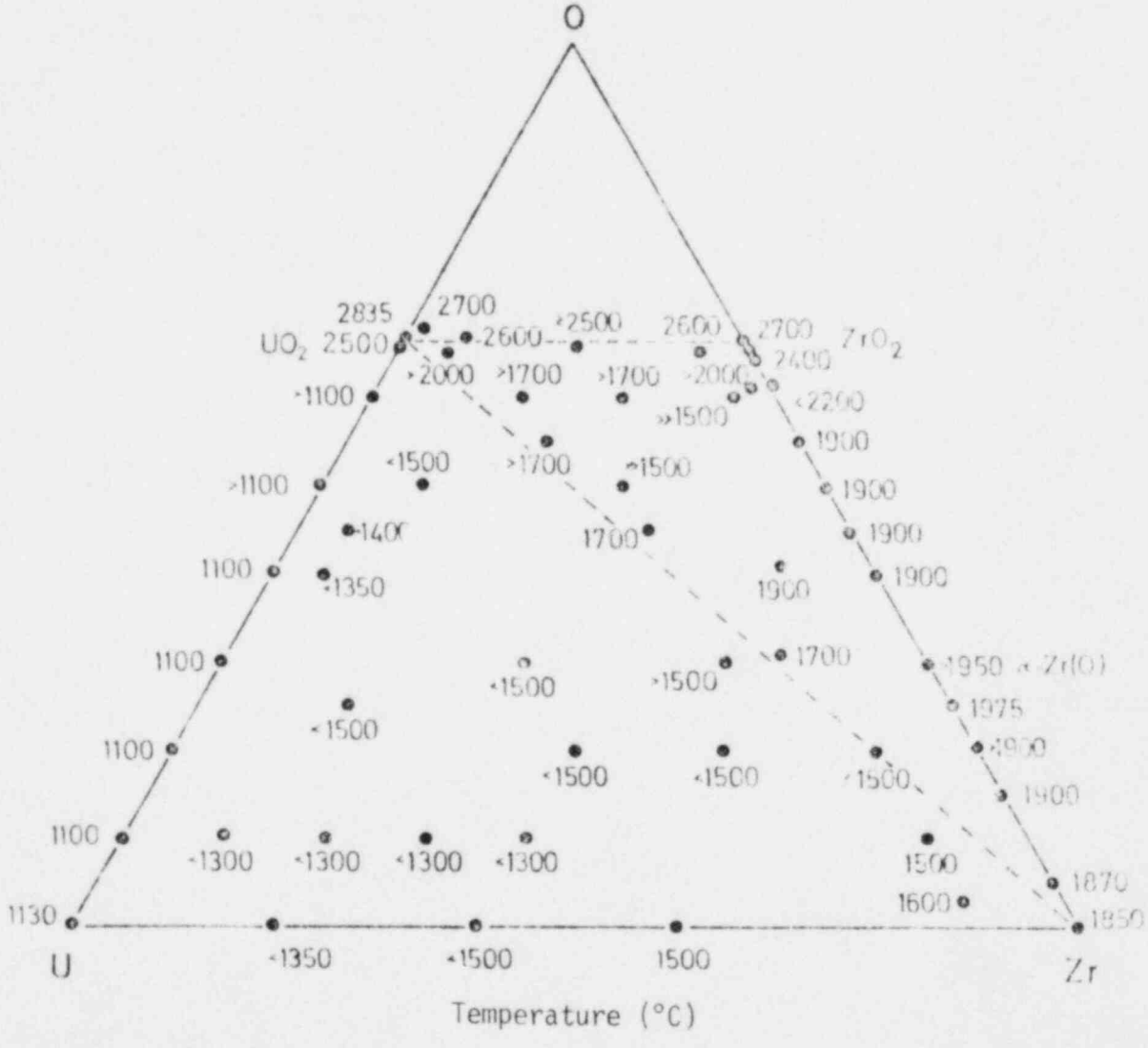

Figure 27. Melting temperatures in the U-Zr-O ternary system, Reference 58.

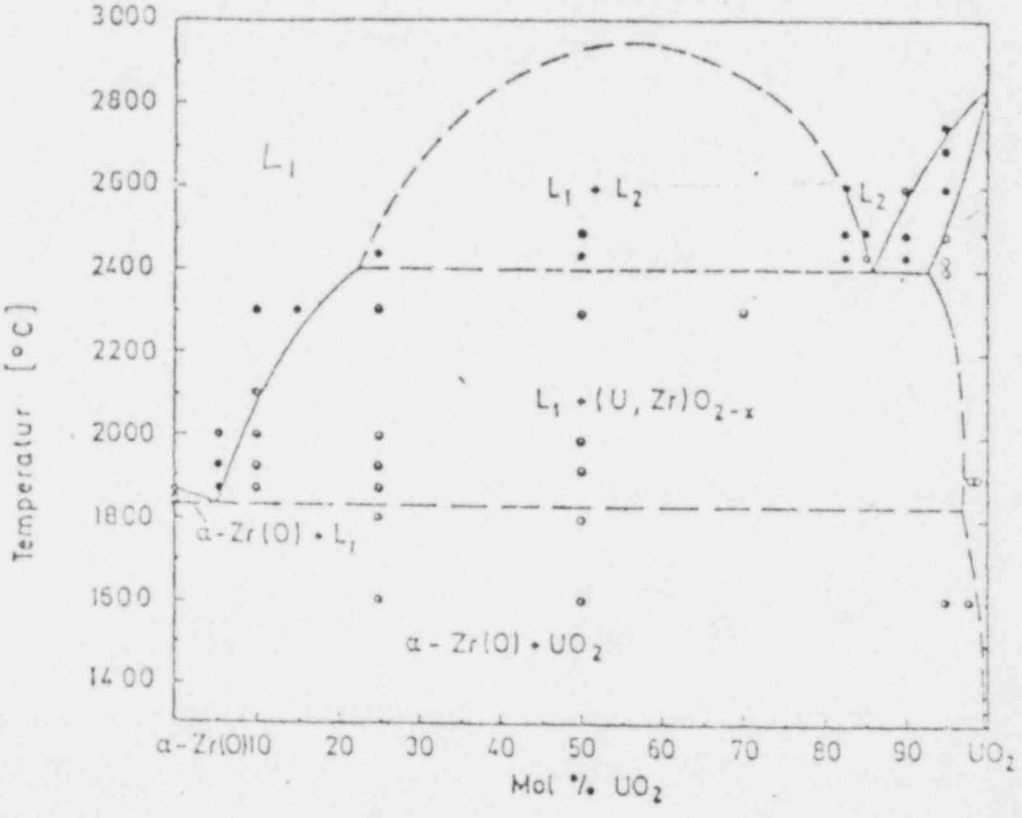

Figure 28. Equilibrium psudo binary-phase diagram between UO_2 and α-Zr(O), Reference 58.

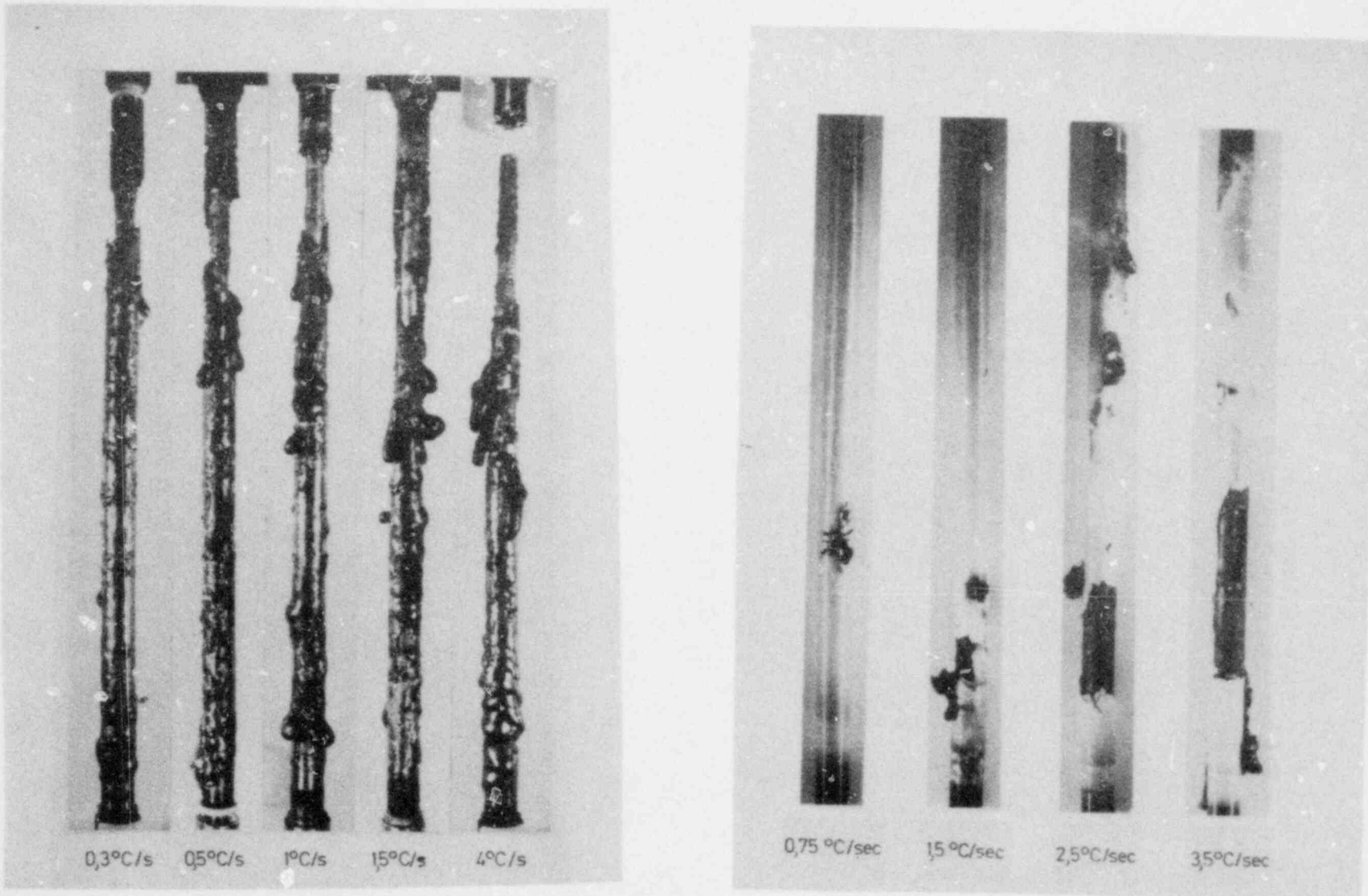

Figure 29. Rods heated in He (a) and steam (b) at different heatup rates, Reference 47.

2123 K, the melt temperature for β-phase zirconium. The molten material from the upper regions moved in smooth, relatively large droplets to lower regions on the rod. The meltdown was a slow continuous process with the melt always in contact with the rod. Variations in heating rate did not significantly influence the final configuration, only the rate of meltdown.

A significantly different meltdown behavior was observed in a steam environment, Figure 29.b. The oxide layer thickness formed during heatup at the different heating rates (from 0.75 to 3.5 K/s) up to 2273K are shown at the upper right of each rod in Figure 30.b. The oxide thickness decreased with increasing heatup rate because of the reduced time at temperature, and the extent of outside oxidation ranged from about 80 percent to less than 40 percent of the original wall thickness. During heatup this oxide layer remained intact up to at least 2173 K. Then small holes formed through which the melt was violently ejected. The oxide layers remained intact at temperature except for the small defects. The formation of cracks and spalling of the ZrO_2 layers occurred during the cooldown.

The melting behavior of rods with inconel spacer in helium and steam atmospheres is shown in Figures 30.a and 30.b. The tests were performed at identical (but undefined) heatup rates. It is apparent that the presence of steam and the subsequent oxidation of the cladding outside surface had a similar affect on the test rod meltdown behavior as described in the preceeding paragraph. That is, the degree of molten material at the test rod surface is relatively insignificant compared with that observed for the test rods in the inert atmosphere.

3.2.2 Review of PBF PCM-1 Test.[53] The fuel rod thermal and mechanical transient that occurred during the PBF test PCM-1 is pertinent to the understanding of cladding melting and the Zr-UO_2 reaction. Test PCM-1 was performed in-pile at initial PWR thermal-hydraulic conditions of pressure and temperature. Following operation at low power levels for preconditioning and power calibration purposes, the peak power of the single fuel rod was

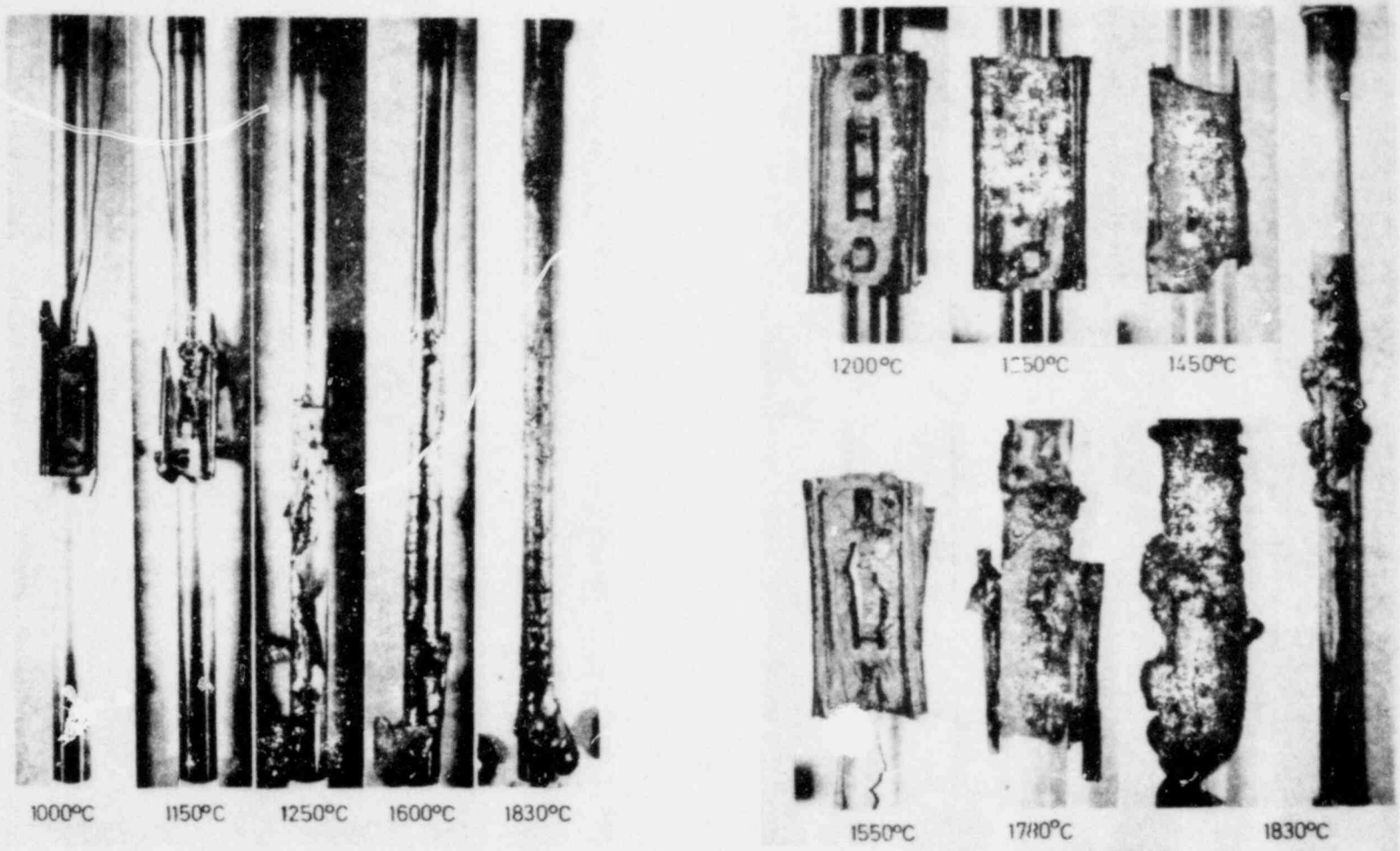

Figure 30. Melting behavior of rods with spacers heated to different maximum temperatures in He (a) and steam (b), Reference 47.

increased to 60 kw/m to initiate film boiling and held constant for 280 seconds from the start of the ramp. The power was then raised to 78 kw/m and held constant for an additional 640 seconds. The peak cladding temperature was estimated from posttest examination to be at least 2100K. Instrumentation indicated initial cladding failure at 520 seconds and severe rod breakup at shutdown. Posttest examination indicated that cladding failure was due to embrittlement with significant cladding breakup during film boiling operation. Fuel fragmentation occurred primarily during quenching at test shutdown.

Examples of the Test PCM-1 zircaloy cladding structure that was oxidized by steam from the outside and reacted with the UO_2 fuel on the inside are shown in Figure 31. The cladding samples shown in Figure 31 are from the same elevation (0.67 m), but different angular orientations. A 220 K circumferential temperature difference existed at this elevation. The microstructures at 0.67 m and above are typical of an unfailed fuel rod with no exposure of the cladding inside surface to steam. The absence of steam exposure at 0.67 m was due to cladding collapse onto the fuel column which sealed the top portion of the rod above the fracture at 0.63 m and isolated the plenum from the failure location. No evidence of cladding melting was apparent at elevations above 0.67 m. Microprobe examination of the fuel-cladding reaction layers indicate that as the oxygen-stabilized alpha layers from the inside and outside of the cladding grew to meet in the center, the U-rich and Zr-rich reaction layers became dispersed within the inner alpha zircaloy layer.

The metallography of the cladding at the 0.30 m elevation is demonstrated by the photographs in Figure 32. An oxide layer on both the inside and outside surfaces with a core of prior molten material is shown. Oxidation of the inner surface occurred after cladding rupture at 520 seconds. The oxidation of the outside surface increased the thermal resistance sufficiently to raise the cladding temperature above 2100 K, the approximate melting temperature of β-phase zircaloy. Microprobe analysis indicated that uranium diffused into the cladding at most only 160 μm. There is no evidence that the

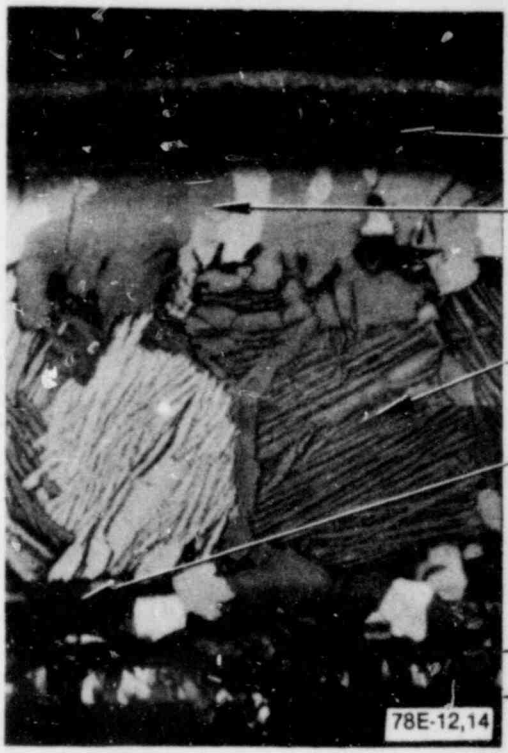

(a) Cladding at 180°

Figure 31. Sev
zir

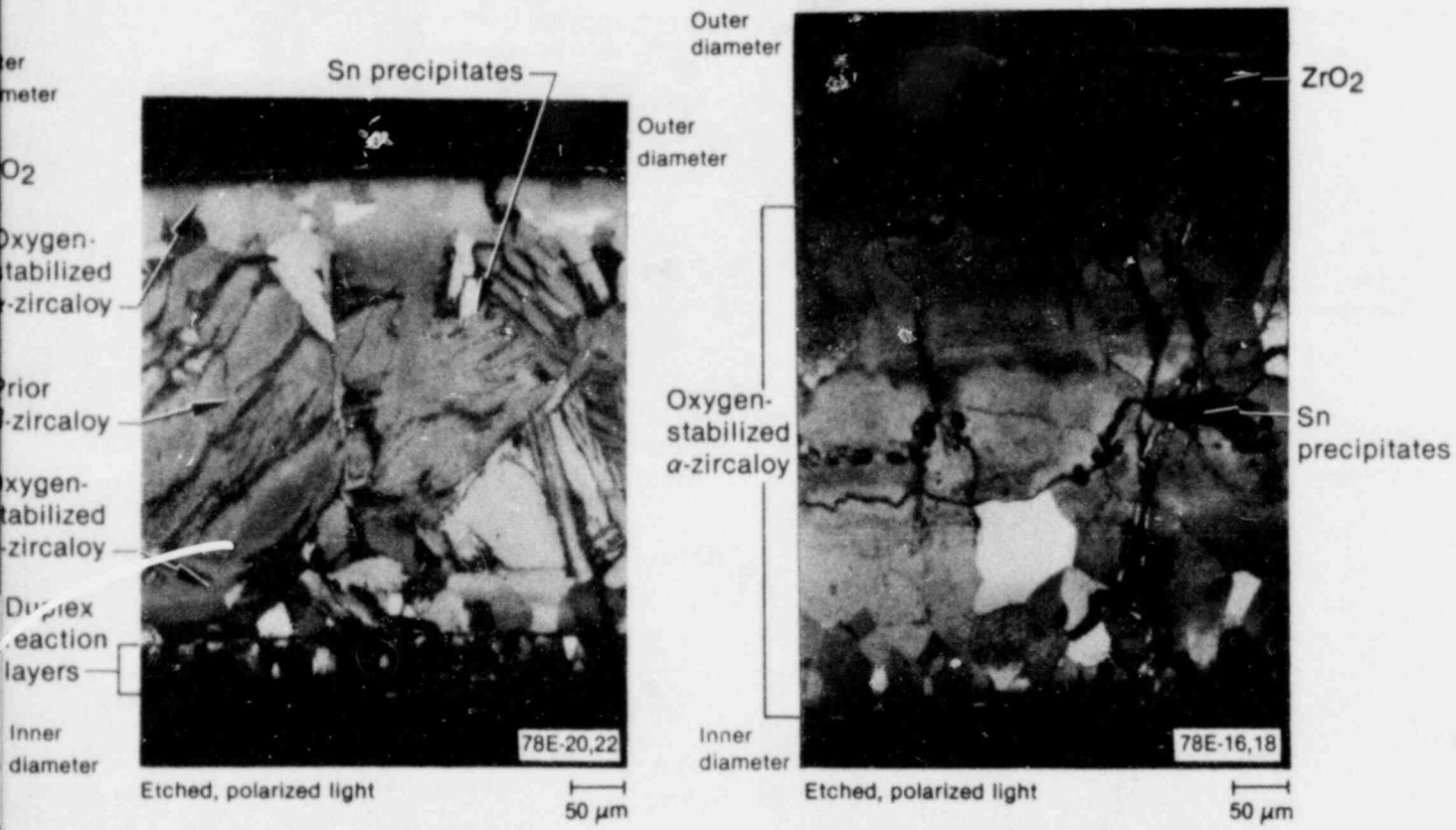

(b) Cladding at 250°

(c) Cladding at 0°

eral orientations of the cladding at 0.67 m showing typical
caloy-UO_2, zircaloy-steam interactions.

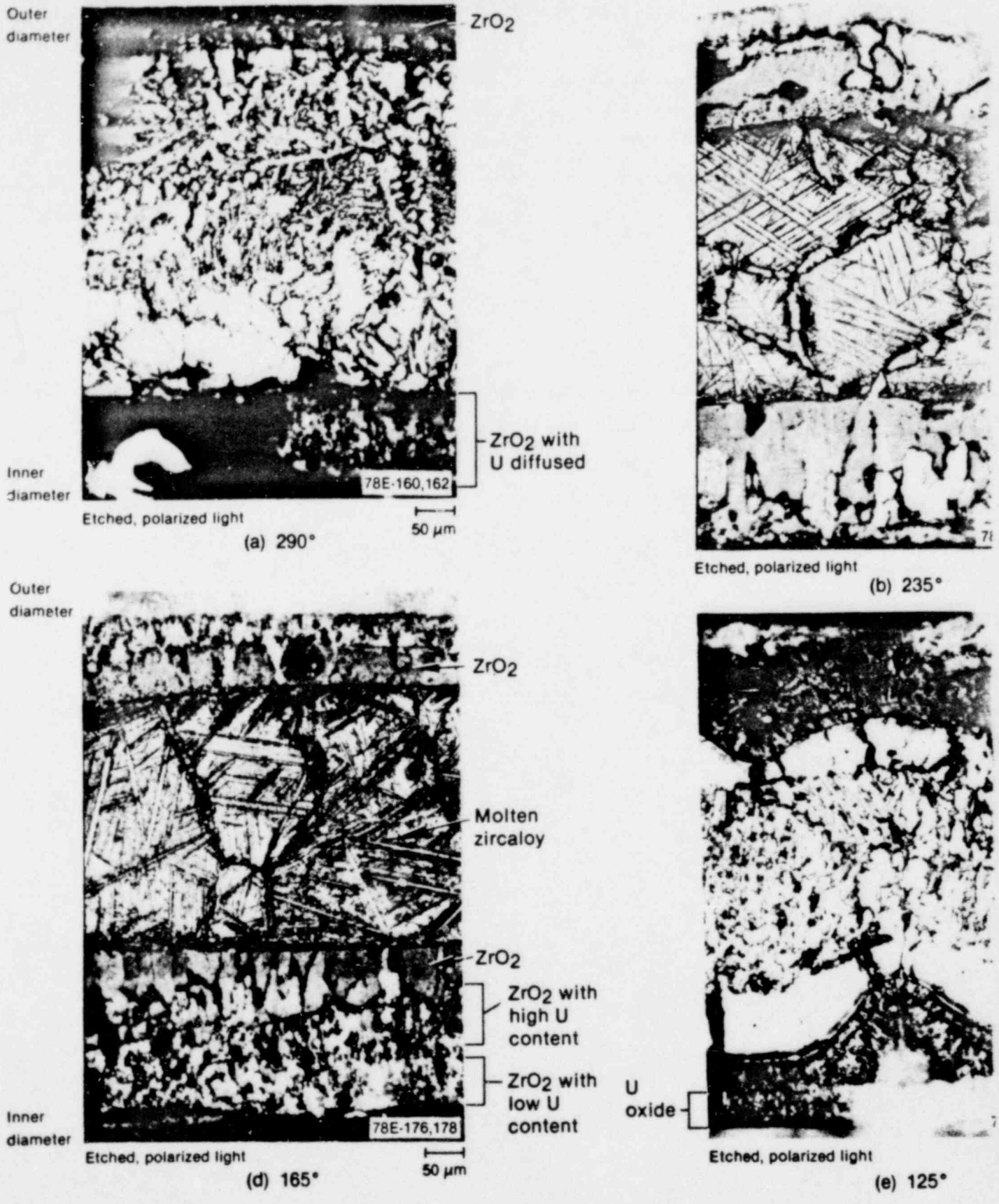

Figure 32. Uranium distribution in the inner oxide layer at sever
0.30 m elevation, Reference 52.

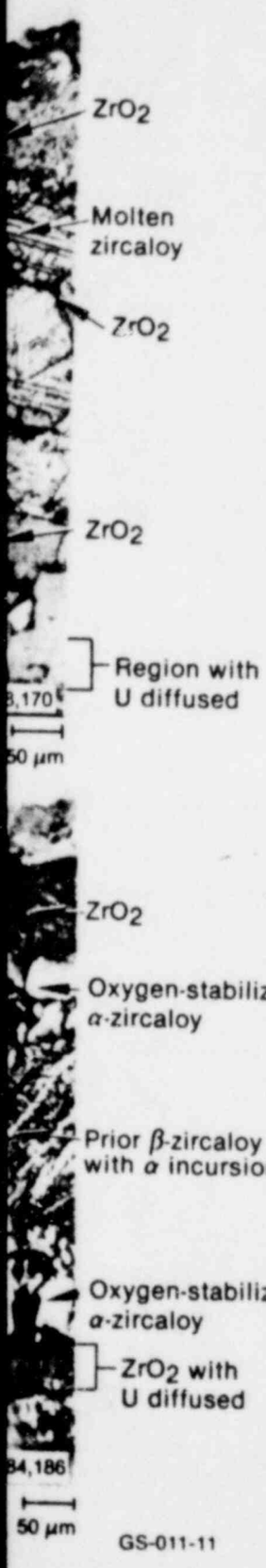

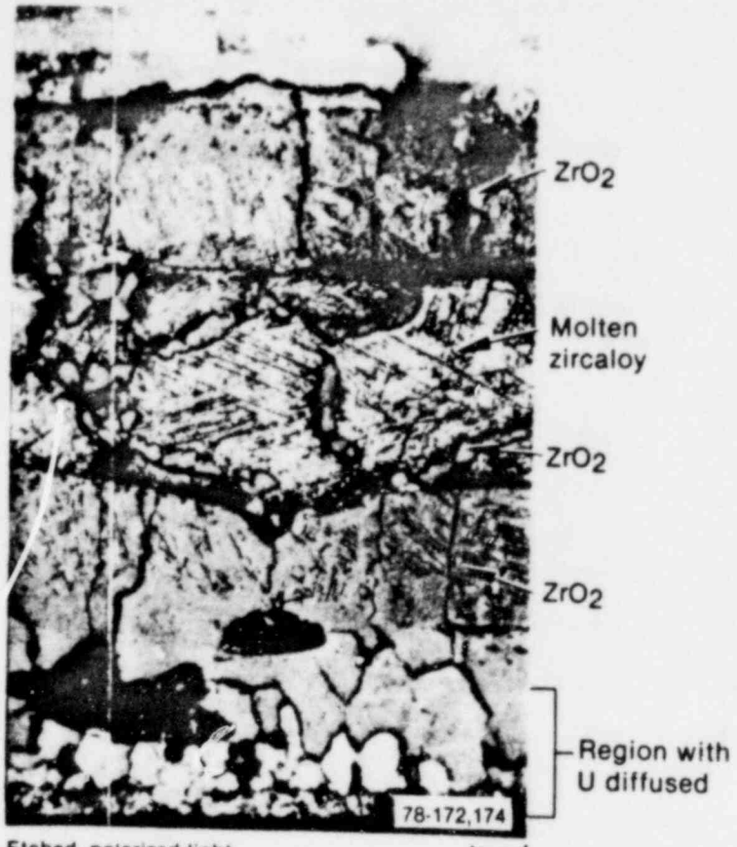

Etched, polarized light

(c) 210°

GS-011-11

orientations of the

molten β-phase zircaloy ever penetrated either the outer or inner surface oxide layer.

There was no evidence in either the KfK or PCM-1 tests that the reduction of the UO_2 by β-phase zircaloy and the subsequent formation of the U-Zr-O eutectic had significant influence on the cladding meltdown. In the KfK out-of-pile tests, the first indication of cladding meltdown was at 2123K, the melting temperature of β-Zr. In the PCM-1 test, the results of the posttest metallographic examination show that the reduction of UO_2 by β-phase zirconium and subsequent diffusion of uranium into the cladding did not produce significant amounts of liquid. In fact, as stated above, the only molten material in evidence was β-phase zircaloy.

3.2.3 Review of KfK Bundle Tests.[49-52] A series of 9-rod electric heater bundle tests have been performed by KfK to evaluate the meltdown behavior of a PWR fuel bundle in steam. The effects of peak cladding temperature, heatup rate, and poison rods and guide tubes on bundle meltdown behavior were reported in the KfK/PNS semi-annual status reports.[49-52] These data and discussions are only preliminary.

Photographs from bundles of simulated fuel rods electrically heated in steam at 4, 2, and 0.25 K/s to temperatures of 2323, 2273, and 2323 K, respectively, are shown in Figure 33 from Reference 50. There was little difference in the fuel behavior observed for 4 and 2 K/s heatup rate. In both cases the outer surface oxidation of the cladding was insufficient to contain the molten zircaloy at temperatures above 2123 K. The cladding melt resulted in intimate contact and dissolution of some of the UO_2 fuel pellets. According to private comment from Dr. S. Hagen of KfK, for some conditions this process may result in liquefaction of a substantial portion of the fuel pellet.

At low heating rates (0.5 K/s) the time at temperature below cladding melting temperature is sufficient to oxidize essentially the

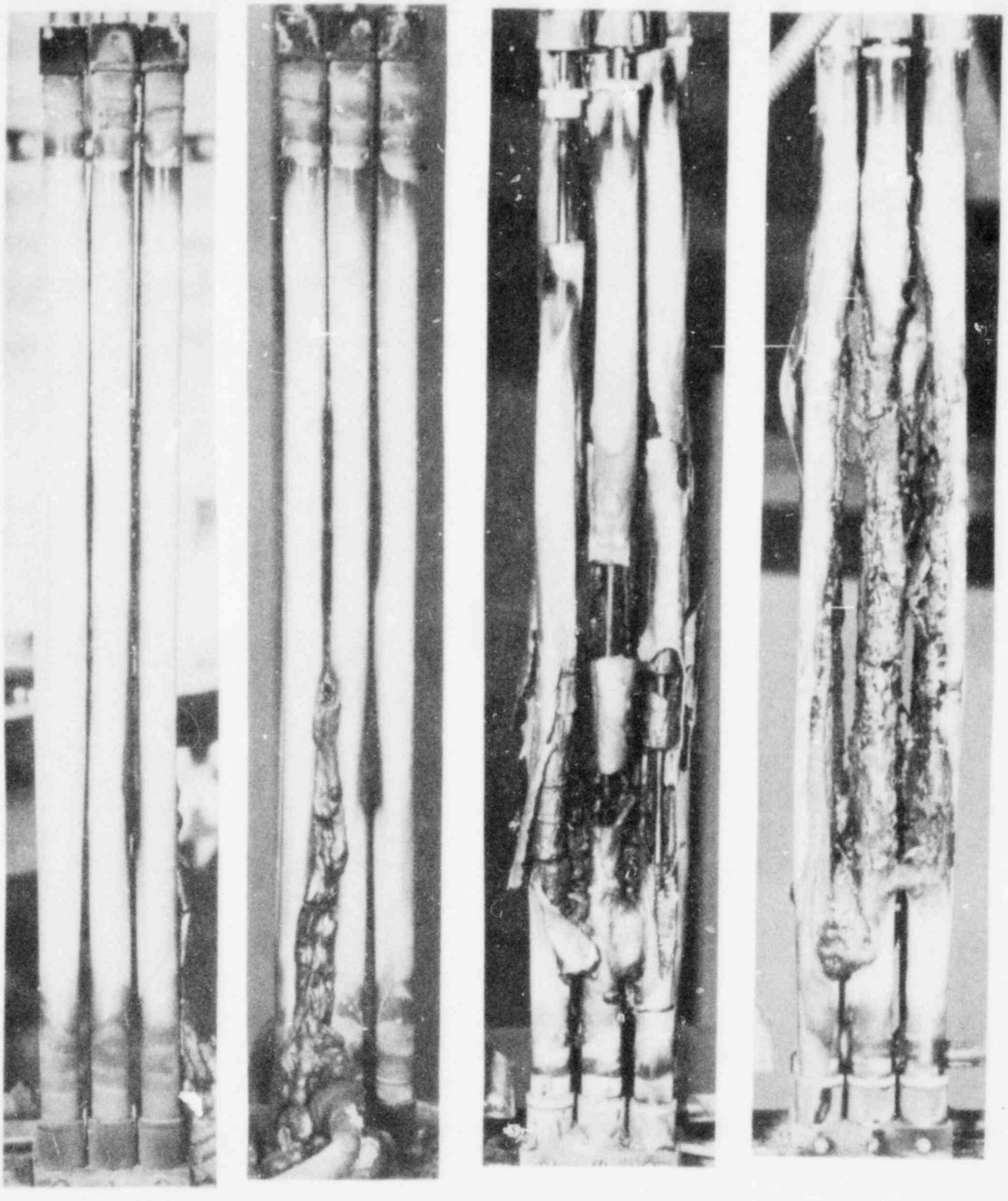

Figure 33. Photographs of bundles heated in steam at 0.25, 2. and 4. K/s to peak temperatures of 2323, 2273 and 2323 K, respectively, Reference 50.

complete cladding wall, if the steam supply is adequate. In the test shown in Figure 33 the steam flow inside the bundle heated at 0.25 K/s was inadequate and resulted in reduced cladding oxidation. Consequently the oxide thickness was insufficient to contain the molten cladding after the melting temperature was exceeded.

The most recently reported data[52] are from tests designed to determine the effects of absorber rods on bundle melting. Three different types of absorber rods were investigated: AgInCd alloy clad in stainless steel, Inconel rods, and boron silicate glass clad in stainless steel. Due to the high vapor pressure of the absorber material at the melting point of the steel cladding, the AgInCd absorber was spewed in small droplets throughout the bundle after temperatures exceeded about 1700 K. The meltdown of the other two types of absorber rods at this temperature resulted in the material slumping down to the bottom of the bundle and eventually freezing. This meltdown behavior as well as the meltdown behavior of Inconel grid spacers[49] indicates that formation of coplanar blockages by previously molten and refrozen core material might be possible even at temperatures significantly below the melting temperature of zircaloy.

3.2.4 Summary of Experimental Results. The out-of-pile experiments conducted on single rods and small bundles by KfK indicate that under conditions possible in a nuclear reactor following a small break LOCA:

- core grid spacers, guide tubes and absorber material might melt and form coplanar blockages at temperatures below the zircaloy melting temperature.

- with a heating rate $\leq$ 0.5 K/s in steam, oxidation will probably prevent significant cladding melting.

- At heating rates above 1.0 K/s or under steam deficient conditions, the remaining metallic zircaloy

will melt at about 2245 K (for α-Zr(O)) and a significant fraction of the UO_2 fuel pellets may be dissolved.

During the PBF PCM-1 Test, temperatures above the zircaloy melting point were reached without any observable dissolution of the fuel. This finding is consistent with the KfK observations because melting of the cladding material did not occur until after the cladding had ruptured and oxidized on the inside surface which prevented intimate contact between the fuel and molten cladding.

The most significant experimental finding with respect to safety considerations is the potential for massive flow channel blockage due to redistribution of molten core structural material or liquified fuel rod material.

4. Fission Gas Release

During normal fuel rod operation gaseous fission products, primarily xenon and krypton, are generated within the UO_2 matrix. Xenon and krypton are virtually insoluble in the fuel matrix, which means that these gases will be rejected from the fuel matrix. The gases are rejected primarily by direct diffusion to and collection or release at grain boundaries. Direct diffusion release is slowed by defect traps (bubbles or dislocations) and subsequent diffusion to the grain boundaries. The fission products coalesce at grain boundaries forming bubbles which are released to the fuel rod free void volume through cracks and pore-gap communication paths. The primary low temperature release mechanisms[54] are (a) by direct flight from the fuel while the gas atom is still an energetic fission fragment (recoil) or (b) by interaction with a fission fragment, a collision cascade of a fission spike with a stationary gas atom near the surface (knockout). Dissolution of uranium dioxide by molten α-Zr(O) would probably release virtually 100%of the gaseous fission products from the dissolved UO_2.

Recoil and knockout are considered secondary modes of gas release, insignificant during a small break LOCA transient because of the high temperatures and will not be discussed further. The diffusion model in MATPRO-11[27] is discussed below and the controlling variables identified and evaluated.

4.1 MATPRO-11 Gas Release Model

The fission gas release model, FGASRL, in MATPRO-11[27] assumes a two step gas release process: (a) release from fuel grains to grain boundaries and, (b) release from the grain boundaries to the fuel rod internal free volume. The fundamental dependence of temperature, grain size, fractional fuel porosity, burnup, fission gas production rate and time on gas release are modeled in FGASRL. The influence of temperature gradients on pore migration, or temperature rise rate which can be important are not considered.

The fission gas reaching the fuel free volume is modeled as a fraction of the fission gas stored at the grain boundaries and the fission gas that reaches the grain boundaries during a time increment. The fraction of grain boundary gas released to the fuel rod free volume is expressed as a function of the fuel density and grain size. This formulation considers only grain boundary fission gas release by bubble interlinkage to the fuel rod free volume. It was assumed that isothermal conditions exist for this development.

Fractional release predictions with FRASRL using the fuel rod operational histories of the model's data base are within $\pm 60\%$ of the experimentally determined fractional gas release.

The diffusion and release mechanisms for cesium and iodine are substantially the same as for xenon and krypton, and release fractions are essentially identical. The model CESIOD,[27] which was developed to predict the release of cesium and iodine, assumes the fuel is a collection of spherical grains and Fick's law of diffusion is valid. The diffusion of xenon and krypton from the UO_2 pellets was

estimated from gas absorption measurements. Different approximations were used to model long- and short-lived isotopes. A more sophisticated treatment of the diffusion process was not justified without including effects from complex chemical reactions. Exact models of the cesium and iodine concentrations in the rod void volume require consideration of the chemical interactions of cesium, iodine, zirconium, and oxygen as well as the details of the diffusion and release mechanisms. Further details of the CESIOD model are presented in MATPRO-11.[27]

These models have not been evaluated against data from slow heatup, high temperature transients such as are expected in this test program. Relatively slow temperature rise rates could substantially affect the fraction of fission gas released. Other release mechanisms which might be significant are discussed in the following subsection.

4.2 Other Mechanisms Influencing Fission Gas Release

Fuel rod fragmentation may occur when the fuel rod is quenched. This fragmentation would primarily occur along grain boundaries, releasing gaseous fission products which have accumulated there. At temperatures above 1900 K, the fuel pellets may desinter to grain size particles when quenched.[43] Fragmentation on this scale would likely result in very high fractional fission gases release. Prediction of the release from this mechanism would require (a) accurate knowledge of the fission product concentrations within grains and trapped at grain boundaries prior to the transient, (b) gas atom and bubble migration rates during the transient, (c) detailed prediction of the grain growth kinetics at temperatures above about 1900 K, and (d) a detailed knowledge of the UO_2 fragmentation and desintering processes.

Dissolution of the UO_2 by molten α-Zr(O) would probably release essentially 100%of the fission gases from the dissolved fuel. This release process is not currently modeled. Conflicting processes are occurring in such a system. Although movement of the gaseous fission

products would be unrestricted when the fuel was liquified, the gas atoms must still escape the liquified material by rising to a free surface. This movement would be either from buoyancy forces or by turbulent transport within the liquid material. With the UO_2 dissolution process, the outer surface of the molten α-Zr(O) would be exposed to steam and oxidization could form a relatively impervious barrier to the release of gaseous fission products.

5. Conclusions

The following conclusions are based upon the preceding discussion regarding fuel behavior during a small break LOCA.

1. Cladding ballooning and rupture would inhibit intimate contact between fuel and cladding(at least over the ballooned region), expose the cladding inside surface to severe oxidation and hydrogen uptake, and release fission products.

2. Cladding oxidation could severely embrittle the cladding and provide significant heat to further increase fuel rod temperatures.

3. Precipitation of zirconium hydrides at low temperatures (< 700 K) could further degrade cladding integrity.

4. Cladding embrittlement depends upon the extent of oxidation, oxygen absorption, hydride precipitation, temperature and cooldown rate.

5. If the cladding is sufficiently embrittled, fuel rod fragmentation may occur from thermal shock during quench.

6. The formation of uranium rich intermetallic compounds probably has little influence on cladding melting.

7. Peak cladding temperature and temperature rise rate with the associated oxidation strongly influence the extent of cladding melting.

8. Dissolution of UO_2 by molten α-Zr(O) could be extensive.

9. Melting of control rods could significantly alter the core geometry.

10. Fractional fission gas release could be very high if the UO_2 were dissolved by molten α-Zr(O) or desintered when quenched.

IV. PROPOSED MODEL FOR LONG TERM COOLING OF A DAMAGED CORE

In Section 2.2 the estimated damage to the TMI-2 plant was discussed. It was concluded that a significant portion of the core may have fragmented and collapsed forming a rubble bed. Measured coolant temperatures at the top of the core possibly indicate that the flow was severely restricted within the central regions of the core, diverting most of the coolant into peripheral bundles.

The test program presented in Section V proposes tests with a fast quench which would create a rubble pile from fragmented fuel rods. It is also proposed that the tests be continued to evaluate the hydrodynamic and heat transfer characteristics of the rubble bed. However, to design relevant tests, a basic understanding of the fluid dynamic and heat transfer processes involved is required. A model is proposed as a first approximation of the hydrodynamics and the heat transfer processes, and the primary controlling parameters are identified.

1. Proposed Model

A schematic representation of the post-quenched state of the TMI-2 core is shown in Figure 34.a. The core consists of a non-homogeneous anisotropic mixture of fragmented fuel rods and previously molten fuel rod material. The fragments are primarily ZrO_2, UO_2 and U_4O_9. The bottom of the rubble pile probably has a parabolic shape, reflecting the variation in heat transfer and relative fuel rod power within the core. When coolant flow is reestablished in such a system, the heat transfer would be characteristic of that in fixed and fluidized pebble beds with the bed fluidization (or regions of the bed) dependent upon the local coolant velocity, bed geometry and local properties. Large chunks of slag from previously molten material would have significant effects on the flow resistance and the local coolant velocity. The heat transfer from these relatively large chunks, if they do not fragment from thermal shock when quenched, would be by conduction and convection.

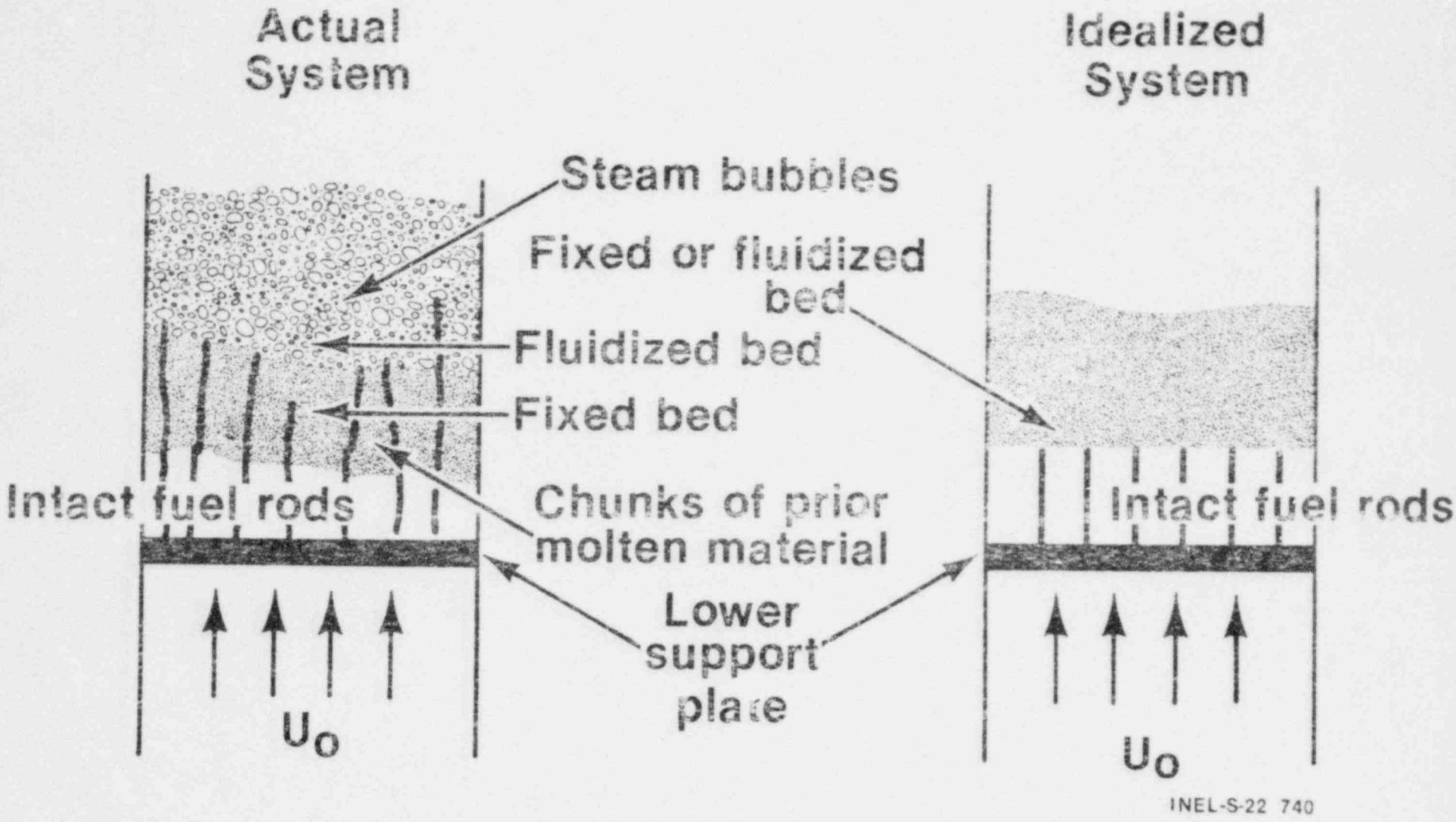

Figure 34. Schematic of damaged core long term cooling model.

Local boiling within the bed could also have significant effects on the local heat transfer. The effect of coolant phase change within the rubble pile is not clearly understood at present.

A simplification of the presumed physical system is shown schematically in Figure 34.b. The rubble bed is assumed to consist of a uniform mixture of ZrO_2 and UO_2 fragments of constant particle size and the bottom of the bed is assumed to be flat. The coolant inlet flow is constant across the bottom of the core and varies only with time. For these conditions, the mode of heat transfer within the rubble bed is primarily dependent upon the fluidization of the bed. For a given system, if the coolant velocity is less than a critical value, U_o, the bed is fixed and the coolant merely percolates through the void spaces between stationary particles. At higher coolant velocity, a point is reached when the particles are all just suspended in the upward flowing liquid. In liquid-solid systems an increase in flow rate above minimum fluidization usually results in a smooth, progressive expansion of the bed. The Nusselt-Reynolds relationship describing the system heat transfer also changes appropriately. At still higher fluid velocities, entrainment of the solid particles will become appreciable, and solids are carried out of the bed with the fluid stream.

2. System Fluid Dynamics

The pressure drop through fixed beds, of non-uniform solid particles has been correlated using Ergun's correlation for pressure drop.[55]

$$\frac{\Delta P}{L} g_c = \underbrace{150 \frac{(1-\epsilon_m)^2}{\epsilon_m^3} \frac{\mu U_o}{(\phi_s d_p)^2}}_{\text{frictional pressure drop}} + \underbrace{1.75 \frac{1-\epsilon_m}{\epsilon_m^3} \frac{\rho_f U_o^2}{\phi_s d_p}}_{\text{kinetic energy losses}} \qquad (1)$$

where

ΔP = pressure drop,

L = height of particle bed,

U_o = superficial fluid velocity (measured on an empty tube) through a bed of solids,

$\bar{d}_p$ = mean particle diameter,

g_c = gravitational conversion factor,

ϵ_m = void fraction in a packed bed

μ = fluid viscosity,

$\bar{\phi}_s$ = mean sphericity of a particle

ρ_f = fluid density,

At low Reynolds numbers, Re $\leq$ 20, the frictional losses predominate and the kinetic energy losses may be ignored. At high Reynolds numbers, >1000, the kinetic energy losses predominate and and the frictional effects may be ignored. At intermediate Reynolds numbers, 20 < Re < 1000, the complete form of Equation (1) must be used to determine pressure drop.

The pressure drop for a given system configuration is dependent upon the particle bed height, bed void fraction, mean particle sphericity and surface mean particle size, all of which are characteristic of the system geometry, as well as the superficial fluid velocity and properties. For an inhomogeneous system, such as the TMI-2 core, large variations in the local superficial velocity must exist to satisfy the system constraint that $\Delta P(z)$ is constant between the lower and upper plenums. Thus, to accurately calculate the thermal-hydraulics of a core rubble bed, these local parameter variations must be known.

The minimum fluidizing velocity, U_{mf}, must also be calculated. The onset of fluidization occurs when the drag forces by upward moving liquid is equal to the weight of particles, or

$$\begin{bmatrix}\text{pressure drop}\\ \text{across bed}\end{bmatrix}\begin{bmatrix}\text{cross sectional}\\ \text{area of Tube}\end{bmatrix} = \begin{bmatrix}\text{volume}\\ \text{of bed}\end{bmatrix}\begin{bmatrix}\text{fraction of}\\ \text{solids}\end{bmatrix}\begin{bmatrix}\text{specific}\\ \text{weight}\\ \text{of}\\ \text{solids}\end{bmatrix} \quad (2)$$

which can be expressed as

$$\frac{\Delta P}{L_{mf}} = (1-\epsilon_{mf})\,(\rho_p-\rho_f)\,\frac{g}{g_c} \quad (3)$$

where

L_{mf} = height of particle bed at minimum fluidizing conditions,
ϵ_{mf} = bed void fraction at minimum fluidizing conditions
g = acceleration of gravity,
ρ_p = particle density,
ρ_f = fluid density,

Equating Equations (1) and (3), the minimum fluidizing velocity is given by,

$$U_{mf} = \frac{25.7}{\bar{\phi}_s \bar{d}_p\, \rho_f}\left\{\left[1 + 5.53 \times 10^{-5}\left(\frac{(\bar{\phi}_s \bar{d}_p)^3\, \rho_f\, (\rho_p-\rho_f)g}{\mu^2}\right)\right]^{1/2} - 1\right\} \quad (4)$$

Note that the minimum fluidizing velocity is dependent only upon properties, the mean sphericity of the particles and the mean particle diameter. The product $\bar{\phi}_s \bar{d}_p$ is the characteristic dimension of the system, assuming effects from the container walls are insignificant. $\bar{\phi}_s$ and $\bar{d}_p$ must be determined experimentally for a core rubble bed, either from representative experiments, available data, or the TMI-2 core when disassembled.

3. Rubble Bed Heat Transfer

Heat transfer in particle beds with coarse solids may be approximated by Equations (5) and (6) for the appropriate range of Reynolds number.[55]

$$Nu_p = 0.3\ Re_p^{1/3},\ Re_p \leq 100 \tag{5}$$

where

$Nu_p = \frac{h_p \bar{d}_p}{k_p}$, Nusselt number

h_p = heat transfer coefficient between the particle surface and the fluid

k_p = thermal conductivity of particle,

and

$$Nu_p = 2 + 1.8\ Pr^{1/3}\ Re_p^{1/2},\ Re_p > 100 \tag{6}$$

where

$Pr = \frac{C_p u}{k_f}$

C_p = specific heat of fluid,

k_f = thermal conductivity of fluid,

A comparison of Equations (5) and (6) with reported results for heat transfer in fixed beds from Reference 55 is shown in Figure 35. The data sets I, and J are for solid-liquid water systems, and the others are for solid-air systems. Data were not shown for Reynolds numbers greater than about 150. In general, Equation (5) underpredicts the solid-water data, and it appears that a transition

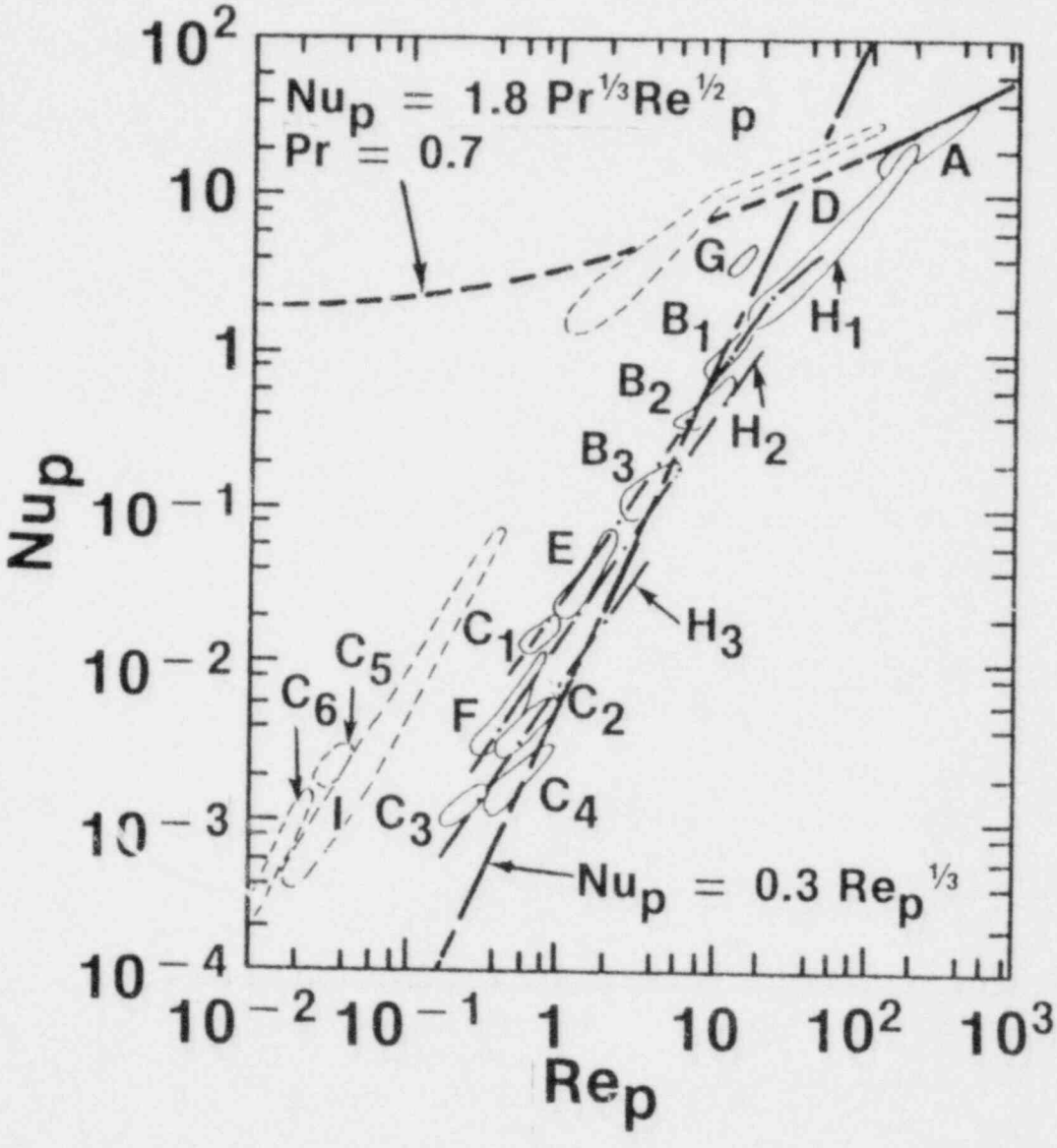

Figure 35. Comparison of heat transfer model with data, C_5, C_6, I and J for liquid water, the others for air, Reference 54.

Reynolds number of approximately 10 may be more appropriate for solid-water systems. The leading coefficient, 0.3 and the exponent, 1/3, in Equation (9) could be adjusted so that Equation (5) would more closely approximate the solid-water data. However, this is not justified as wide variations in the data are common, and data from experiments representative of a "nuclear rubble pile" are necessary to adjust these coefficients and exponents with confidence.

4. Conclusions

A relatively simple model of the fluid-dynamics and heat transfer within a core rubble bed was proposed. This model provides a mechanism by which to specify experimental conditions or perform an evaluation of the hydrodynamic and heat transfer characteristics of the rubble beds formed during the PBF experiments (proposed in Section V). Data are required from representative separate effects tests to determine the coefficients in the Nusselt number-Reynolds number power law relationship, and to assess the model at Reynolds numbers greater than about 150.

V. SEVERE CORE DAMAGE ASSESSMENT TEST PROGRAM

The test requirements and objectives for the PBF severe core damage test program are discussed in Section VI.1. The controlling parameters which were identified in Sections II and III are consolidated and organized.

The proposed PBF test program for severe core damage tests is presented in Section V.3. An out-of-pile separate effects test program is also suggested to obtain data on the basic hydrodynamic and heat transfer characteristics of a highly fragmented PWR core using fuel rod fragments from the PBF PCM and IE test programs which are currently in storage at the INEL.

1. Test Requirements and Objectives

This program, performed as part of the NRC Severe Core Damage Assessment Program, will provide a series of highly controlled and instrumented tests with nuclear fuel rods during small break loss-of-coolant accident conditions. The tests will be conducted to progress from the initial reduction in coolant flow and initiation of boiling through cladding melting and redistribution of liquified fuel rod material, followed by quench and fuel rod fragmentation. The hydrodynamic and heat transfer characteristics of the rubble pile will also be examined. As it is not feasible to perform sufficient tests in PBF to systematically evaluate all aspects of fuel rod behavior and damaged core coolability, the tests (inclusive of all tests in the severe core damage assessment program) are structured to provide the most relevant data over the complete range of anticipated fuel rod behavior. The data obtained from these tests will be used to bench mark out-of-pile data which are necessary to complete a systematic evaluation of fuel rod behavior during these types of transients.

The primary experiment objectives for the program are:

1. To examine the primary fuel rod damage mechanisms and the controlling processes during system conditions of decreased pressure and steam cooling, and

2. Examine the hydrodynamic and heat transfer characteristics of a rubble pile formed from previously molten and fragmented fuel rods.

Detailed test objectives have been defined to ensure that the more general primary experiment objectives are attained. They are:

1. Evaluate the effect of cladding ballooning and rupture on oxidation, hydrogen uptake, embittlement, and fuel rod melt down.

2. Confirm existing zircaloy cladding oxidation correlations at temperatures above 1773 K, and the embrittlement and fuel rod fragmentation criteria at quench temperatures.

3. Characterize fuel rod fragmentation and UO_2 desintering when quenched.

4. Determine the extent of UO_2 dissolution by molten zircaloy, and characterize the redistribution and solidification of liquified fuel rod material.

5. Monitor fission product release during heatup and evaluate the effect of UO_2 dissolution and fragmentation on fission product release.

6. Evaluate the hydrodynamic and heat transfer characteristics of the rubble bed with respect to fuel rod fragment size and coolant flow rate.

The primary fuel rod damage mechanisms and the controlling variables are summarized in Table 1.A. The relationship between the controlling variables and fuel rod damage mechanisms is indicated only

TABLE 1. SUMMARY OF FUEL ROD DAMAGE MECHANISMS AND CONTROLLING VARIABLES (A), AND DIRECT COUPLING BETWEEN MECHANISMS (B)

	FUEL ROD DAMAGE MECHANISMS						
Controlling Variable	Cladding Ballooning and Rupture	Cladding Oxidation 2	Hydrogen Uptake and Hydride Precipatation 3	Cladding Embrittlement 4	Cladding Melting and UO_2 Dissolution 5	Fuel Rod Fragmentation 6	Fission Gas Release 7
Peak Cladding Temperature	X	X	X	X	X	X	X
Temperature Rise Rate	X	X			X		X
Time at Temperature		X	X		X		X
Cladding Cooldown Rate		X	X			X	
Rod Internal Pressure	X						
Fuel Rod Damage Mechanisms							
1		X			X		X
2	X		X	X	X		
3				X			
4						X	
5						X	X
6							X
7	X						

if the influence is direct. Direct couplings between damage mechanisms are indicated in Table 1.B. A direct coupling between a fuel rod damage mechanism, shown as the numbered column on the left, and another, shown across the top of the Table is indicated by an "X." The influence is from the damage mechanisms, listed in the column on the left, to those listed across the top of the table.

The values of the controlling variables during the test program are listed in Table 2. A peak cladding temperature of at least 2300 K was selected to ensure melting of the metallic zircaloy. Cladding temperature rise rate will be varied to obtain different degrees of cladding oxidation prior to exceeding the zircaloy melting temperature. At 0.5 K/s the cladding should totally oxidize before reaching 2250 K, whereas at 4.0 K/s less than 50% of the cladding will oxidize. The remainder of the cladding will melt, and as it slumps and contacts the UO_2, considerable UO_2 may be dissolved. These heatup rates will be held constant until the desired peak temperature is reached. The third temperature rise rate will approximate the predicted cladding temperature history during the conditions that have been postulated for the TMI-2 accident. The time at peak temperature will be adjusted to obtain the desired degree of cladding oxidation. Cladding cooldown will be either slow, by radiation to the flow shroud, or a quench. The slow cooldown will preserve the test bundle for posttest examination, and the quench will fragment the test rods. Postquench flow rate will be varied to examine the hydrodynamic and heat transfer characteristics of the test bundle rubble pile. The test rods will be prepressurized to approximately 3 MPa to induce cladding ballooning and rupture. Two lower priority tests, SBL-5 and -6, have been specified with an initial fuel rod prepressurization of only 0.1 MPa. During these tests the cladding will collapse thus maximizing potential fuel/cladding chemical interaction.

2. Feasibility of PBF Testing.

An analytical evaluation of the thermal performance of the proposed PBF test configuration is currently in progress. The analysis is being performed with the MOXY/SCORE[56] digital computer

TABLE 2. TEST PARAMETERS

PEAK CLADDING TEMPERATURE	2300 K
CLADDING TEMPERATURE RISE RATE	0.5, 4 k/s[a]
TIME AT PEAK TEMPERATURE	to be determined
CLADDING COOLDOWN	~10, $\geq$100 k/s
POST-QUENCH COOLANT FLOW RATE	>0 to ~10 cm/s
ROD INTERNAL PRESSURE	0.1, ~3 MPa

a. Controlled to approximate the best estimate of the TMI-2 core temperature history.

program. The results from this analysis will be documented upon completion.

The primary concerns regarding the performance of these tests in PBF are (1) the fission heat requirement to compensate for radiative and convective heat transfer from the test bundle when cladding temperatures are approximately 2300 K and (2) the relatively small size of the test bundle. Fuel centerline melting could occur if the required fission heat were approximately 26 kw/m or greater, and the relatively large radial temperature gradients within a test rod at such power levels is undesirable. Both of these conditions are atypcial of the actual state of the fuel rod during an accident.

The relatively small size of the test bundle (either 4 x 4 or 5 x 5) could severely restrict the validity of the results if the tests were primarily intended to be demonstrative. However, the tests are intended to examine, phenomenologically, the fuel rod damage mechanisms that occur during system conditions of decreased pressure and steam cooling, and the hydrodynamic and heat transfer characteristics of the rubble bed formed during quench. If the tests are structured and performed correctly, and properly instrumented the desired data should be obtained.

3. Test Program

A scoping test plus seven additional tests are proposed in Table 3. The system and fuel rod conditions for each test, and a summary of the anticipated fuel rod behavior during each test are tabulated. The test program is divided into five tests of high priority and three relatively low priority tests. The high priority tests will provide the basic information regarding: (a) the fragmentation of a highly oxidized fuel rod bundle; (b) cladding melting, UO_2 dissolution, and redistribution and re-solidification of the liquified material; (c) the state of the test bundles prior to quench; and (d) the hydrodynamic and heat transfer characteristics of a rubble pile composed primarily of ZrO_2 and UO_2 fragments versus

TABLE 3. TEST PROGRAM

TEST	ROD PRESSURE (MPa)	PEAK CLADDING TEMP (K)	CLADDING TEMP RISE RATE (K/s)	TEST TERM-INA-TION	LONG TERM COOLING FLOW RATE (cm/s)	COMMENTS
SCOPING TEST	3	2300	0.5	SLOW COOL-DOWN	N/A	CLADDING BALLOONING AND RUPTURE; EXTENSIVE OXIDATION, HYDROGEN UPTAKE, AND EMBRITTLEMENT; FISSION PRODUCT RELEASE WHEN CLADDING RUPTURES
SCD-1	3	2300	4.0	SLOW	N/A	DEGREE OF OXIDATION SIGNIFICANTLY REDUCED BECAUSE OF INCREASED HEAT UP RATE AND CLADDING MELTING. MOLTEN ZIRCALOY COULD DISSOLVE SIGNIFICANT FRACTION OF UO_2. GROSS FISSION PRODUCT RELEASE COULD OCCUR.
SCD-2	3	2300	0.5	QUENCH	VARIABLE (~0.0-10)	SAME AS SCOPING TEST EXCEPT FOR QUENCH. POST-QUENCH FLOW RATE WILL BE VARIED TO EVALUATE RUBBLE BED HYDRODYNAMIC AND HEAT TRANSFER CHARACTERISTICS.
SCD-3	3	2300	4.0	QUENCH	VARIABLE (~0.0-10)	SIMILAR TO TEST #1. QUENCH WILL FRAGMENT FUEL ROD. POST-QUENCH FLOW RATE WILL BE VARIED TO EVALUATE RUBBLE BED HYDRODYNAMIC AND HEAT TRANSFER CHARACTERISTICS WITH RESOLIDIFIED FUEL ROD IN RUBBLE BED.

TABLE 3. (continued)

TEST	ROD PRESSURE (MPa)	PEAK CLADDING TEMP (K)	CLADDING TEMP RISE RATE (K/s)	TEST TERM-INA-TION	LONG TERM COOLING FLOW RATE (cm/s)	COMMENTS
SCD-4	3	2300	SEE COMMENTS	QUENCH	VARIABLE (~0.0-10)	HEATUP RATE WILL APPROXIMATE BEST ESTIMATE OF TMI-2 FUEL ROD HEATUP, OTHERWISE SIMILAR TO TEST #3.
SCD-5	0.1	2300	4.0	SLOW COOL DOWN	N/A	SIMILAR TO TEST #6 CLADDING COLLAPSE AND WAISTING; EXTENSIVE OXIDATION AT CLAD OUTSIDE SURFACE, SEVERE CLADDING EMBRITTLEMENT; INCREASED POTENTIAL FOR REDUCTION OF UO_2 BY MOLTEN ZIRCALOY.
SCD-6	0.1	2300	4.0	QUENCH	VARIABLE (~0.0-10)	CLADDING COLLAPSE AND WAISTING; EXTENSIVE OXIDATION AT CLAD OUTSIDE SURFACE, SEVERE CLADDING EMBRITTLEMENT; INCREASED POTENTIAL FOR REDUCTION OF UO_2 BY MOLTEN ZIRCALOY.
SCD-7	3	2300	4.0	RAPID QUENCH	VARIABLE (~0.0-10)	REPLACE ONE OF THE CENTER RODS WITH A CONTROL ROD. EVALUATE THE EFFECT OF MOLTEN MATERIAL FROM THE CONTROL ROD ON THE RUBBLE BED COOLING CHARACTERISTICS.

a rubble pile composed for resolidified cladding and dissolved UO_2, and UO_2 fragments. The lower priority tests are suggested to provide additional information regarding the chemical interaction between zircaloy and UO_2 at temperatures greater than 2245 K for comparison with the results from SCD-1, -3 and -4. Test SCD-7 is suggested to examine the effect from the destruction of a simulated control rod on the response of the surrounding fuel rods.

A series of separate effects tests performed out-of-pile (in the INEL hot cell facility) with fuel rod fragments from the PBF PCM and IE test programs is suggested. Data from these tests would be used to determine the coefficients and exponents in the Nusselt number-Reynolds number heat transfer relationship. These tests would systematically evaluate pressure drop as a function of bed height, mean particle size and sphericity, bed composition (i.e. UO_2 and ZrO_2 fragments, and prior molten material), and superficial fluid velocity. The minimum fluidizing velocity and the terminal fluid velocity for particle entrainment would be determined as a function of bed composition and the characteristic dimension of the bed ($\bar{\phi}_s \bar{d}_p$). Heat transfer data would also be obtained over an applicable range of Reynolds numbers. The temperature distribution within the rubble pile would be measured to ascertain an average heat transfer coefficient. Additional planning is required to optimize a test plan utilizing the available fuel rod fragments and experimental capabilities of the INEL hot cell facilities.

VI. EXPERIMENT REQUIREMENTS

The test train design, fuel rods, instrumentation and postirradiation examinations which are required to obtain necessary data from the proposed tests are discussed in this section.

1. Test Train Operational Requirements

The test conditions for the proposed severe core damage tests will be more severe than any encountered in previous PBF tests because of the very high temperatures, presence of molten cladding and dissolved UO_2, and the relatively long time required to perform the tests. The test train must be designed to withstand these severe conditions and provide the necessary containment to prevent damage to the IPT, if possible.

The system operational requirements necessary to perform a test are as follows. After completion of the preconditioning operation, the reactor power will be decreased to about 0.1 MW and the system pressure will be decreased to about 7 MPa and held constant. The coolant flow to the test bundle will be shut off and the test bundle will uncover by boiling. When the coolant reaches the desired level, near the bottom of the bundle, the coolant flow will be increased (and adjusted as necessary) to maintain the desired liquid level. Reactor power will be increased to initiate cladding heatup, and the fission heat will be controlled to maintain the desired fuel rod heatup rate. The degree of fission heat required to compensate for radiative and convective heat transfer from the bundle is being evaluated as part of the feasibility study, see Sec V.2. After reaching a peak cladding temperature of at least 2300 K, the test will be terminated. Test termination will consist of reactor scram followed by a slow cooldown (i.e., radiation to the flow shroud) to preserve the bundle structure for posttest examination, or a quench to fragment the highly embrittled fuel rods. Tests which are subjected to a quench will also include a series of low flow tests to evaluate the hydrodynamic and heat transfer characteristics of the rubble pile.

During some of the tests, significant molten and liquified fuel rod material will be formed which will slump and redistribute into lower regions of the test train. This liquified material must be contained or at least prohibited from damaging the IPT. Explosive vaporization of water from molten fuel/coolant interaction (MFCI) may also be possible during quench. The potential for an energetic steam explosion for this system is assessed in Appendix A. Based upon the current understanding of the state-of-the-art and available data, it was concluded that the potential for a steam explosion could not be definitively ascertained. The question of steam explosions from MFCI when the system is reflooded must be addressed in greater detail to insure the safe conduct of tests and possibly for consideration in the test train design.

The minimum bundle size for testing will be a 4 x 4, 16-rod bundle fabricated from 17 x 17 PWR fuel, (see Section VI.2). If space within the IPT permits, a 25-rod bundle should be used. Grid spacers should be placed at about 0.20 and 0.71 m from the bottom of the active portion of the fuel rods. The axial power profile should be flattened between 0.30 and 0.61 m, possibly by using a stainless steel sleeve of varying wall thickness.

2. Fuel Rods

Eighty test rods of 17 x 17 PWR design will be required to complete the high priority tests if a 4 x 4 bundle is used. The basic fuel rod dimensions are summarized in Table 4.

3. Instrumentation

The fuel rod and test train instrumentation is summarized in Tables 5 and 6, respectively, and shown schematically in Figure 36 for both a 16-rod and a 25-rod bundle. Fuel rod measurements specified are; fuel centerline temperature, cladding temperature, cladding axial elongation, fuel rod internal pressure, and plenum gas temperature.

TABLE 4. TEST FUEL ROD NOMINAL DIMENSIONS

Characteristics	Nominal Value
Fuel	17 x 17
Material	UO_2
Pellet OD (mm)	8.192
Pellet Length (mm)	13.46
Pellet Enrichment (wt ^{235}U)	a
Density (TD)	95
Fuel Stack Length (m)	0.935
End Configuration	Dished
Burnup (MWd/t)	0.0
Centerhole Diameter (mm)	1.85
Insulator Pellet	
Material	Same
Length (mm)	a
Diameter (mm)	a
Cladding	
Material	Same
Tube OD (mm) 9.50	9.50
Tube ID (mm)	8.357
Wall Thickness (mm)	0.572
Fuel Rod	
Plenum Volume (cm^3)	a
Fill Gas	Same

a. To be determined--nominal value will be specified in the Experiment Specifications Document.

TABLE 5. FUEL ROD MEASUREMENT REQUIREMENTS

Measurement	Location	Range	Accuracy	Time Response	Resolution
Cladding Surface Temperature	TBD[a], see Figure 36	280-2300 K	±2.8 K or 2% of reading which ever is larger	100 msec	2.8 K
Fuel Centerline Temperature	TBD[a], see Figure 36	280-2800 K	±20 K, or 2% of reading which ever is larger	500 msec	3.3 K
Cladding Axial Elongation	Top of fuel rod, see Figure 36	0 to 12.7 mm	±10% of reading or ±0.5 mm which ever is larger	100 msec	0.1 mm
Plenum Pressure	Plenum of rods indicated in Figure 36	0.1 to 15.5 MPa	3% of reading or ±0.34 MPa, which ever is larger	250 msec	0.01 MPa
Plenum Temperature	Plenum of rods indicated in Figure 36	280-1700 K	±3% of junction reading	100 msec	±8.3 K

a. Axial elevation to be determined from pre-test predictions.

TABLE 6. TEST TRAIN AND SYSTEM MEASUREMENT REQUIREMENTS

Measurement	Location	Range	Accuracy	Time Response	Resolution
Fuel Rod Power Profile (flux wire)	Outside surface of flow shroud.	N/A	N/A	N/A	N/a
Neutron Axial Flux Profile	Positioned between flow shroud and IPT flow tube at fuel rod midplane, ±150 mm and ±300 mm.	7.5×10^{13} n/cm^2-s	±2%	100 msec	±2%
Coolant Temperature	Inlet and outlet of flow shroud. Strings of 3 T/C's located between 0 and 0.45 m positioned within the bundles as shown in Figure 36.	280–2500 K	±2.8 K or 2% of reading which ever is larger	100 msec	2.6 K
Coolant Differential Temperature	Between shroud inlet and outlet	0–30 K	±0.1% of reading	100 msec	±0.1% of reading
Coolant Volumetric Flow	Inlet and outlet of flow shroud	0.0–10.0 l/s	±5% of reading	30 msec	±2%

TABLE 6. (continued)

TABLE 6. (continued)

Measurement	Location	Range	Accuracy	Time Response	Resolution
Coolant Pressure	At top of flow shroud	0.1-68.9 MPa	±0.77 MPa or ±2% of reading which ever is larger	100 μsec	±0.5 MPa
Coolant Pressure	Upper and lower plenum of IPT	0.1-15.5 MPa	±0.77 MPa or ±2% of reading which ever is larger	100 μsec	±0.3 MPa
Coolant Differential Pressure	Between shroud inlet and outlet	0.01-0.7 MPa	±5% of reading	10 msec	±1% of reading

a. To be determined from pretest predictions.

16-rod bundle

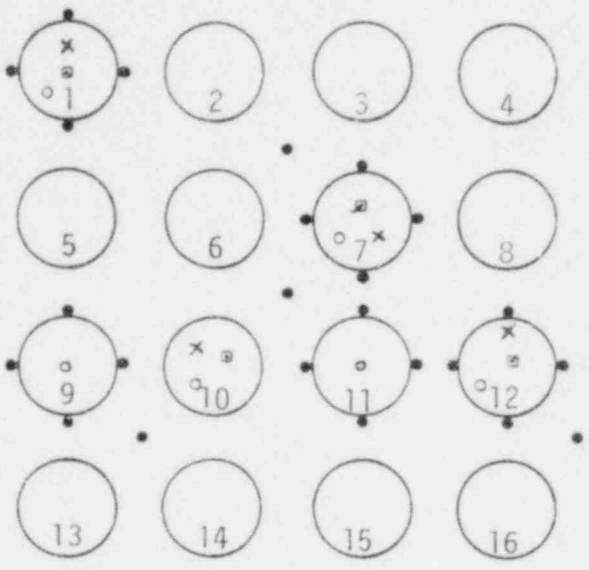

Legend

x LVDT

o Fuel centerline T/C

⊡ Plenum pressure transducer with T/C

• Clad T/C or coolant T/C string

25-rod bundle

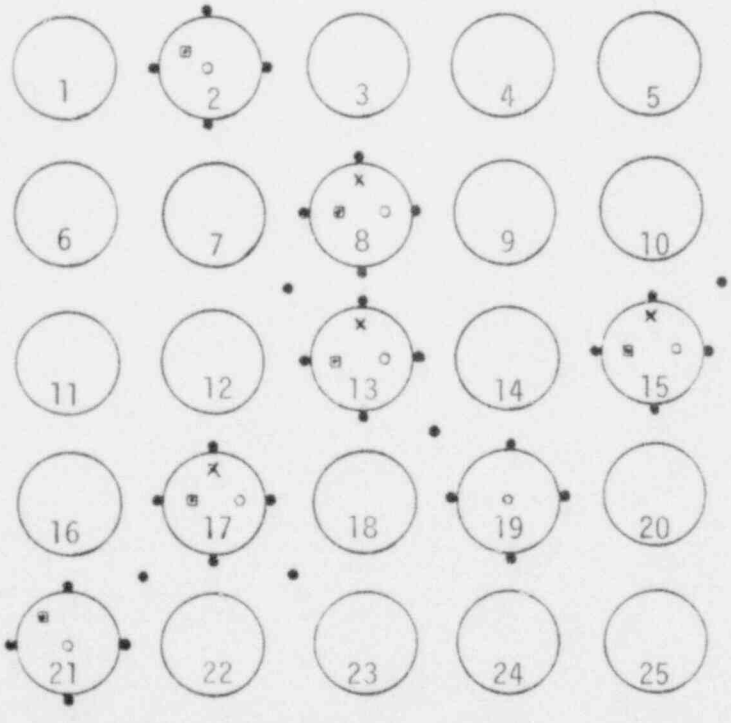

Figure 36. Schematic of test bundle instrumentation.

Measurements to be made within or on the test train are: net axial flux profile, hydrogen release, coolant temperature, coolant differential temperature, coolant volumetric flow, coolant pressure, and coolant differential pressure. Detailed measurements will be made of coolant temperatures in the lower one-third of the bundle on those tests where the test bundle is fragmented. The coolant temperature and mass flow measurements are required to determine the average heat transfer coefficient of the fragmented fuel rods. Measurement of coolant pressure differential is required to characterize the fluid dynamics within the rubble bed.

4. Postirradiation Examination

The requirements listed in Table 7 represent general guidelines for the posttest examination. The specific posttest examination requirements should be tailored to the individual objectives and conditions for each test. Severe fuel rod damage primarily from cladding ballooning and rupture, oxidation, cladding melting with UO_2 dissolution, and fuel rod fragmentation (during some tests) will occur. For those tests terminated with a slow cooldown, the posttest examination will be structured to provide detailed characterization of the conditions of the fuel rod, potential modes of fuel rod failure, and redistribution of previously molten and liquified material. Selected fuel rods will be sectioned to examine the details of cladding oxidation, the zircaloy/UO_2 chemical interaction and fuel restructering.

For those tests with extensive fuel rod fragmentation, the posttest examination will be primarily geared toward providing a detailed quantitative description of the rubble pile composition, particle size and distribution, and redistribution of prior molten and liquefied material. Fuel rod fragments will be selected for detailed evaluation of oxygen content and embrittlement of the cladding, maximum cladding and fuel temperature, and fuel/cladding chemical reaction.

TABLE 7. POSTIRRADIATION EXAMINATION REQUIREMENTS

Requirement	Exam Purpose
Nondestructive Examinations	
1. Fuel rod and test bundle visual examination and photographic record.	Document general rod and bundle appearance, defects, ruptures, oxidation, waisting and ballooning.
2. Test bundle geometry.	Bundle dimensions, channel spacing, extent of fragmentation, redistribution of prior molten material, and particle size distribution.
3. Fuel rod dimensions.	Rod length, diameter and bow.
4. Axial power profile.	Flux wire analysis.
5. Gamma scanning.	Axial distribution of fission products, particularly Cs-137 and I-131.
6. Neutron radiography.	Fuel stack condition (e.g. pellet cracking, central void, axial gaps, redistribution of liquified material).
Destructive Examination	
1. Fission gas analysis and void volume measurement.	Fission gas release to gap and system.
2. Metallography.	Fuel structure (grain size, densification, pore distribution, fragmentation); fuel-cladding chemical interaction, fuel dissolution; cladding structure (microstructure, oxidation, hydriding, microhardness, failures).
3. Chemical analysis.	Fuel fission gas concentration, fuel burnup.
4. Cladding ring compression sample.	Cladding ductility at quench and room temperatures.

VII. CONCLUSIONS

The range of system response and the primary modes of fuel rod behavior that could occur during a small break LOCA transient were determined from a review of RELAP4/MOD7 calculations of the response of a PWR system to a range of small break LOCA's and the TMI-2 accident. The system response is, in general, characterized by a slow depressurization and very low core inlet flow which could allow the core to boil dry. The fuel rods would then heat up and the rate of heatup would primarily depend upon the rod surface heat transfer and decay heat. The primary fuel rod damage mechanisms are cladding ballooning and rupture; oxidation, and embrittlement; and cladding melting with UO_2 dissolution. Extensive fission product would also occur. The primary controlling parameters were also identified.

A model describing the heat transfer within a severely damaged and fragmented core is needed. A simple model based on the fluid dynamics and heat transfer in idealized pebble beds is proposed. The model is primarily dependent upon the superficial fluid velocity, the product of mean particle diameter and mean particle sphericity, and physical properties of the particles and coolant.

A series of eight tests is proposed to examine the primary fuel rod damage mechanisms during system conditions of decreased pressure and steam cooling. The primary controlling parameters are varied parametrically during the test program to provide the desired fuel behavior data and data regarding the hydrodynamic and heat transfer characteristics of the rubble pile. Out-of-pile tests are proposed to obtain the basic hydrodynamic and heat transfer data necessary to specify the coefficients in the proposed heat transfer model.

VIII. REFERENCES

1. United States Nuclear Regulatory Commission, Reactor Safety Research Program, A Description of Current and Planned Reactor Safety Research Sponsored by the Nuclear Regulatory Commissions Division of Reactor Safety Research, NUREG-75/058, June 1975.

2. Nuclear Safety Analysis Center, Analysis of Three Mile Island - Unit 2 Accident, NSAC-1, July 1979.

3. J. M. Broughton and P. E. MacDonald, Light Water Reactor Fuel Behavior Program Description: PBF-LOCA Experiment Requirements, Aerojet Nuclear Co., January 31, 1975.

4. J. M. Broughton, Light Water Reactor Fuel Behavior Program Description: PCM Fuel Behavior Experiment Requirements, SRD-106-76, May 1976.

5. L. S. Thompson et al., Light Water Reactor Fuel Behavior Program Description: RIA Fuel Behavior Experiment Requirements, RE-S-76-187, October, 1976.

6. D. W. Croucher and M. K. Charyulu, Experiment Requirements for the Study of Anticipated Transients with and without Scram, TFBP-TR-308, January 1979.

7. L. J. Siken et al., FRAP-T A Computer Code for the Transient Analysis of Oxide Fuel Rods, NUREG/CR-0840, TREE-1281, June 1979.

8. S. R. Fisher et al., RELAP4/MOD6 A Computer Program for Transient Thermal-Hydraulic Analysis of Nuclear Reactors and Related Systems, User's Manuel, CDAP-TR-003, January 1978.

9. S. R. Behling and C. A. Dobbe, Small Break Calculations for the B&W Oconee Reactor, WR-CD-79-006, May 1979.

10. C. B. Davis, Audit Calculations of Small Cold Leg Breaks in a Combustion Engineering Pressurized Water Reactor, CAAP-TR-055, September 1979.

11. C. A. Dobbe, Audit Calculations for Westinghouse PWR Small Cold-Leg Breaks, CAAP-TR-054, August 1979.

12. G. P. Marins and J. M. Marks, Calculation of Fuel Rod Temperatures Reached in the Three Mile Island-2 Incident, NRC Memorandum for Files, October 25, 1979.

13. P. L. Rittenhouse, Progress in Zircaloy Cladding Failure Modes Research, ORNL-TM-3188, December 1970.

14. D. O. Hobson and P. L. Rittenhouse, Deformation and Rutpure Behavior of Light-Water Reactor Fuel Cladding, ORNL-4727, October 1971.

15. P. L. Rittenhouse, et al., The Effect of Light-Water Reactor Fuel Rod Failure on the Area Available for Emergency Coolant Flow Following a Loss-of-Coolant Accident, ORNL-4752, January 1972.

16. D. G. Hardy, High Temperature Expansion and Rutpure Behavior of Zircaloy Tubing, CONF-730304, Topical Meeting on Water-Reactor Safety, March 1973.

17. R. H. Chapman, Results and Status of ORNL Single Rod and Multirod Bundle Tests in a Steam Environment, Joint US-NRC/GfK-PNS LWR Safety Research Information Exchange Meeting, Karlsruhe, West Germany, June 12-14, 1978.

18. R. H. Chapman, et al., Zircaloy Cladding Deformation in a Steam Environment with Transient Heating, Fourth International Conference on Zirconium in the Nuclear Industry, Stratford-on-Avon, England, June 26-29, 1978.

19. F. Erbacher et al., Ballooning in Zircaloy Fuel Rod Cladding in a Loss-of-Coolant Accident, ANS Thermal Reactor Safety Meeting, Sun Valley, Id, July 31-August 5, 1977.

20. F. Erbacher et al., Fuel Rod Behavior in the Refilling and Reflooding Phase of LOCA Burst Tests with Indirectly Heated Fuel Rod Simulators, Zircaloy Cladding Review Group Meeting, Idaho Falls, Id, May 23, 1977.

21. F. Erbacher et al., Interaction between Thermo-Hydraulics and Fuel Clad Ballooning in a LOCA, Results of REBEKA Multirod Burst Tests with Reflooding, Sixth Water Reactor Safety Research Information Meeting, Gaithersburg, Md., November 6-8, 1978.

22. E. D. Hindle, Zircaloy Fuel Clad Ballooning Tests at 900-1070 K in Steam, ND-R-6(s), June 1977.

23. E. D. Hindle and C. A. Mann, Zircaloy PWR Fuel Clad Deformation Tests Under Mainly Convective Cooling Conditions, Zircaloy Cladding Program Review Meetings, Idaho Falls, Id, June 25, 1979.

24. J. R. Larson et al., PBF-LOCA Test Series Test LOC-11 Test Results Report, NUREG/CR-0618 TREE-1329, April 1979.

25. T. R. Yackle, et al., PBF-LOCA Test Series Test LOC-3 Quick Look Report, TFBP-TR-328, July 1979.

26. E. H. Karb, Results of the FR2 Nuclear Tests on the Behavior of Zircaloy Clad Fuel Ro..., Sixth Water Reactor Safety Research Information Meeting, Gaithersburg, Md, November 6-8, 1978.

27. D. L. Hagrman and G. A. Reymann, MATPRO-VERSION II A Handbook of Materials Properties for use in the Analysis of Light Water Reactor Fuel Rod Behavior, NUREG/CR-0497 TREE-1280, February 1979.

28. S. L. Seiffert and R. R. Hobbins, Oxidation and Embrittlement of Zircaloy-4 Cladding from High Temperature Film Boiling Operation, NUREG/CR-0517 TREE-1327, April, 1979.

29. J. V. Cathcart, Quarterly Progress Report on the Zirconium Metal-Water Oxidation Kinetics Program Sponsored by the NRC Division of Reactor Safety Research for April-June 1976, ORNL/NUREG/TM-41, August 1976.

30. R. B. Bird et al., Transport Phenomena, John Wiley and Sons, Inc., 1960.

31. R. A. Perkins, Zirconium Metal Water Oxidation Kinetics II, Oxygen-18 Diffusion in β Zircaloy, ORNL/NUREG/TM-19, 1976 pp. 33.

32. R. E. Pawel et al., Anomalous Oxide Growth During Transient Temperature Oxidation of Zircaloy-4, Oxidation of Metals, 14, 1, 1980.

33. P. Hofmann and C. Politis, "Chemical Interaction Between UO_2 and Zry-4 in the Temperature Range Between 900 and 1500 C", Paper Presented at the Fourth International Conference on Zirconium in the Nuclear Industry, Stratford-on-Avon, England, June 26-29, 1979.

34. C. D. Cann and A. Atrens, "A Metallographic Study of the Terminal Soiubility of Hydrogen in Zirconium at Low Hydrogen Concertrations," Journal of Nuclear Materials 88, 1980 pp. 42-50.

35. C. J. Scatena, Fuel Cladding Embrittlement During a Loss-of-Coolant Accident, NEDO-10674, General Electric, October 1974.

36. H. M. Chung et al., Light Water Reactor Safety Research Program: Quarterly Progress Report, October-December 1978, ANL. 79-18, May 1979.

37. D. O. Hobson and P. L. Rittenhouse, Embrittlement of Zircaloy-Clad Fuel Rods By Steam During LOCA Transients, ORNL-4758, January 1972.

38. R. E. Pawel, "Oxygen Diffusion in Beta Zircaloy During Steam Oxidation," Journal of Nuclear Materials, 50, pp. 247-258, 1974.

39. H. M. Chung, et al., Light Water Reactor Safety Research Program: Quarterly Progress Report, January-March 1978, ANL-59-49, June 1978.

40. H. M. Chung and T. F. Kassner, "Zircaloy Embrittlement Criteria," presented at the Zircaloy Cladding Program Review Meeting, Idaho Falls, Idaho, June 25, 1979.

41. B. A. Cook, Fuel Rod Material Behavior During Test PCM-1, NUREG/CR-0757, TREE-1333, June 1979.

42. D. K. Kerwin, Fuel Rod Materials Behavior During Test PCM-5, NUREG/CR- , (to be published).

43. A. W. Cronenberg and T. R. Yackle, An Assessment of Intergranular Fracture Within Unrestrictured UO_2 Fuel Due to Film Boiling, NUREG/CR-0595, TREE-1330, March 1979.

44. H. M. Chung et al., Light Water Reactor Safety Research Program: Quarterly Progress Report, July-September 1979, ANL-78-3, January 1978.

45. H. M. Chung et al., Light Water Reactor Safety Research Program: Quarterly Progress Report, October-December 1977, ANL-78-25, May 1978.

46. C. Politis, Investigations of the Ternary Uranium-Zirconium Oxygen System, KfK 2167, October 1975.

47. P. Hofmann, Chemical Interactions Between UO_2 and Zircaloy-4 in the Temperature Range Between 1000 and 1500° C, Presented at American-German-Japan Workshop on Fuel Rod Behavior Under Accident Conditions, Idaho Falls, Id, June 25-29, 1979.

48. S. Hagen, et al., "Phenomena and Material Behavior During Meltdown of PWR Fuel Rods," Presented at the OECD Committee on the Safety of Nuclear Installations, Specialists Meeting on the Behavior of Water Reactor Fuel Elements Under Accident Conditions, Spatinal, Norway, September 1976.

49. Projekt Nukleare Sicherheit, Halbjahresbericht 1976/1, KfK 2375, p 393, Kernforschungszentrum, Karlsruhe September 1976.

50. Projekt Nukleare Sicherheit, Halbjahresbericht 1977/2, KfK 2600, p 416, Kernforschungszentrum, Karlsruhe May 1978.

51. Projekt Nukleare Sicherheit, Halbjahresbericht 1978/1, KfK 2700, p 4300-46, Kernforschungszentrum, Karlsruhe, (to be published)

52. Projekt Nukleare Sicherheit, Halbjahresbericht 1978/2, KfK, p 4300-46, Kernforschungszentrum, Karlsruhe, (to be published).

53. B. A. Cook, Fuel Rod Material Behavior During Test PCM-1, NUREG/CR-0757, TREE-1333, June 1979.

54. D. R. Olander, Fundamental Aspects of Nuclear Reactor Fuel Elements, Technical Information Center, Office of Public Affairs, Energy Research and Development Administration, 1976.

55. D. Kunii and O. Levenspiel, Fluidization Engineering, John Wiley Sons, Inc., 1969.

56. D. R. Evans and M. M. Giles, The MOXY/SCORE Core Heat Transfer Code: Model Description and User's Guide, SRD-129-76, June 1976.

APPENDIX A
POTENTIAL FOR VAPOR EXPLOSION

During the severe core damage tests, the fuel rods will be severely embrittled, and extensive fragmentation and fuel desintering may occur during quench. At the high fuel rod temperatures (ie ~2300 K) the cladding will melt and a significant fraction of the fuel may be dissolved. The liquefied core material would flow into the bottom regions of the test bundle, where the water level is maintained at about 10 cm above the bottom of the fuel. Rapid quenching of the test bundle could result in an energetic vapor explosion if the liquefied fuel rod material and fuel rod fragments are rapidly dispersed within the coolant and if there were an appropriate triggering mechanism.

The present theories of vapor explosion phenomena are briefly reviewed and the primary models which have been postulated are discussed. The potential for the PBF tests to satisfy the basic criteria for vapor explosions to occur are then assessed.

1. Physics of Explosive Vaporization

Results from recent research indicate that a vapor explosion is characterized by the following:

1. A period of stable film boiling

2. Destabilization of film boiling by either thermal or pressure induced means, or both

3. Initimate contact between the "hot" and "cold" liquids

4. Extensive fragmentation and intermixing of the hot liquid with the cold liquid, resulting in a large effective heat transfer area causing rapid coherent coolant vaporization

5. Sufficient system constraint to cause severe shock pressurization.

In the PBF tests, the hot liquid could be liquified fuel rod material molten UO_2, and/or fuel rod fragments intermixed with desinted UO_2. The cold liquid is the coolant water. The preceding scenario is illustrated schematically in Figure A.1.

At the present time, there is little agreement as to the details of the actual physical phenomena involved in such processes. For example, there is little agreement on the mechanism of fragmentation of the hot liquid, the rate at which it occurs, and the ultimate particle size that can be expected. Likewise, the question of the energy transfer mechanism between fuel and coolant is unanswered. It has been proposed by some investigators that rapid phase-transformation by spontaneous nucleation is a necessary condition for obtaining a vapor explosion,[1,2] whereas others[3-10] have postulated that a nucleate-type boiling process from finely divided fuel intermixed with coolant can produce vapor at sufficient rate to obtain shock pressurization of the system. The current understanding and modeling of these phenomena are summarized in the following paragraphs.

2. Fragmentation - Intermixing Process

Both in-pile fuel-failure tests and out-of-pile molten metal dropping experiments indicate that the fragmentation/intermixing process is primarily thermal in nature, with hydrodynamic influences having an added effect. Nevertheless, because no one model has yet been accepted which accurately calculates the rate of breakup and particle sizes, emperical evidence must be used for parametric evaluation such as Mizuta's[1] correlation shown below.

$$f(\log D) = 58.1 \exp \frac{-(\log D - 2.27)^2}{0.944}$$

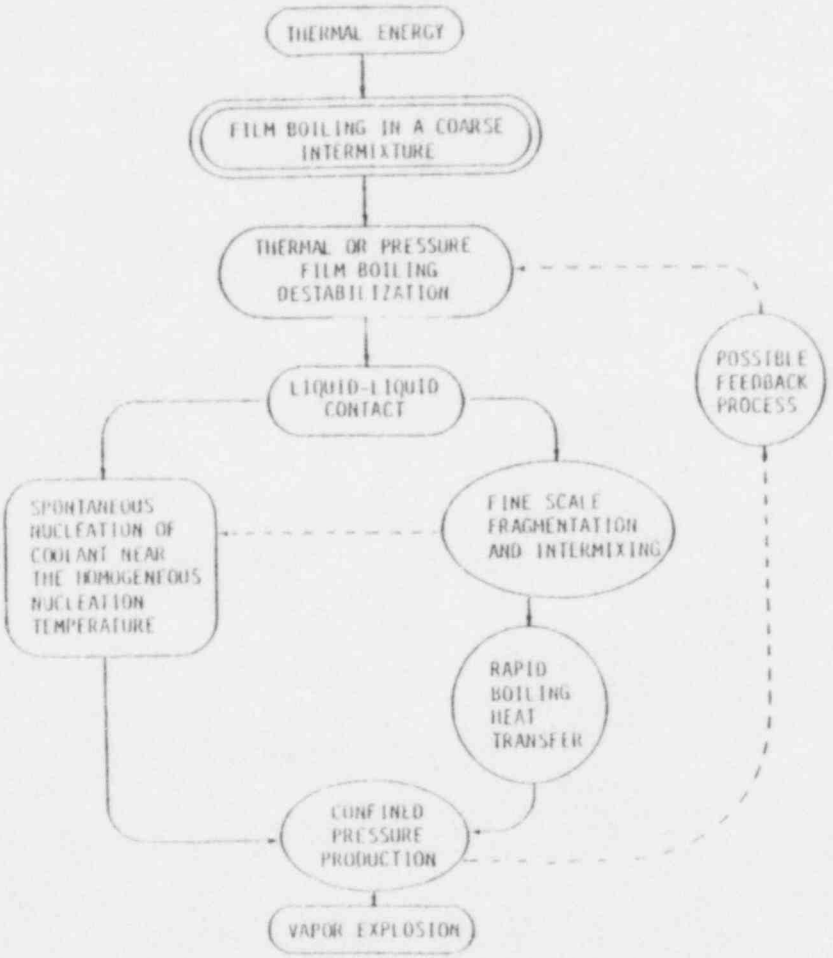

Figure A.1. Possible chain of events in large scale vapor explosion, Reference A-16.

Where D is the particle diameter (μm). This correlation is based primarily on fragmentation data obtained from controlled small-scale experiments (some of which cannot be considered vapor explosion events), rather than a large-scale vapor explosion which might occur in a nuclear reactor. Thus, the correlation is subject to questions of prototypicality.

Based on the results of parametric calculations[1] and the results of the SPERT-ID[2] destructive experiments, an appropriate breakup and intermixing time is on the order of a few milliseconds. Further evidence that such mixing and fragmentation occurs on a millisecond time scale can be found from analysis of numerous other experiments. Therefore, a time for breakup and intermixing alone of several milliseconds was suggested by Cronenberg and Benz.[3]

For the particular system associated with the relatively rapid inundation of the hot core by coolant when terminating a small break LOCA transient, the potential for extensive fragmentation and intermixing of the core material definitely exists. Fragmentation of the liquified fuel rod material would not necessarily be typical of that observed in previous experiments. The liquified material could be in contact with the solid UO_2 and it would probably have solid ZrO_2 in suspension. Fragmentation of the uranium and zirconium dioxide would probably be induced by thermal stresses resulting from quench. Results from the in-pile PBF PCM-1 test[18] show that when very high temperature UO_2 is subjected to severe thermal shock, such as usually occurs during quench, that UO_2 pellets can "de-sinter" into very fine particles approximately the size of individual grains.

3. Heat Transfer-Pressurization Process

For a vapor explosion to occur, intimate fuel-coolant contact must be established with resulting rapid vaporization and shock pressurization. Essentially only two mechanistic models have been proposed which attempt to describe the actual mechanisms involved and

the kinetics of such processes. These models are the spontaneous nucleation/pressure suppression model by Fauske and Henry,[4-6] and the pressure detonation model of Board and Hall[7,8]. According to the spontaneous nucleation model, the necessary criteria for large scale vapor explosions are summarized as follows:

1. Liquid-liquid systems,

2. Liquids must be at greatly different temperatures,

3. The interface temperature (T_I) upon contact must be greater than or equal to the spontaneous nucleation temperature of the working fluid.

In addition to the above, other system parameters which affect or may even preclude explosive interactions are:

1. System constraint,

2. Elevated ambient pressures,

3. Supercritical interface temperatures in a free contacting mode.

The concept upon which the spontaneous nucleation model is based is graphically illustrated in Figure A.2.

Figure A.3 is a one dimensional illustration of the Board-Hall pressure detonation concept. The model assumes that a strong shock front propagates steadily through a region of coarsely mixed molten fuel and coolant, the initial pressure trigger being considered sufficient to cause collapse of any preexisting vapor. As the pressure wave passes the interaction region, the flow velocity differential between the dense fuel and lighter coolant are hypothesized to be sufficient to cause fine-scale fragmentation. As a result, the front leaves behind finely fragmented fuel in intimate

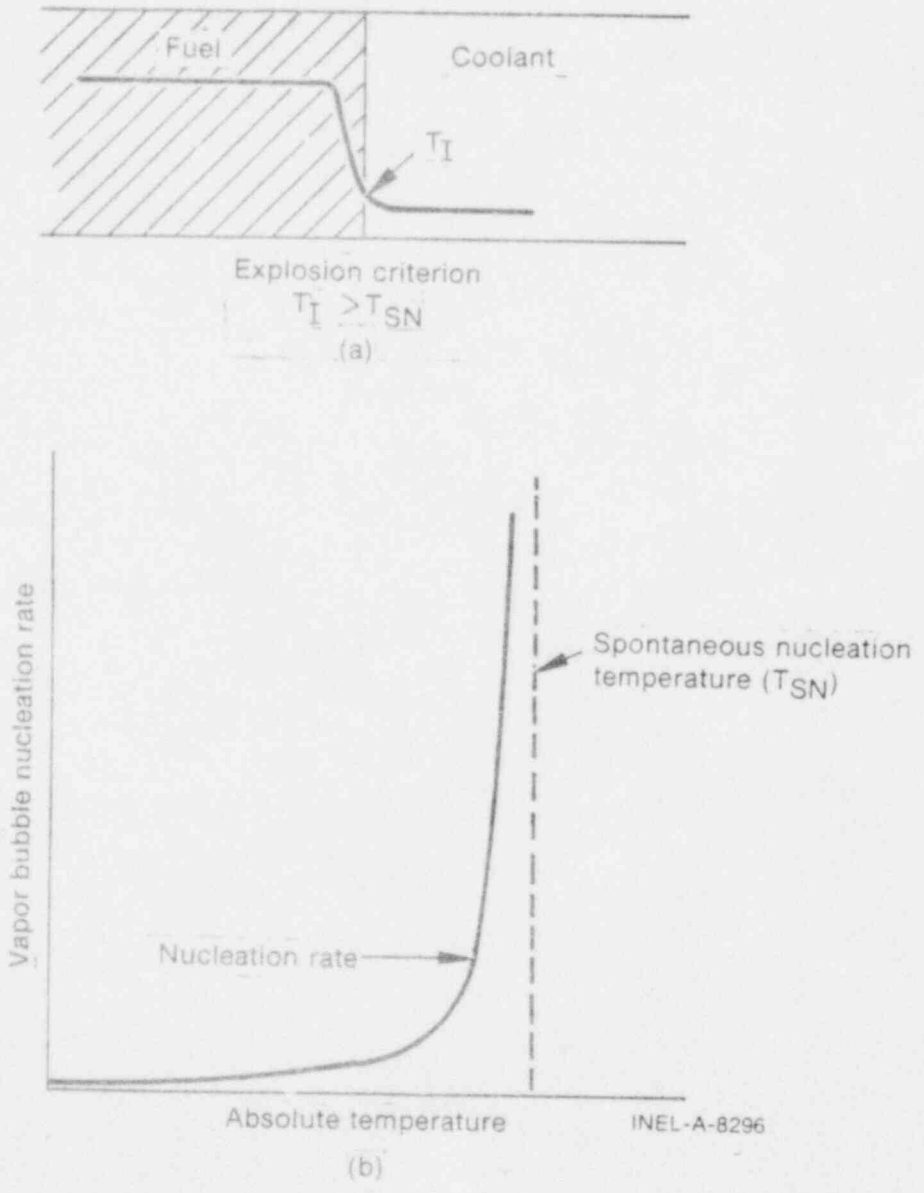

Figure A.2. Illustration of spontaneous nucleation model, Reference A.3.

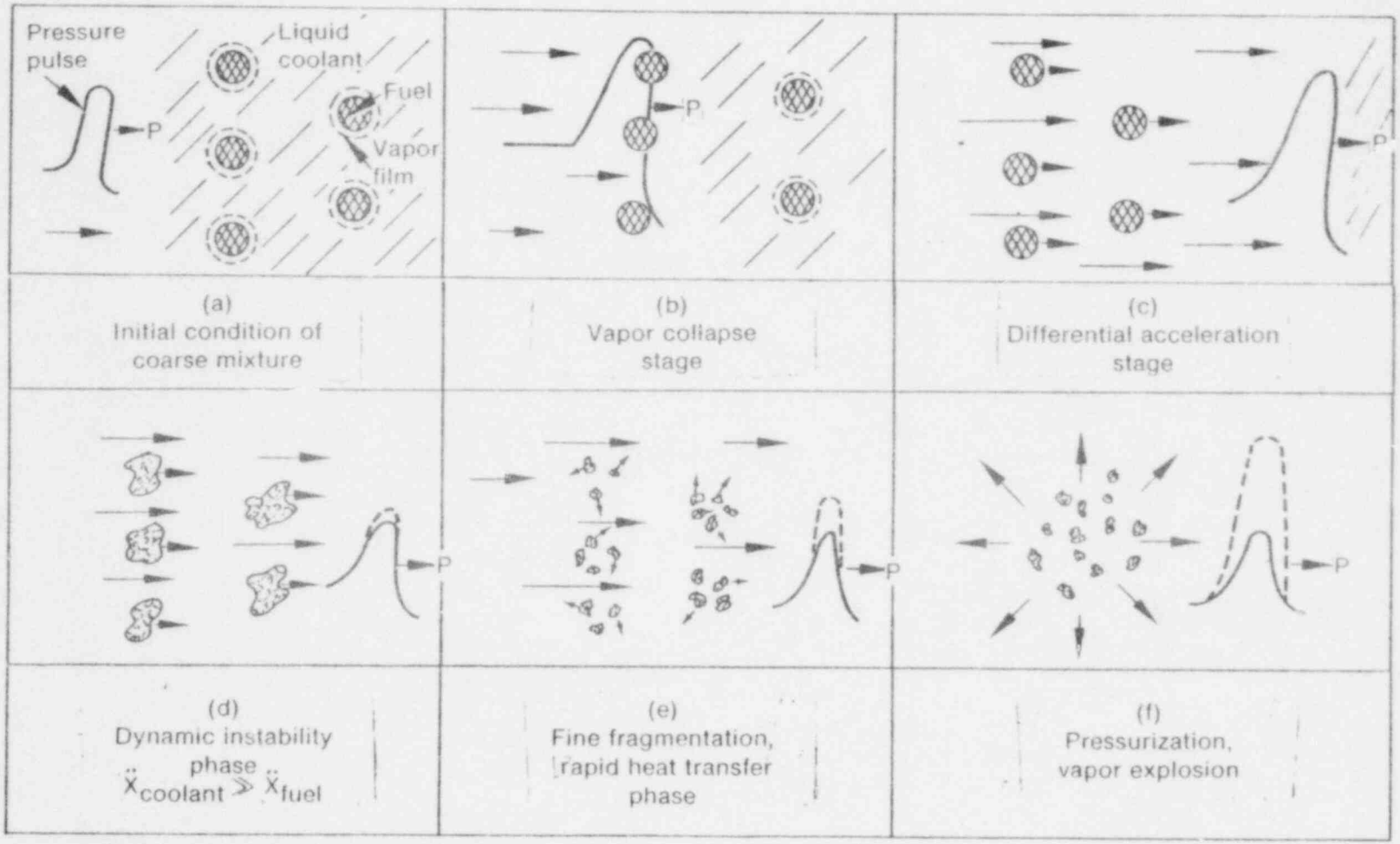

Figure A.3. Descriptive illustration of pressure detonation model, Reference A.3.

contact with the coolant, resulting in vaporization sufficiently rapid to cause shock pressurization and explosion. Some uncertainties with respect to the model are: the source of the initial pressure pulse, the requisite condition of a predispersed coarse mixture, and the mechanism for rapid, fine fragmentation by dynamic instability.

Cronenberg and Benz[3] have reviewed vapor explosion phenomena with respect to nuclear reactor safety assessment and concluded the following. Although each of the vapor explosion models has merit, neither has gained wide acceptance as an acceptable description of the actual phenomena involved or as encompassing all possible scenarios that could lead to explosive vaporization. It is their opinion that the spontaneous nucleation model is one mechansim by which vapor explosions can be accounted for; however, it ma not be considered the only criterion upon which vapor explosion potential should be judged. An 'a priori' conclusion that a vapor explosion will not occur if the instantaneous contact temperature between fuel and coolant is below the spontaneous nucleation temperature or if the system pressure is greater than the critical pressure of the working fluid, cannot suffice if it can be demonstrated that progressive fragmentation-heat transfer-pressurization models can lead to explosive vaporization. The work of Board and Hall is an attempt at such an approach; however, serious questions arise as to the original hydrodynamic assumptions and associated fragmentation dynamics. Thus, further investigation of this concept appears warranted.

Extensive investigations with simulant fluid experiments appear to support the interface-spontaneous nucleation concept of Fauske and Henry. However, most simulant fluid experiments have been carried out to test particular model assumptions rather than to assess all-encompassing conditions which could lead to shock-type explosive vaporization. For example, the water-hammer experiments of Wright and Humberstone[4] produced vapor explosions with molten aluminum impacted upon water (which satisfies the contact interface-nucleation criterion); however, such experiments have not been conducted for molten UO_2 impacted upon sodium (which would not satisfy the contact

interface-nucleation criterion), yet explosive vaporization under such conditions appears possible. Therefore, $T_I > T_{SN}$ is not considered to be a necessary condition for explosive vaporization, but rather, just one mechanism by which rapid vaporization can be accounted for. Further experimental verification of required conditions is thus deemed necessary before either the pressure detonation concept or other plausible scenarios can be completely discounted or accepted in reactor safety assessment.

The detonation concepts require pressure- or thermal-induced film boiling destabilization and subsequent fragmentation. The spontaneous nucleation concept requires at least an order of magnitude increase in the vapor nucleation rate at the spontaneous nucleation temperature. Considering the ideas presented in these modeling concepts and experimental result, it appeared to Cronenberg and Benz[3] that destabilization of quiescent film boiling, due to either pressure or thermal conditions, or both, resulting in rather violent nucleate-type boiling and fragmentation into a large surface heat transfer area, satisfies the conditions for explosive vaporization. The fact that the predicted homogeneous nucleation temperature is not significantly different from a thermodynamic prediction of the minimum film boiling temperature[9-11] (Liedenfrost point) and that contact-wetting conditions affect both, indicates that experiments which have been interpreted in light of spontaneous or homogeneous nucleation temperature[12,13] may also be explained by a film boiling destabilization temperature. In addition, pressure effects have been shown to also cause film boiling collapse. The recent work of Lienhard,[14] Dhir,[15] Gunnerson and Cronenberg,[16,10,11] and Bankoff et al.[17] with respect to understanding the conditions for film boiling stability should help in understanding vapor explosion criteria.

With our current understanding of explosive vaporization it is not possible to predict that a vapor explosion is possible or impossible for the rapid quenching of a high temperature, partially molten PWR core. The fact that a vapor explosion did not occur when TMI-2 was quenched is not conclusive evidence that such an explosion

is impossible. Many of the key parameters considered important to the process are satisfied. For instance, contact interface temperatures for all core materials are greater than the spontaneous nucleation temperature, extensive amounts of liquified core material could be present, and extensive fragmentation of UO_2 fuel at high temperatures can occur.

Mechanisms which could restrict or even prevent a vapor explosion include the following. The system pressure will range from 2.75 to 10.0 MPa which would preclude the occurence of a vapor explosion according to Fauske and Henry. The system constraints of the rubble pile formed by quenching could prevent intimate contact between the coolant and the hot material.

4. REFERENCES

A-1. H. Mizuta, "Fragmentation of Uranium Dioxide After Molten UO_2-Na Interaction," Nuclear Science and Technology, 11 1974 pp. 480-487.

A-2. R. W. Miller, A. Sola, R. K. McCardell, Report of the SPERT-1 Destructive Test Program on an Aluminum Plate-Type Water-Moderated Reactor, IDO-16883, 1964.

A-3. A. W. Cronenberg and R. Benz, Vapor Explosion Phenomena with Respect to Nuclear Reactor Safety Assessment, NUREG/CR-0245, July 1978.

A-4. H. K. Fauske, On the Mechanisms of UO_2-Na Explosive Interaction, Nuclear Science and Engineering, Volume 51, pp. 95, 1973.

A-5. H. K. Fauske, "The Role of Energetic Mixed-Oxide-Fuel-Sodium Thermal Interactions in Liquid Metal Fast Breader Reactor Safety," Proceedings of the Third Specialist Meeting of Sodium/Fuel Interaction in Fast Reactors, Tokyo, March 22-26, 1976.

A-6. R. E. Henry and K. Myazaki, "Effects of System Pressure on the Bubble Growth from Highly Superheated Water Droplets," Annual ASME Winter Meeting; Topic in Two-Phase Heat Transfer and Flow Section, San Francisco, California, December 10-15, 1978.

A-7. S. J. Board and R. W. Hall, "Recent Advances in Understanding Large-Scale Vapor Explosings," Proceedings of 3rd Specialist Meeting on Na/Fu[illegible]nteractions in Fast Reactors, Tokyo, Japan, March 22-26, 1976, pp. 249-284.

A-8. S. J. Board, R. W. Hall, R. S. Hall, "Detonation of Fuel-Coolant Explosions," Nature, 254(March 1975) pp. 319-321.

A-9. P. Spiegler et al., "Onset of Stable Film Boiling and the Foam Limit," International Journal of Heat and Mass Transfer, 6(1963) pp. 987-994.

A-10. F. S. Gunnerson and A. W. Cronenberg, On the Thermodynamic Superheat Limit for Liquid Metals and Its Relation to the Leidenfrost Temperature (to be published), Journal of Heat Transfer, 1978).

A-11. F. S. Gunnerson and A. W. Cronenberg, "A Thermodynamic Prediction of the Temperature for Film Boiling Destabilization and Its Relation to Vapor Explosion Phenomena," Transactions of the American Nuclear Society Annual Meeting, San Diego, California, June 18-22, 1978, p. 449.

A-12. R. E. Henry, H. K. Fauske, L. M. McUmber, "Vapor Explosion Experiments with Simulant Fluids," Proceedings of the American Nuclear Society Conference on Fast Reactor Safety, Chicago, Illinois, October 1976.

A-13. R. E. Henry and H. K. Fauske, "Nucleation Characteristics in Physical Explosion," Proceedings of 3rd Specialist Meeting on Na/Fuel Interaction in Fast Reactors, Tokyo, Japan, March 22-26, 1976, pp. 596-623.

A-14. J. H. Leinhard and P. T. Y Wong, "The Dominant and Unstable Wavelength and Minimum Heat Flux During Film Boiling on a Horizontal Cylinder," Journal of Heat Transfer, 86, May 1964, pp. 220-226.

A-15. V. K. Dhir and G. P. Purohit, Subcooled Film-Boiling Heat Transfer From Spheres, ASME Paper: 77HT-78 (1977).

A-16. F. S. Gunnerson and A. W. Cronenberg, "A Correlation for the Leidenfrost Temperature for Spherical Particles and Its Application to FCI Analysis," Transactions of the American Nuclear Society, 25, (1977) pp. 381-383.

A-17. S. G. Bankoff et al., "Destabilization of Film Boiling in Liquid-Liquid Systems," Proceedings of the 6th International Heat Transfer Conference, Toronto, Canada, August 1978.

A-18. A. W. Cronenberg and T. R. Yackle, An Assessment of Intergranular Fracture Within Unrestructured UO_2 Fuel due to Film Boiling Operation, NUREG/CR-0595, TREE-1330, March 1979.